國立交通大學

光電工程研究所

博 士 論 文

場序全彩液晶顯示器之時空域調變技術設計與評估

Design and Evaluation of Spatiotemporal Modulation for
Field-sequential-color LCDs

研 究 生：鄭裕國

指導教授：謝漢萍 博士

中 華 民 國 九十九 年 一 月

場序全彩液晶顯示器之時空域調變技術設計與評估

Design and Evaluation of Spatiotemporal Modulation for

Field-sequential-color LCDs

研 究 生： 鄭裕國　　　　Student：Yu-Kuo Cheng

指導教授： 謝漢萍　　　　Advisor：Han-Ping D. Shieh

國 立 交 通 大 學

光 電 工 程 研 究 所

博 士 論 文

A Dissertation
Submitted to Institute of Electro-Optical Engineering
College of Electrical and Computer Engineering
National Chiao Tung University
in partial Fulfillment of the Requirements
for the Degree of
Doctor of Philosophy
in
Electro-Optical Engineering
2010
Hsinchu, Taiwan, Republic of China

中 華 民 國 九十九 年 一 月

場序全彩液晶顯示器之時空域調變技術設計與評估

博士研究生：鄭裕國

指導教授：謝漢萍　博士

國立交通大學　　光電工程研究所

摘　　要

　　近年來，為滿足低耗能、高效率之綠色環保訴求，顯示器學界、業界再次興起研發場序全彩液晶顯器的熱潮。然而，受限於當前液晶顯示器系統的信號寫入模式與液晶模態的響應速率，不僅尚未攻克基本的色度難題，諸如色域縮減、接續色場混雜干擾及背光亮度侷限等，更遑論潛在的視覺效應，色分離現象，仍待克服。本研究探討上述色度難題成因，並提出對應之解決方案，同時建置評估色分離現象之指標。

　　本論文提出一種新穎的雙色場混色驅動法及其搭配之系統架構，以實現無彩色濾光片之場序全彩液晶顯示器。該混色驅動法採用可空間調控之彩色背光模組以提供額外的空間自由度，滿足三原色系統除了兩個時間自由度外所需之維度，得以呈現全彩影像。採用本架構之系統，最大特色在於擁有最長的單色場時間週期，一方面使現有之商業化液晶模態，例如多區域垂直配向液晶模態，可適用於本系統，降低成本，另一方面則可通過充裕的時間調配，無須犧牲前述之色度參數。除此之外，採用本驅動法之單一色場，通常由雙原色混成，故雙色場通常為非高對比之對立色，例如紅－綠、黃－藍;而對比敏感度的降低，有助於抑制色分離條紋的感知。最後，所提出之心理物理指標，相對對比敏感度，已初步驗證其評估色分離現象的適用性，將可作為評量、反饋於系統優化的參考項目。

Design and Evaluation of Spatiotemporal Modulation for Field-sequential-color LCDs

Doctoral Student: Yu-Kuo Cheng

Advisor: Dr. Han-Ping D. Shieh

Institute of Electro-Optical Engineering
National Chiao Tung University

Abstract

Field-sequential-color (FSC) liquid-crystal-display (LCD) has been driven by the demand for energy-efficient Green display in recent years. The driving scheme and slow LC response, however, have led to issues such as color gamut shrinkage, color crosstalk between successive fields, and insufficient backlight intensity, etc., not to mention the visual artifact, color break-up (CBU). This research is to study those colorimetric issues and the feasible solution, based on spatial-temporal modulation, and to develop a methodology to evaluate CBU.

A novel two-field driving scheme and the associated system have been proposed to facilitate the FSC LCD without color filters. A spatially-modulated color backlight is implemented to provide degrees of freedom in spatial domain in addition to the two temporal ones for conveying full-color information. This configuration of FSC LCD specifically features the feasibility of commercial LC modes, e.g. Multi-domain Vertical Alignment (MVA), without sacrificing the mentioned colorimetric properties. Additionally, the innate nature of reduced contrast sensitivity between two primary-mixed fields suppresses the CBU to be less sensitive than that appears in the fundamental three-field FSC LCD. Finally, the psychophysical index, relative contrast sensitivity (RCS), has demonstrated the applicability to evaluate CBU among various driving schemes, which can be a useful feedback for system optimization.

Acknowledgement

Table of Contents

Figure Captions

VIII

List of Tables

Chapter 1

Introduction

1.1 Green Concept

Green concept is pervading all present-day walks of life because of the alarming crisis of energy shortage and environment deterioration. Being driven by this demand, Green display or Eco-display has turned into an emerging, main theme of display development. New display devices are expected to feature some properties, such as material recycling, power saving, non-toxic (e.g. mercury-free and/or lead-free) stuff, carbon dioxide reduction, etc. Among those considerations, power saving of a liquid-crystal-display (LCD) system inspires the research of this thesis because the LCD has dominated the markets of television and monitor nowadays. This property will become more and more significant, say, for the enlarging display size since the power efficiency of most LCDs, currently, is merely of around 6% ~10%.

Whenever power-saving or, equivalently, power efficiency promotion is thought of in recent years, either field-sequential-color (FSC) LCD [1,2] or high-dynamic-range (HDR) LCD [3,4] always recurs in our mind. The optical efficiency of the FSC LCD is promoted, ideally up to a factor of 3, by removing the color filter. Meanwhile, the electric power of the HDR LCD is saved by applying a spatially-modulated backlight. Therefore, the integration of the merits of these two types of LCD is regarded as a promising idea to innovate an LCD system, which is supposed to be of considerable reduction of power consumption with compatible display performance as the conventional LCDs.

Some physical limitations and visual artifacts, however, restrain the development of FSC LCDs. At the same time, some restrictions have been observed to degrade the performance of the HDR LCD. The concerned issues will be described later; the strategic designs on optics and driving algorithm are, thus, elaborated to facilitate the FSC LCD with a spatially-modulated backlight.

1.2 Historical Review

Both spatial and temporal color synthesis methods, based on the principle of additive color mixing, were developed in modern display history. In 1950, a temporal FSC broadcast system for color television, proposed by the Columbia Broadcasting System, was standardized by the Federal Communications Commission for use in the USA [5]. Three primary field pictures were shown at 144 Hz, which equals to 48 full-color images per second. This decision, however, was soon set aside in 1953 due to some system limitations and objectionable visual artifacts, flicker and color break-up (CBU) [6]. Then, the spatial mosaic configuration, tri-chromatic phosphor triad, sprang up due to simplicities of design and manipulation. Consequently, the application of the mosaic method culminated in the cathode-ray tube (CRT) display in the past decades.

1.3 Conventional LCD

In the commencement of the LCD system, the mosaic method remains to be the main design norm for simplicity. The so-called "conventional LCD," as shown in **Fig. 1-1**, is defined as an LCD system consisting of an LC module and a constant white backlight module.

1.3.1 System Configuration

The LC module is composed of a series of functional layers. Briefly speaking, a bottom polarizer, a bottom glass, a thin-film-transistor (TFT) array, an LC layer, a color filter (CF) film, a top glass, and a top polarizer are stacked from the backlight side to the observation side. Particularly, each pixel comprises tri-chromatic, namely red, green, and blue, sub-pixels, independently controlled by the corresponding units of TFT circuit. The pixel size is designed to be beyond the spatial discrimination ability of the human visual system (HVS), such that the tri-chromatic light from three sub-pixels is explained by the HVS as if emanating from the same position. This mechanism is what spatial color synthesis means. As for the backlight module, cold cathode fluorescent lamp (CCFL), the typical light source, is gradually replaced by white light-emitting-diode (LED) after the advanced improvement of electro-optical transfer efficiency and cost reduction. It is worth noting that the "LC module" defined here is somewhat different from that termed in the industrial LCD manufacturing processes. The backlight module is isolated from the usual LC module because of the manifest significance in this thesis.
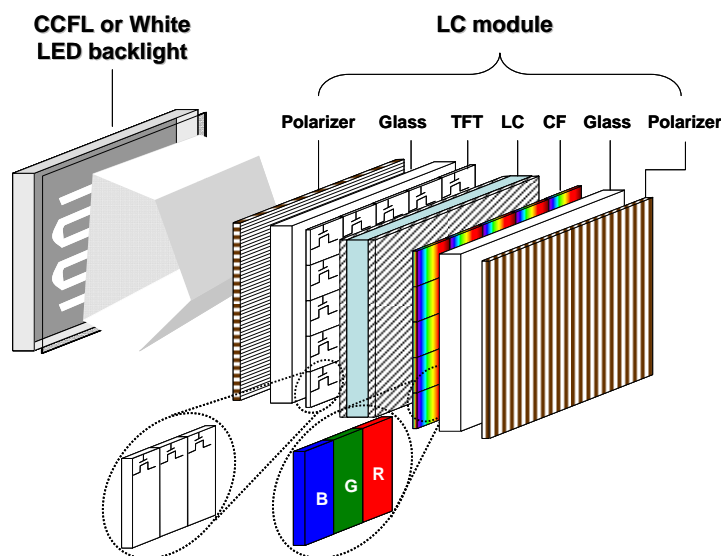
Fig. 1-1 *Configuration of a conventional LCD*

1.3.2 Operation Principle

The digital data of an image, through a series of signal processes, are transformed into analog signals. Row data lines of the TFT array circuitry switch on TFTs' gate electrode on the same row simultaneously. Electric charges, in proportion to the image data, are then delivered to the storage capacitor of each pixel through column data lines. The timing chart of the data registration and the following LC response are illustrated in **Fig. 1-2**, in which one column of LC module is selected since all columns experience identical timing, i.e. the field time T_f. The symbol τ denotes the data registration time of each row. In the conventional LCD, the value of τ is estimated according to one frame time divided by the number of row. For the jth row, after the time of $[(M-j)*\tau + j*\tau]$, the LC cell starts the molecule transition for the time duration T_{lc} till the stable state. $(M-j)*\tau$ represents the data registration time for the previous frame while $j*\tau$ for the current frame. Successively, the LC cell keeps the stable state for the hold time period T_h until the electric field is altered in the next frame. This nature gives the name of hold-type display, in contrast with the impulse-type display, e.g. CRT. It is worth noting that each row of LC cells, in the conventional LCD, actually undergoes the same time duration, T_f-τ, for receiving light illumination because of the constant backlight. The timing of such operation mode reveals inadequate to the application of FSC LCD, which will be discussed in detail in **Section 1.4.3.2**.

4
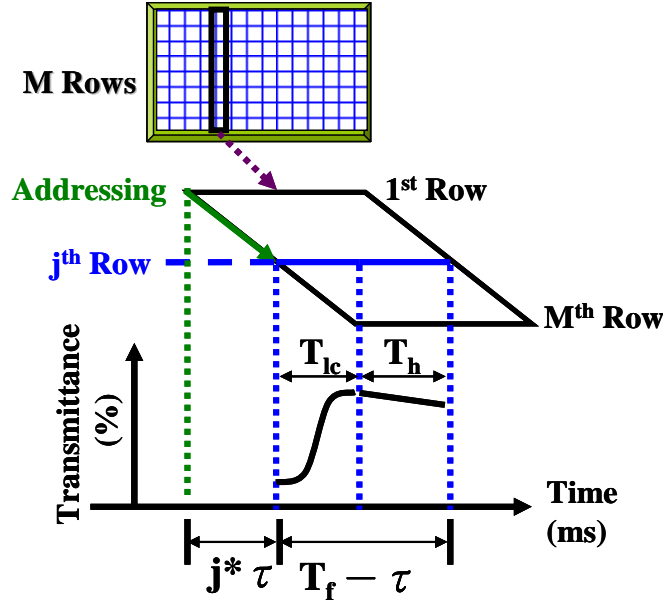
Fig. 1-2 Timing chart of data registration and LC response

The incident un-polarized white light from the backlight module is first filtered by the bottom polarizer to become single polarized light into the LC module. The amount of light leaving the LC module is dependent on the final polarization state of light reaching the top polarizer, which is regulated by the LC layer, functioning as a light polarization modulator. The polarization modulation of light by the LC layer is determined by the rotation of LC molecules, driven by the external electric filed across the LC cell according to the electric charges accumulated in the storage capacitor, as shown in **Fig. 1-3**. White light into the LC module then experiences spectral modulation when passing through the CF of a sub-pixel to convert into color light, green CF as an example in **Fig. 1-3**. The red and blue light can be obtained following the same mechanism, except for the red and blue CF in the red and blue sub-pixel.
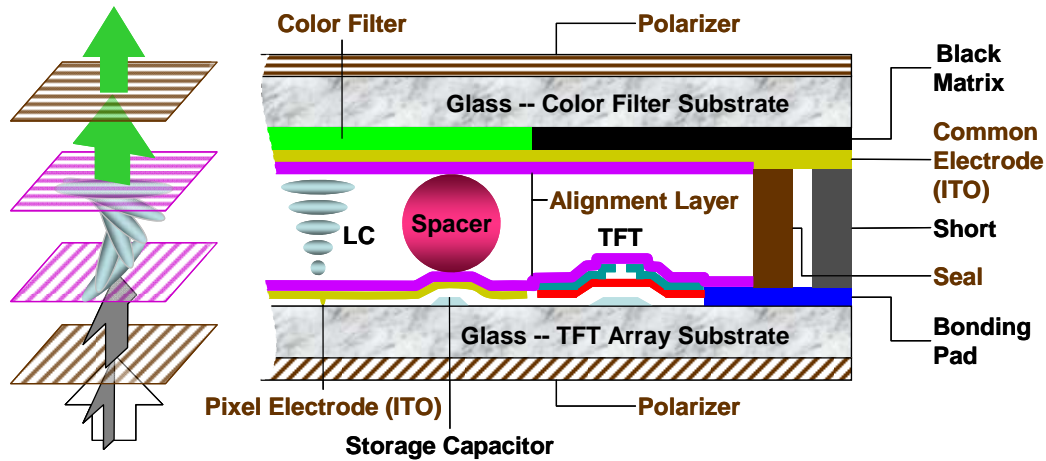
Fig. 1-3 *Partial cross-section of the LC module*

1.3.3 Optical Throughput

The pair of polarizers, the CF film, and the aperture ratio of a pixel are the three main factors decreasing the optical throughput of an LC module. Theoretically, a pair of orthogonal polarizers allows, at most, passing through 50% of radiometric energy of un-polarized light. The transmittance of the CF film, in average, is of around 33.3%. The aperture ratio of a pixel is defined as the ratio between the area where light can pass through and the total area of the pixel. The black matrix in the CF film, covering the underneath opaque regions of TFT devices, circuit paths, etc., primarily determines the area through which light can pass, as shown in **Fig. 1-3**. In practice, the aperture ratio may vary within the range of 65% ~ 85%, depending on the LC cell design. The overall optical throughput of these three components is estimated to be 12.5% when the aperture ratio is taken as of 75%. In most cases, the optical throughput of 8%~10% is the typical, reasonable estimation as some minor mechanisms, e.g. light absorption and reflection, are considered. As a result, about 90% of incident light energy from backlight module is wasted in the LC module. Low optical throughput of the conventional LCD, thus, concerns the researchers and manufacturers in the LCD industry due to the emerging demand for power saving.

1.4 Field-sequential-color (FSC) LCD

In view of optical throughput, the FSC concept recurs since removing the CF can promote optical efficiency by a factor of 3. Ideally, the optical throughput of the LC module without the CF can be improved to be of 37.5% (= 50% * 75%). Besides, the aperture ratio can increase because only one unit of TFT circuit is required in a pixel. Around one-fourth to one-third of the cost can be reduced as well. Recently, some FSC projectors have demonstrated that CBU can be suppressed by means of multi-field driving scheme [7]. All these positive features newly inspire the researches of FSC LCDs in recent years [8,9,10,11].

1.4.1 System Configuration

An FSC LCD has the similar structure to a conventional one, except for some critical modifications. The primary difference in the LC module is that there are no sub-pixels in a pixel along with the removal of the CF, as shown in **Fig. 1-4**. The TFT layer is thus of less number of TFT units than that of the conventional LC module. The backlight module is no longer emitting white light all the time, but successive red, green, and blue light in time sequence. Red/green/blue LEDs are the preferred light sources because of the short switching time and high color saturation.
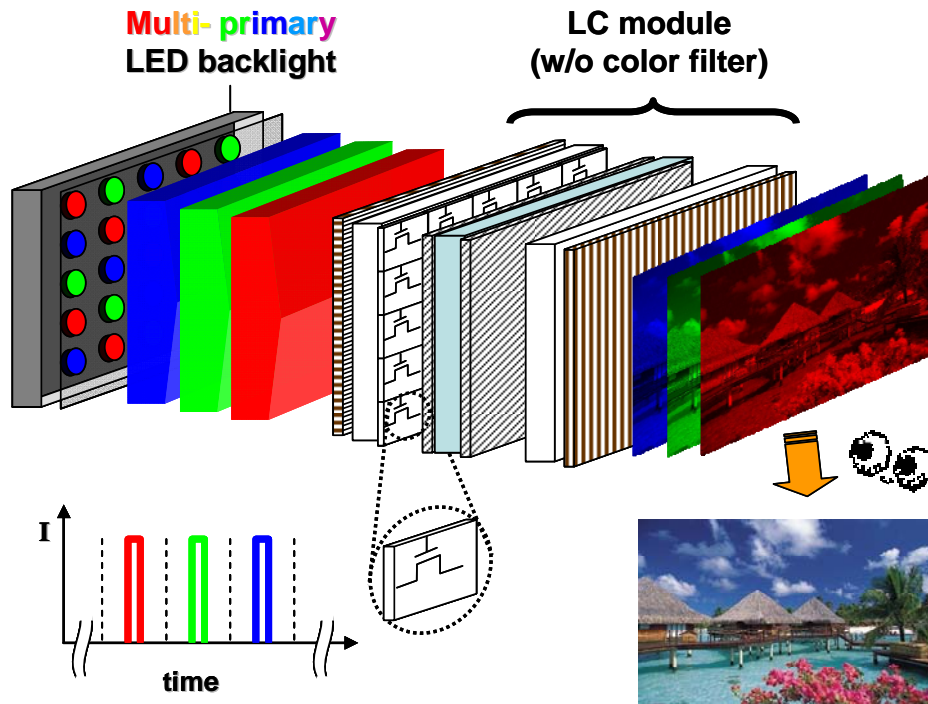
Fig. 1-4 *Configuration of an FSC LCD*

1.4.2 Operation Principle

The FSC method manipulates the signals in time domain. At first, one frame period, e.g. 16.7ms at refresh rate 60Hz, is divided into three fields, each of 5.56ms. Accordingly, each frame image is decomposed into a set of three primary field images. During a field time, red field for example, the red image signals are addressed into the pixel. After LC transition, the backlight module emanates uniform red light into the LC module. The green and the blue stimuli are obtained in the similar manner at the corresponding field time, as shown in **Fig. 1-4**. The HVS receives the primary stimuli and integrates for a frame period. When the refresh rate of the LCD is beyond the temporal discrimination threshold of the HVS, a full-color image is formed as if those three filed images were seen at the same time.

1.4.3 Issues

In spite of the aforementioned advantages, the FSC method applied to the LCD, however, encounters more serious challenges than those to the CRT. First, the visual artifacts, flicker and CBU, are potential to incur annoying perception. Second, the physical constraints, row data registration and LC response time, induce extra side effects, which affect final output luminance and color performance. These issues are introduced here and some strategies to those issues are described briefly.

1.4.3.1 Visual Artifacts

Flicker

Flicker in FSC display is mainly referred to "luminance" flicker, which is the luminance change perceived by observers. The "chrominance" flicker, caused by the hue change between the primary colors, is less significant and is always disregarded because CBU is the major visual artifact in color. Luminance flicker arises from the periodic luminance variation between blue channel and the other two primary colors, especially the green channel. In general, the ratio of maximum luminance between the three channels is of roughly 3:7:1 in the order of red, green, and blue, as shown in **Fig. 1-5**. The ratio varies with specific system design. The variation between the primary channels, especially blue and green ones, produces a high-contrast visual signal to the HVS, which easily results in an objectionable flashing to observers.
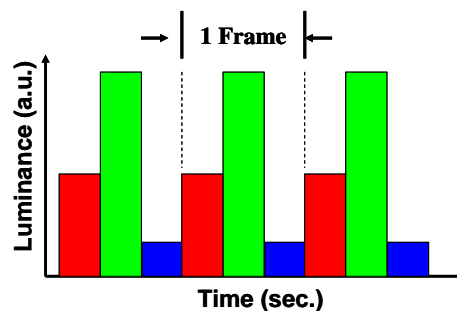
Fig. 1-5 An example of maximal luminance of the three primary channels

Color Break-up (CBU)

CBU occurs occasionally when the field of view of an observer moves relatively to an FSC display. If the speed of the relative motion exceeds the field refresh rate of an FSC display, the three primary field images may not coincide on the retina. Color fringes or color bands are probably observed along the direction of relative motion; an example image is shown in **Fig. 1-6** on the right. This phenomenon is termed as CBU or rainbow effect, which leads to annoying perception experience and, thus, degrades the visual quality.

Fig. 1-6 A normal image (left) vs. the CBU image (right)

Prior Solutions

The two most effective methods to suppress flicker and CBU in FSC projectors are field-rate acceleration [12] and multi-field driving scheme [7]; the latter can regarded as the modified version of the former with extra advantages.
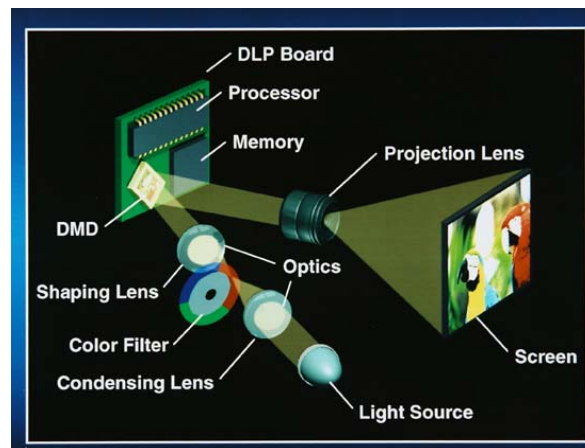
Fig. 1-7 1-chip DLP® projection [12]

10

The method of field-rate acceleration has been implemented successfully in commercial products of 1-chip Digital Light Processing® (DLP®) projector, as shown in **Fig. 1-7**. The basic principle of 1-chip projection is to synchronize the Digital Micro-mirror Device (DMD) with the color light, obtained when white light from the lamp passing through the rotating color wheel. In the very beginning, the 1-chip projection runs in the mode of three primary fields per frame, and serious flicker and CBU occur. Later on, two manipulations to speed up the field rate, as shown in **Fig. 1-8**, are developed to suppress the visual artifacts. The field rate of the first configuration, shown in **Fig. 1-8(a)**, is 360Hz when the 6-segmentation (RGBRGB, where R denotes red, G green, and B blue) color wheel rotates at 60Hz. Similarly, the field rate of the second one, shown in **Fig. 1-8(b)**, is 480Hz since the 4-segmentation (RWGB, W for white) color wheel rotates at 120Hz. When the field rate increases, the separate color-fringe width of each field is reduced in comparison with the 180Hz-field-rate under the same viewing conditions. The HVS is less sensitive to both high-frequency luminance and chrominance variation [13,14], so the flicker and CBU are suppressed effectively with the increasing field rate.
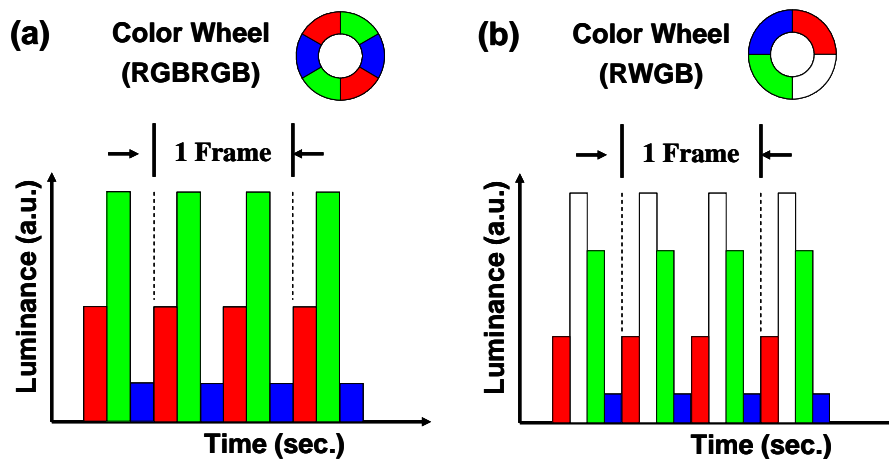
Fig. 1-8 *Two manipulations of field-rate acceleration method: (a) RGBRGB segmentation of color wheel rotating at 60Hz, and (b) RWGB segmentation of color wheel rotating at 120Hz, where W denotes white*

The multi-field driving scheme is the advanced version of the method of field-rate acceleration. More than the three primaries, R, G, and B, are displayed in a frame, such as RYGB, RGBCY, RGBCYM, etc., where Y, C, and M denote yellow, cyan, and magenta, respectively. Although incurring rather complexity of color-managing algorithm, the driving scheme possesses extra advantages in addition to that from the method of field-rate acceleration. Firstly, the color gamut of multi-primary system, in general, is wider than that of three-primary one. Secondly, the luminance is redistributed more uniformly to the multi fields, so helps to alleviate flicker. Finally and the most important of all, the contrast sensitivity between the primaries of separate color fringes is reduced that is useful to suppress CBU.

In summary, those driving schemes introduced in the section are promising for flicker and CBU suppression, and have led the development of FSC LCDs. However, the increment of field number in a frame lessens the time necessary for the row data registration and LC response. Consequently, insufficient time for the system operation results in degradation of display performance, introduced below.

1.4.3.2 Physical Constraints

That slow response of most LC modes obstructs the progress of FSC LCDs has grown into a well-known common consensus. On the contrary, the engineering challenge arisen from the row data registration catches little attention. The influences from these two fundamental features of LCD are clarified here.

Row Data Registration

In the conventional LCDs, each row of LC cells receives equivalent amount of incident light from the constant backlight. The rotation state of LC cells on each row is not changed until the next cycle of data refreshment. Nevertheless, it becomes difficult to synchronize the primary backlight emanation with the row data registration in the FSC LCDs. Data registration, from the first (top) to the last (bottom) rows, spends a field time. The immediate question is when the backlight is turned on. Three occasions of turning backlight on are illustrated in **Fig. 1-9**. **Fig. 1-9(a)** shows that the backlight is switched on according to the first row. That is, the backlight, shown as a translucent red block, is turned on and lasts the hold-time of the first row. It is worth noting that some bottom rows are still in the hold-time with image data of the preceding field. The color light in the present field incident on the LC cells with data of the preceding field incurs enormous stimuli – crosstalk. As the actuation of backlight is based on the middle row, as shown in **Fig. 1-9(b)**, the crosstalk may occur in both the preceding and the succeeding fields. Finally, crosstalk mainly shows up in several top rows of the succeeding field when the backlight is in synchronization with the bottom row, as shown in **Fig. 1-9(c)**.

One way for crosstalk reduction is to shorten the time period of backlight illumination. However, the overall output luminance of the display system may be reduced as well. A feasible solution, multi-division scanning backlight [15,16], is proposed to save as much time as possible for both backlight illumination and LC response. This spatial backlight design and the operation will be introduced in detail in **Chapter 3**.
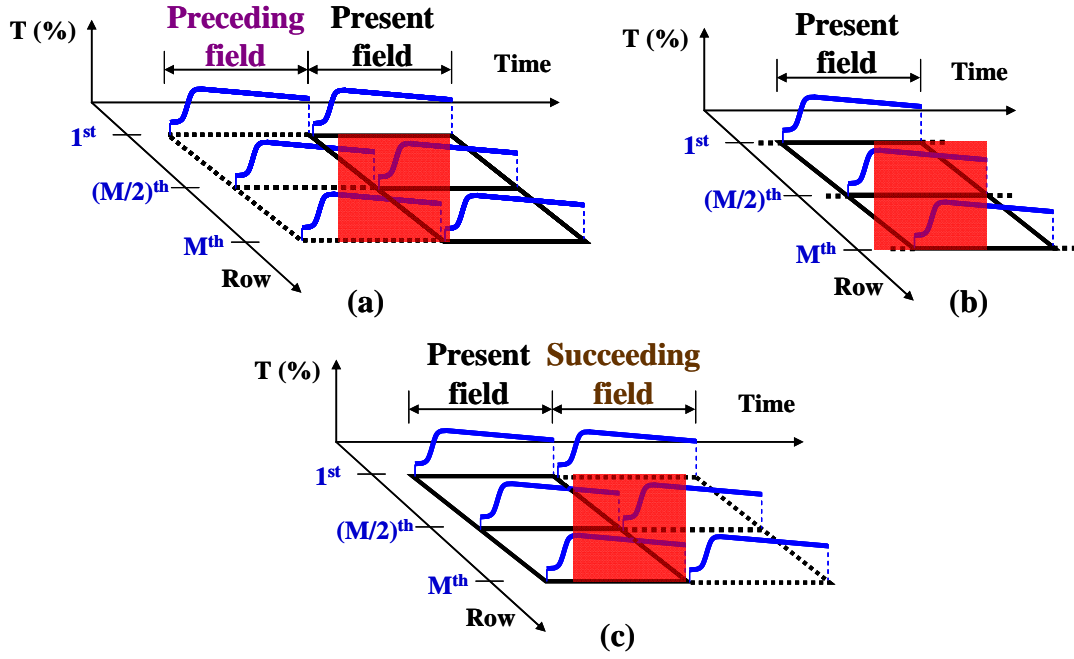
Fig. 1-9 *Backlight illumination during the hold-time of LC cells according to (a) the 1st row (top), (b) the (M/2)th row (middle), and (c) the Mth row (bottom), respectively, which will induce cross-talk with respect to the preceding field, both the preceding and the succeeding fields, and the succeeding field in the corresponding case.*

LC Response Time

Color gamut shrinkage is the serious side effect when the slow-response LC mode is implemented in the multi-field driving scheme. Take a Twisted Nematic (TN) LC mode with response time of more than 16.7ms for example, as shown in **Fig. 1-10(a)** [17]. The polarization state of LC cell is gradually changing during a frame time so the spectral transmittance varies dynamically. Thus, the same incident backlight, equivalently, undergoes different spectral filtering at every small time interval among a frame period, successively. As a result, the integration of output stimuli for a frame time produces a de-saturated optical stimulus, whose colorimetric coordinate moves toward the inner white point. Therefore, the color gamut is shrunk along with the increasing frame (/field) rate, as shown in **Fig. 1-10(b)** [18]. As a result, it has become a guiding rule that the backlight illumination had better await

the LC cells reaching the stable state to prevent from primary de-saturation. This is the very reason why fast-response LC modes are required for the FSC LCDs.

(a)   (b)
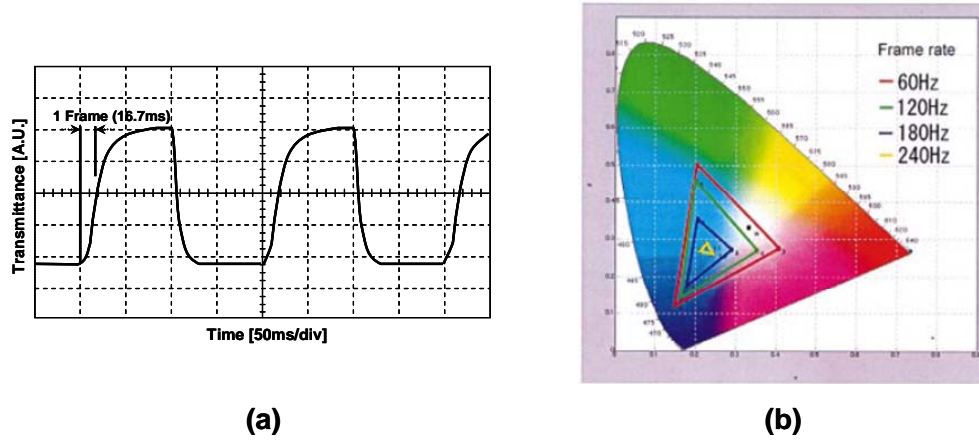
Fig. 1-10 (a) TN LC mode with response time more than 16.7ms to achieve stable sate [17]; (b) color gamut is shrunk along with increasing frame rate as slow-response LC mode is used [18].

As a comparison, it is worth exploring why the multi-filed driving scheme can be applied to 1-chip DLP® projection. First, the timing of the data registration in the light valve, DMD, is different from that in the LCDs. The data registration of the memory array, underneath the micro mirrors, is processed simultaneously while the micro mirrors are latched to certain orientation for reflection. The incident primary light can synchronize the data registration easily without crosstalk and trade-off of illumination intensity, occurring in the FSC LCD. Second, the optical switching time of DMD is of ~2μs [19] so the saturation of primary stimuli and, thus, the color gamut is independent of the field rate, but only the spectral characterization of the color filters on the color wheel.

In summary, crosstalk, trade-off on maximum output intensity, and shrinkage of color gamut, are the three main issues degrading the system performance. Particularly, those issues occur even in the basic three-field FSC LCD, and get more serious when the response of LC mode is not fast enough, say, the response time of

15

4ms~8ms of most current LC modes. Hence, it is recommended that the system performance, i.e. colorimetric characteristics, must first be achieved to be similar to that of the conventional LCDs before starting the suppression of visual artifacts. A two-field driving scheme (referred to **Chapter 4**), the main theme of this thesis, is effective to solve the issues arisen from the physical constraints. Since the spatially-modulated backlight of the high-dynamic-range (HDR) LCD plays a significant role in the proposed method, the concept of the HDR LCD is introduced in the following.

1.5 High-dynamic-range (HDR) LCD

The HDR LCD is prominent for the apparently wider dynamic range of luminance than that of the conventional LCD. Meanwhile, the ability of power-saving of such kind of LCD has received much attention. The brief concept of the HDR LCD is introduced since the spatially-modulated backlight is one of the major components of the proposed configuration of the FSC LCD.

1.5.1 System Configuration

After the HDR LCD was proposed, the luminance range of an LCD system extends remarkably [3,4]. This enhancement is achieved by replacing the traditional full-on, constant backlight with the spatially-modulated one, as shown in **Fig. 1-11**. Radiant energy emanating from the backlight surface can vary spatially, which is regarded as a low spatial resolution image, and then be modulated by the front LC panel to form an image with clear details. The image reproduction on an HDR LCD is based on **Eq. (1-1)**, where L and I denote the incident and the output luminance of an LC pixel, and T the transmittance of that pixel. The suffixes "o" and "r" are acronyms of "original" and "reproduced", respectively. The reproduced

transmittance, T_r, can be derived by **Eq. (1-1)** when the reproduced incident backlight luminance, L_r, is known, and vice versa. It is worth noting that the reproduced output luminance, I_r, is a function of the incident luminance, I_o. If the goal of image reproduction on an HDR LCD is aimed at the exact colorimetric reproduction, I_r is simply set equal to I_o. Otherwise, set the lowest I_r less than the lowest I_o and then re-scale I_r as a function of I_o to widen the dynamic range. High contrast ratio is achieved without increasing the maximum luminance.

$$I_r = f(I_o), \quad \text{where} \quad I_o = L_o \times T_o \quad \text{and} \quad I_r = L_r \times T_r \qquad (1\text{-}1)$$
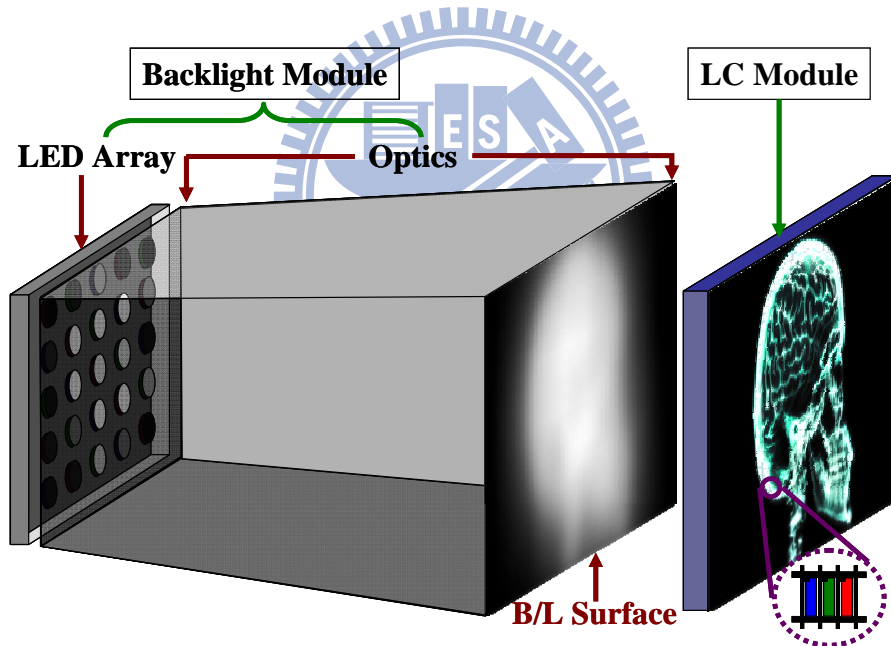
Fig. 1-11 *The configuration of the HDR LCD, which comprises a spatially-modulated backlight with white LEDs and an LC module with color filter [3,4].*

1.5.2 Signal Derivation

An LCD with a spatially-modulated backlight is controlled by both the LED and the LC cell driving signals, which can be derived in either "forward" or "backward"

pathways. The "forward" process determines the LC signals from the backlight information, briefly following the sequence from target luminance, I, obtaining the LED signal, d_{BL}, and then the LC signals, d_{LC}, as shown in the flowchart **Fig. 1-12**. Shortly speaking, the process follows the procedure: step 1 first, then step 3, and finally step 6. On the contrary, the "backward" process determines the LED signals based on known LC signals, that is, changing the sequence of deriving d_{LC} and d_{BL} in the "forward" process [20]. That is the order: step 1 first, then step 6, and finally step 3. It is worth noting that I, d_{LC}, and d_{BL} must be threefold for three-primary color mixing. In addition, I, as shown in **Fig. 1-12**, must be adjusted according to **Eq. (1-1)** to be I_r before running the signal processing flow. Both pathways are of equal importance and applied to the proposed two-field driving scheme.

I : output (/target) luminance of single pixel (normalized)
d_{BL} : LED driving signal
d_{LC} : LCM driving signal
L : incident backlight luminance onto single pixel
p : light spread function
T : transmittance of single pixel

r_1 : transfer function of LED
r_2 : transfer function of LCM
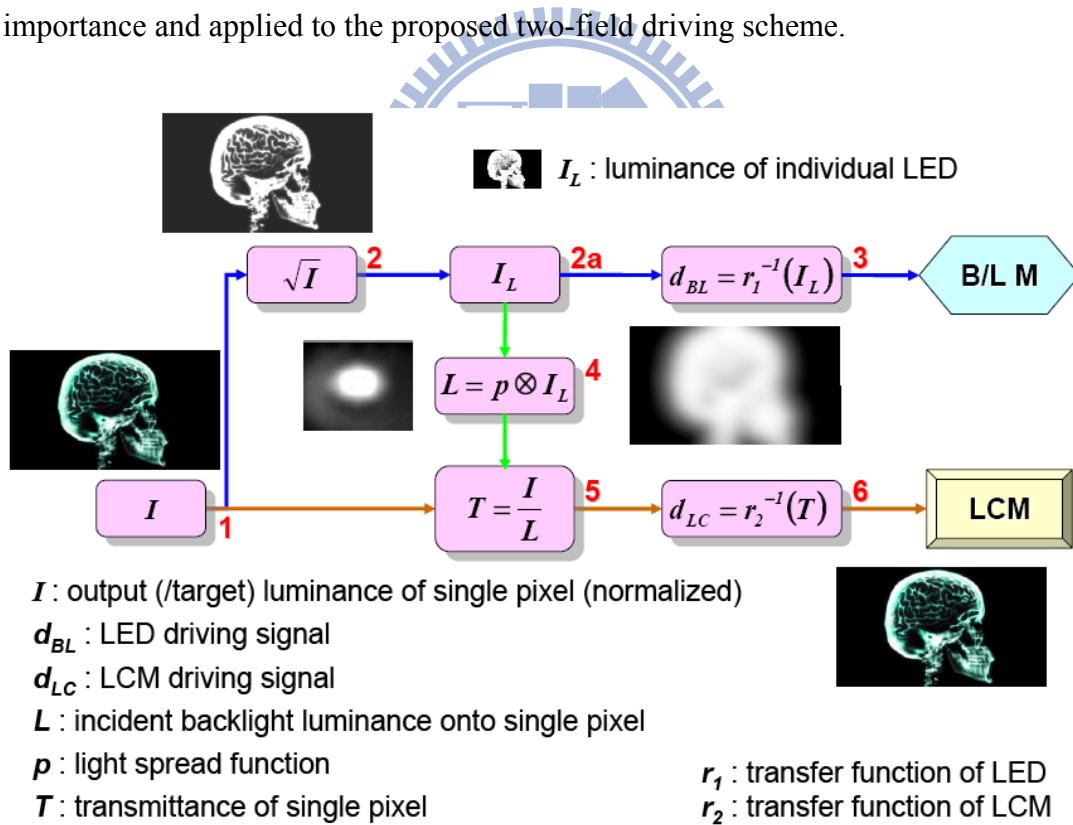
Fig. 1-12 *Flowchart of deriving driving signals for backlight module (B/L M) and LC module (LCM) [3,4]*

1.5.3 Issues

Backlight luminance distribution, L, at step 4 is the critical connection between d_{BL} and d_{LC}. In the "forward" pathway, L is obtained by linear superposition, **Eq. (1-2)**, in which $I_L(n)$ denotes the intensity of nth LED and $p(x, y; n)$ the light spread function (LSF) of the nth LED corresponding to LC pixel at position (x, y). As for the "backward" one, the estimated LED intensity, $\hat{I}_L$, is acquired by pseudoinverse computation, **Eq. (1-3)**, where $\hat{I}_L$, $\hat{L}$, and $\hat{p}$ are the equivalent matrix forms of I_L, L, and p after moderate rearrangement.

$$L(x, y) = \sum_n p(x, y; n) \cdot I_L(n) \qquad (1\text{-}2)$$

$$\hat{I}_L = \left(\hat{p}^T \cdot \hat{p} \right)^{-1} \cdot \hat{p}^T \cdot \hat{L} \qquad (1\text{-}3)$$

The accuracy of L strongly affects the colorimetric performance of images displayed on an LCD with a spatially-modulated backlight. In the "forward" process, L is, in fact, seldom obtained using **Eq. (1-2)** because of the computation loading and the considerable cost of memory if all the numbers of LSF of each LED is stored. That is, LSF of each LED generally varies at different position due to the interaction, e.g. reflection, with boundary walls of the backlight module. Hence, a great amount of LSF must be recorded faithfully if **Eq. (1-2)** is applied. Instead, convolution computation is used in practical situations [4]. However, the necessary condition, spatial shift invariance, for applying convolution is always violated in real cases, which result in inaccurate L leading to inaccurate compensation of LC cells. The influences of incorrect estimation of L on colorimetric performance are discussed in **Chapter 2**; a solution, special optical design of backlight unit, to this and the other issues is proposed in **Chapter 3**.

1.6 Motivation and Objective

The motivation is aroused by the issues from applying the multi-field driving scheme to the FSC LCD. The multi-field driving scheme, based on reduction of color fringe width, has been verified to effectively suppress visual artifacts in projection displays. In fact, this solution has become the guiding rule in developing the FSC LCD. Nevertheless, when the multi-field method is applied, time duration of single filed grows into the critical design parameter. If being with insufficient field time, the physical constraints of LCDs will lead to deteriorated system performance: field crosstalk, reduction of output intensity, and shrinkage of color gamut. Comparatively, an FSC LCD without those colorimetric issues must be of higher priority than that without the visual artifacts, CBU and flicker, at the opening of evolving the FSC LCD. Thus, a novel two-field driving scheme, contrary to the multi-field fashion, is proposed since it can increase the filed time that is beneficial for improving backlight intensity and maintaining color gamut.

The objective of this research is threefold. The first is to work out a framework of the FSC LCD running at two fields per frame. The goal falls on a feasible **algorithm** for the two-field driving scheme. An apparent difficulty immediately occurs at how three-primary information can be conveyed faithfully via two fields. For that matter, a spatially-modulated color backlight is incorporated since such system possesses three spatial degrees of freedom, which can compensate for the lack of the third degree of freedom in time domain. However, issues on colorimetric reproduction and operation efficiency are observed when an LCD adopts such kind of backlight. A **color model** and a specific **optical design** of the backlight together compose the second objective. Thirdly, a **metric** for CBU evaluation based on the HVS is proposed and CBU suppression of the two-field method is compared with others.

1.7 Organization of Dissertation

This dissertation is divided into six chapters. The context is schematically illustrated by **Fig. 1-13**. **Chapter 1** goes through the brief introduction to the FSC LCD and the HDR LCD, followed by challenge issues. Besides, motivation and organization have also provided. **Chapter 2** explains the development of a specific color model necessary for an LCD system with a spatially-modulated backlight module. **Chapter 3** presents a novel concept of super-Gaussian LSF particularly adequate for the system with a spatially-modulated backlight module. A special optical design of light guide unit to realize the desired LSF is also described. **Chapter 4** elaborates the manipulations to fulfill an LCD operated by the two-field driving scheme. The suppression of CBU based on reduction of contrast sensitivity is disclosed. **Chapter 5** introduces a useful index for CBU quantification based on the human visual system. The applications of the index are given. **Chapter 6** gives the conclusions and future works.
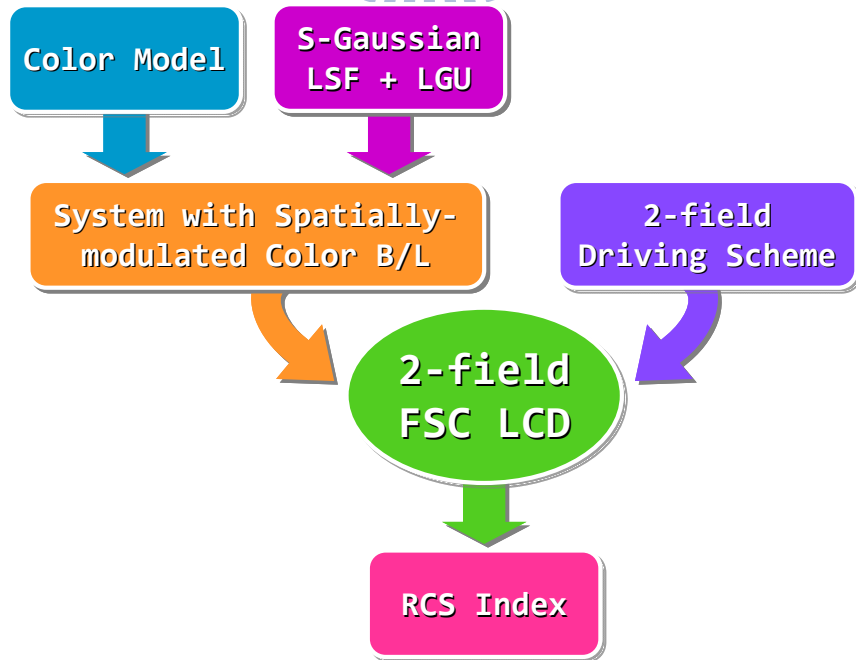
Fig. 1-13 *Organization of the research topics of this thesis*

Chapter 2

Colorimetric Characterization

2.1 Introduction

The colorimetric characterization of a display medium is the very fundamental profile for color reproduction across multi-media. The standard process flow of color reproduction is schematically summarized in **Fig. 2-1**. The "profile" is the device model that correlates the input signals from the device-dependent color space with tri-stimulus values in the device-independent color space, such as CIE XYZ or CIE LAB. If the ambient conditions are regarded, color appearance model (CAM), e.g. CIECAM02 [21], must be applied to transform those device-independent tri-stimulus values into perceptual attributes, e.g. lightness, chroma, and hue, denoted as J, C, and h, respectively. Since the viewing conditions and the device characteristics are rarely identical in practice, gamut mapping is indispensible between the source and the destination situations. After achieving the reproduced perceptual attributes, the color transformation is executed in inverse sequence from reversing the CAM to obtain the corresponding device-independent tri-stimulus values and then the profile to deduce driving signals for the destination devices. Theoretically, the reproduced perception in the destination situation is assumed to be similar to that of the original one. First of all, the color model or profile derived by colorimetric characterization bases the entire process and even other applications of color manipulations, such as white balance.
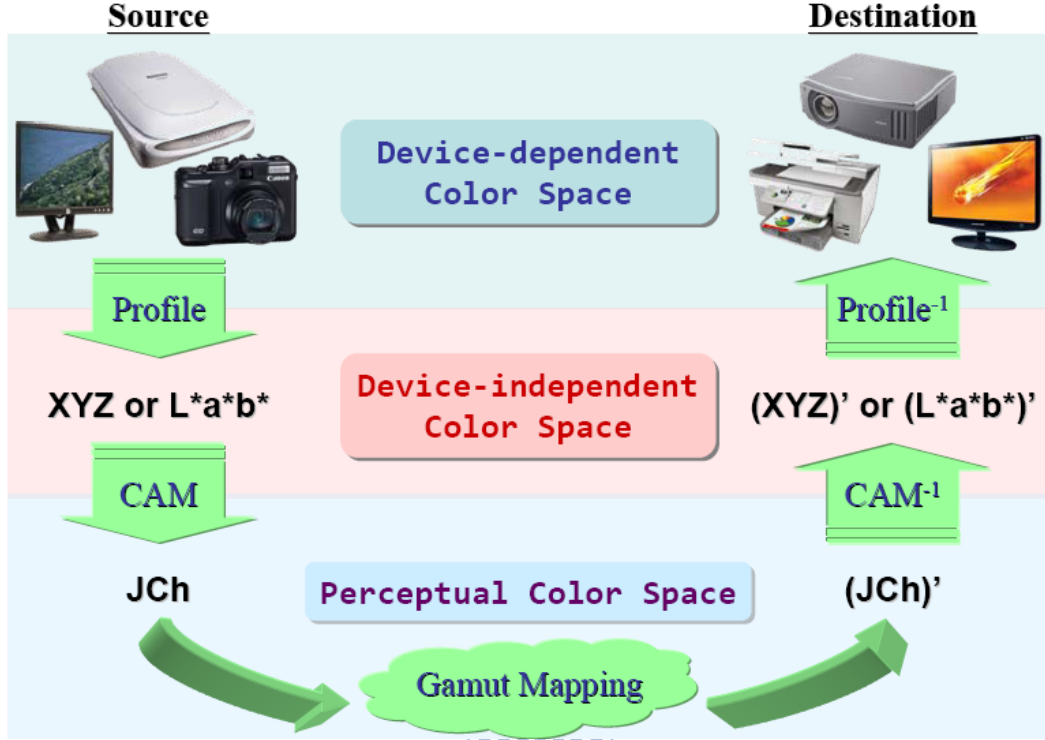
Fig. 2-1 *Standard process flow of color reproduction*

In contrast with the advanced progress on system implementation, the exploration of colorimetric properties of the HDR LCD gets only rare attention [22,23,24]. Currently, **Eq. (2-1)** is assumed to be the ideal color model for the HDR LCD, where ***I***, ***L***, and ***γ*** denote output luminance, backlight luminance distribution, and non-linear behavior between input digit, ***d***, and the resultant ***I***, respectively. ***N*** in the term, 2^N-1, denotes the bit-depth of the signal format of a display medium. If not explicitly declared, bit-depth 8 is usually the value. Besides, **Eq. (2-2)** is the transfer equation being commonly used [25].

$$I = L\left(\frac{d}{2^N - 1}\right)^\gamma \qquad (2\text{-}1)$$

$$I_r = I_o \;\Rightarrow\; d_r = \left(\frac{L_o}{L_r}\right)^{1/\gamma} \times d_o \qquad (2\text{-}2)$$

The issues from the model expressed by **Eq. (2-1)** are obviously twofold, though. First, the leakage light of an LCD at dark level is not accounted for. Second, the non-linearity of the opto-electronic transfer function (OETF) is not precisely an exponential one. A pair of chromatic diagrams of three primaries, shown in **Fig. 2-2**, measured on two images displayed on an LCD system with a spatially-modulated backlight. The mosaic image contains patches with all the twelve sets of input digits of those in the red, green, and blue color-ramp images. The result reveals important information that such an LCD system possesses one-to-many color mapping. Namely, for a set of input digits, $(d_r\ d_g\ d_b)$, it may correspond to more than one set of colorimetric tri-stimulus values. Actually, this is the third property by which cannot be provided by **Eq. (2-1)**. More details about the measurement and color difference calculation will be described in **Sections 2.3** and **2.4**. Therefore, an adequate color model is an inevitable requirement when this type of LCD is being in vogue.
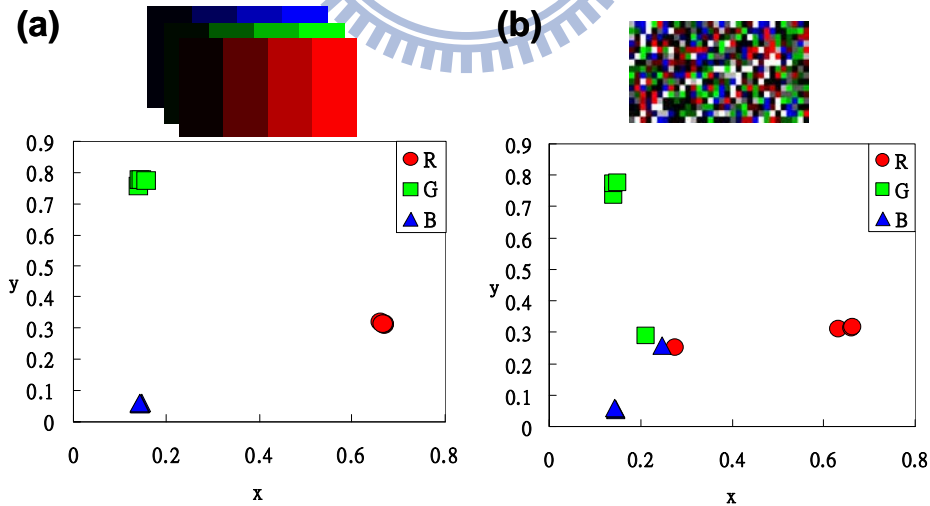
Fig. 2-2 *Chromatic diagrams of three primaries measured on (a) color-ramp images and (b) a mosaic image, displayed on an LCD with a spatially-modulated backlight*

2.2 Color-modeling Principle: Two-stage Approach

An effective principle for colorimetric characterization is called two-stage approach [26]. The first stage accounts for the non-linear behavior between the input digits and the radio-metric scalars, simply expressed by an OETF. The OETF can be an analytic physical model of the display device, e.g. CRT [27,28], or a recorded look-up table (LUT), which is suitable for an LCD and will be introduced in the next section. The second stage successively transforms the radio-metric scalars into the resultant tri-stimulus values by linear algebraic matrix. Because of the similarity of system construction, current task is appropriate to refer to the prior colorimetric characterization of the conventional LCD.

2.2.1 Conventional LCD

If a conventional LCD possesses channel scalability and independence, the model, expressed by **Eqs. (2-3)** and **(2-4)** [29], can achieve acceptable accuracy of predicting device-independent colors. Based on the two-stage approach, the process of characterizing a conventional LCD is illustrated by **Fig. 2-3**. Three one-dimensional look-up tables (LUTs) of the radio-metric scalars are built first, accounting for the OETF of LC cells as a function of input digits of each channel. Those radio-metric scalars, denoted by R, G, and B in **Eq. (2-3)**, range from zero to unity, where d_r, d_g, and d_b are input digits of red, green, and blue channel, respectively. The linear conversion between radio-metric scalars and resultant tri-stimulus values, are then constructed, as shown in **Eq. (2-4)**. $[X_{i,max} \ Y_{i,max} \ Z_{i,max}]^T$ are the maximal tri-stimulus values of channel i, which denotes r, g, and b for the corresponding three primaries. The tri-stimulus values of "flare" term, $[X_k \ Y_k \ Z_k]^T$,

accounts for the non-zero radiance at black level [27,28]. Flare term should be treated carefully in modeling an LCD because it is mainly responsible for the instable primaries [30].

$$R = LUT(d_r)$$
$$G = LUT(d_g)$$
$$B = LUT(d_b)$$
$$0 \le R, G, B \le 1$$

$$\begin{bmatrix} X \\ Y \\ Z \end{bmatrix} = \begin{bmatrix} X_{r,\max} - X_k & X_{g,\max} - X_k & X_{b,\max} - X_k \\ Y_{r,\max} - Y_k & Y_{g,\max} - Y_k & Y_{b,\max} - Y_k \\ Z_{r,\max} - Z_k & Z_{g,\max} - Z_k & Z_{b,\max} - Z_k \end{bmatrix} \begin{bmatrix} R \\ G \\ B \end{bmatrix} + \begin{bmatrix} X_k \\ Y_k \\ Z_k \end{bmatrix}$$

(2-3)

(2-4)
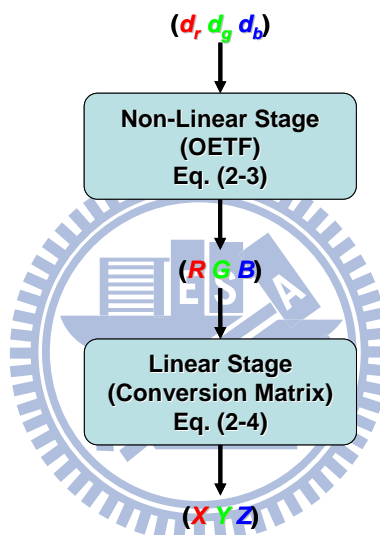
Fig. 2-3 *Color model of a conventional LCD following the two-stage approach*

If channel scalability and independence, on the contrary, are violated, complex models should be considered [31,32,33]. An effective methodology is to statistically improve the model performance [30], in spite of the aforementioned issues and the measurement uncertainty of equipment. In summary, this methodology is based on **Eqs. (2-3)** and **(2-4)**, and performs non-linear optimization to minimize the mean CIEDE2000 color difference, calculated by the CIE (Commission Internationale de L'Eclairage) 2000 color difference formula [34], of test colors sampling the display's gamut. Three one-dimensional LUTs in **Eq. (2-3)** and all the tri-stimulus parameters in **Eq. (2-4)** are dynamically adjusted in every iterative process.

In summary, the model expressed by **Eqs. (2-3)** and **(2-4)** can moderately represent the two properties, non-ideal exponential behavior of OETF and non-zero radiance at black level, to which the simple model, **Eq. (2-1)**, is inapplicable. Nevertheless, one set of input digits into **Eqs. (2-3)** and **(2-4)** can merely obtain a unique set of output tri-stimulus values, that is, one-to-one mapping. One-to-many mapping phenomenon observed in the LCD with a spatially-modulated backlight remains an issue to be solved.

2.2.2 LCD with a Spatially-modulated Backlight

The colorimetric characterization is performed on the system primarily consists of an LC module with CF and a spatially-modulated backlight with white LEDs, as shown in **Fig. 1-11**. Obviously, the color model of the conventional LCD, as shown in **Fig. 2-3**, cannot form the one-to-many mapping relationship observed in an LCD with a spatially-modulated backlight. It is presumed that the corresponding LED and LC driving signals should play significant roles in the process of colorimetric characterization. The signal derivation of the target system needs to be discussed in detail instead of the brief introduction given in **Section 1.5.2**, in which merely the "forward" and the "backward" processes are defined.

Signal Derivation Revisited

The process of deriving LED and LC driving signals has been illustrated in the flowchart, as shown in **Fig. 1-12** [4]. I is the normalized luminance of each pixel and the square root of I is to increase the normalized luminance value of each pixel. I_L is the luminance value of each LED. Since the number of LED is less than that of LC pixels, step 2 to step 2a is treated as a down-sampling procedure. After inversely converting I_L by LED response function r_I, step 3, the driving signals, d_{BL}, of each

LED are deduced. Step 4 is the convolution of I_L and p_1, the LSF of single LED, to obtain the normalized backlight luminance, L. The outcome of the target value divided by the convolution result, step 5, denotes the transmittance, T, of each LC pixel. Accordingly, the driving signals of each LC pixel, d_{LC}, are obtained after inversely transforming the transmittance by the LC response function, r_2, at step 6. Particularly, this process is performed three times for the three primary channels. The final outcomes are LED driving signal, d_{BL}, and the set of LC driving signals, ($d_{LC,r}$ $d_{LC,g}$ $d_{LC,b}$), which are then re-symbolized by (d_r' d_g' d_b'), for short.

Proposed Color Model

As for the one-to-many mapping behavior, a hypothesis is made that the flare term in **Eq. (2-4)** is no longer constant, neither the other matrix parameters. Thus, the normalized backlight luminance L is suggested to be incorporated into **Eqs. (2-3)** and **(2-4)** that are then modified into **Eqs. (2-5)** and **(2-6),** accordingly. If linearity is hold between the backlight luminance and the maximal tri-stimulus values of each channel, **Eq. (2-6)** can be further simplified in the form of **Eq. (2-7)**. As a result, the proposed model for current system configuration is composed of signal derivation for d_{BL} and (d_r' d_g' d_b'), and **Eqs. (2-5)** and **(2-7)**, finally.

$$
\begin{aligned}
R &= LUT(d_r') \\
G &= LUT(d_g') \\
B &= LUT(d_b') \\
0 &\le R, G, B \le 1 \\
0 &\le L \le 1
\end{aligned}
\tag{2-5}
$$

$$
\begin{bmatrix} X \\ Y \\ Z \end{bmatrix} = \begin{bmatrix} X_{r,\max}(L) - X_k(L) & X_{g,\max}(L) - X_k(L) & X_{b,\max}(L) - X_k(L) \\ Y_{r,\max}(L) - Y_k(L) & Y_{g,\max}(L) - Y_k(L) & Y_{b,\max}(L) - Y_k(L) \\ Z_{r,\max}(L) - Z_k(L) & Z_{g,\max}(L) - Z_k(L) & Z_{b,\max}(L) - Z_k(L) \end{bmatrix} \begin{bmatrix} R \\ G \\ B \end{bmatrix} + \begin{bmatrix} X_k(L) \\ Y_k(L) \\ Z_k(L) \end{bmatrix}
\tag{2-6}
$$

$$
\begin{bmatrix} X \\ Y \\ Z \end{bmatrix} = \begin{bmatrix} X_{r,\max} - X_k & X_{g,\max} - X_k & X_{b,\max} - X_k \\ Y_{r,\max} - Y_k & Y_{g,\max} - Y_k & Y_{b,\max} - Y_k \\ Z_{r,\max} - Z_k & Z_{g,\max} - Z_k & Z_{b,\max} - Z_k \end{bmatrix} \begin{bmatrix} R \\ G \\ B \end{bmatrix} L + \begin{bmatrix} X_k \\ Y_k \\ Z_k \end{bmatrix} L
\tag{2-7}
$$

In comparison, the proposed color model, different from that of the conventional LCD, requires a pre-process for the system driving signals, as shown in **Fig. 2-4**. Those sets of extra information explain well why the one-to-many mapping occurs in current system configuration. That is, a set of input digits can derive interim information of backlight intensity and compensated LC signals, which result in diverse output tri-stimulus values. It is worth noting that if the same LC module is implemented in the two types of LCD, the LUTs are identical because the transmittance of the LC cells is independent of the backlight luminance.
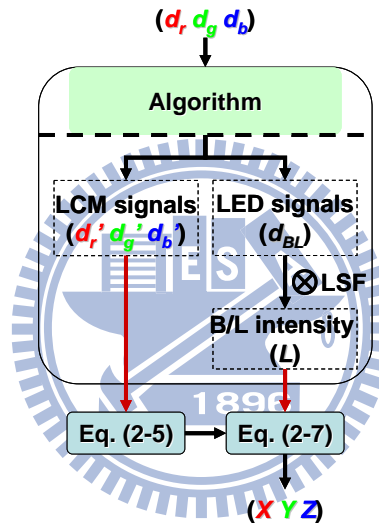
Fig. 2-4 *Color model of an LCD with a spatially-modulated backlight*

2.3 Experiment

The chromaticity property of an LCD with a spatially-modulated backlight is explored first by examining the primary stability under different illumination distributions of backlight. Then, the accuracy of the proposed model, expressed by **Eqs. (2-5)** and **(2-7)**, is evaluated by color difference between the predicted and the measured colorimetric values. Comparison will be made between the proposed model and the model dedicated for the conventional LCD, expressed by **Eqs. (2-3)**

and **(2-4)**, so as to verify the necessity of the proposed model. The measurement is done by means of the spectro-radiometer SR-UL1R [35], under the setup of 2° measuring angle, at which working luminance range is $0.005 \sim 3,000 \text{cd/m}^2$.

A.   Testing Platform

An LCD system with a spatially-modulated backlight is constructed as the testing platform. 8-by-8 groups of three-in-one LED are implemented as light source for the 37" LCD of resolution 1920-by-1080 pixels. Each LED group contains 18 LEDs. Those LEDs work as white light source by controlling the embedded red, green, and blue LEDs in synchronization, although they can be operated independently. The maximum luminance of the system is about 507cd/m^2, and the minimum could be of less than 0.05cd/m^2. The contrast ratio, thus, was of greater than 10,000:1. This system can function as both the conventional LCD and the LCD with area-adaptive backlight distribution by turning all LEDs full-on and by adjusting LEDs dynamically, respectively.
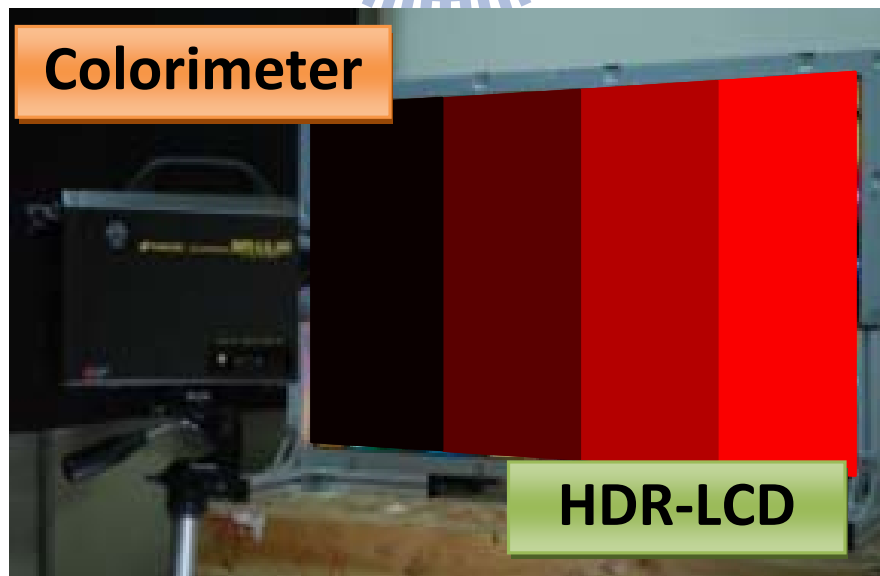
Fig. 2-5 *Experiment setup*

B. Preliminary Measurement

The three one-dimensional LUTs are important in both modes of operation. In assumption, LUTs only characterize the OETF of the LC cells and are not associated with the backlight luminance. Therefore, the LUTs can be created following the same procedures as that in the conventional LCD. First, all the LEDs in the backlight module are turned full-on, like the case of the conventional LCD. Second, input digits of eleven equal steps, from 0 to 255 for eight-bit signal depth, are the input signals for each primary, respectively. Finally, optimization of least-square-error of colorimetric difference is performed iteratively to obtain the LUTs in **Eq. (2-3)** and the parameters in **Eq. (2-4)**. In addition, the channel scalability and independence are also verified.

C. Testing Images

According to the one-to-many mapping relationship, the resultant tri-stimulus values of a set of digit counts are expected to vary with image content. The backlight distribution is postulated to be the key factor affecting the final tri-stimulus values. The color-ramp and mosaic images, as shown in **Fig. 2-6**, are thus designed to evaluate the proposed model and that for the conventional LCD since two different, regular and random, manners of backlight profiles are induced, which are beneficial to clarify the effect of backlight distribution.

(a)   (b)
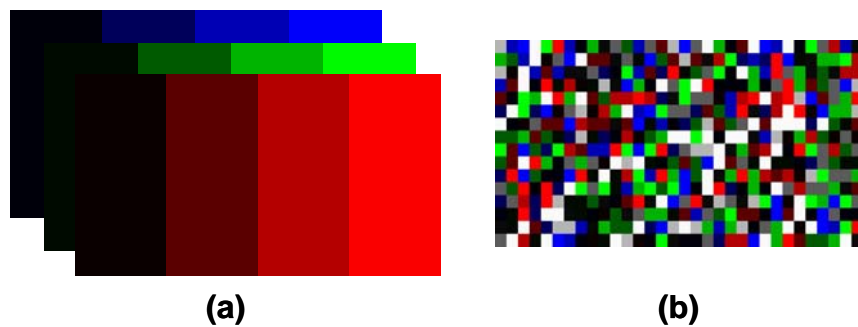
Fig. 2-6 *(a) color-ramp and (b) mosaic images are designed as the test images*

The digit counts of uniform patches in the red ramp image, as shown in **Fig. 2-6(a)** for example, are set as (10 0 0), (90 0 0), (180 0 0), and (250 0 0) from left to right. Those digits are chosen because they cover the range from low to high luminance levels. Green and blue ramp images are in the same fashion, except for inter-changing the order of primary channel. The colorimetric data are measured at the center of each uniform patch. The mosaic image consisted of 32-by-16 rectangular patches, as shown in **Fig. 2-6(b)**, including all the sets of digit counts in the color-ramp images. Moreover, more than one color patches can be of the same set of digit counts at random position in the image. The tri-stimulus values are measured on twelve color patches chosen arbitrarily and corresponding to each color ramp. Some achromatic (white, gray, and black) patches are also added in the image in order to extend the spatial luminance variation of backlight distribution.

2.4 Result and Discussion

The first observation is exactly the one-to-many mapping, which initiates this study and has been introduced by the measured chromaticity, as shown in **Fig. 2-2**. A postulation that backlight distribution induces the diversity of resultant tri-stimulus values has been made to build up the proposed color model. Here gives the qualitative insight into this phenomenon by means of the designed images.

Based on colorimetry, the chromaticity coordinate, (x y), is calculated by **Eq. (2-8)**. In combination with **Eqs. (2-6)**, **(2-7)** and **(2-8)**, the chromaticity diagrams, shown in **Fig. 2-2**, can be reasonably correlated with the percentage of the term $L^*[X_k\,Y_k\,Z_k]^T$ in the resultant $[X\,Y\,Z]^T$. Briefly speaking, if the percentage increases, the chromaticity coordinate moves closer to the central position, and vice versa. Take the red-ramp image for example. The radio-metric scalars are both zeros. The resultant tri-stimulus values can be obtained by **Eq. (2-9)**. Since R and L tend to vary

in the same manner from left to right, as observed in **Fig. 2-6(a)** and **Fig. 2-7(a)**, the percentage of the term $[X\ Y\ Z]^T$ changes little. Therefore, the chromaticity of red primary is almost the same, so are the other two channels. On the contrary, the backlight distribution of the mosaic image varies randomly, as shown in **Fig. 2-7(b)**. The chromaticity diagram shown in **Fig. 2-2(b)** is just the result of an arbitrarily-chosen set of twelve color patches. If another set of twelve color patches are measured at different position, the chromaticity diagram may change as well if the percentage of the term $[X\ Y\ Z]^T$ of each selected color patch is different.

$$\begin{cases} x = \dfrac{X}{X+Y+Z} \\ y = \dfrac{Y}{X+Y+Z} \end{cases} \tag{2-8}$$

$$\begin{bmatrix} X \\ Y \\ Z \end{bmatrix} = \begin{bmatrix} X_{r,\max} - X_k \\ Y_{r,\max} - Y_k \\ Z_{r,\max} - Z_k \end{bmatrix} RL + \begin{bmatrix} X_k \\ Y_k \\ Z_k \end{bmatrix} L \tag{2-9}$$

(a)   (b)
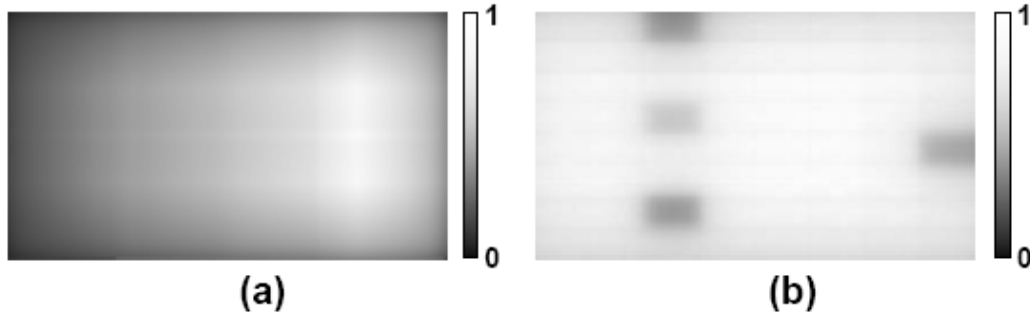
Fig. 2-7 *Two backlight distributions, corresponding to (a) color-ramp and (b) mosaic images, respectively*

The second test is aimed at examining the effectiveness of the proposed model and that for the conventional LCD. CIEDE2000 color difference, as shown in **Fig. 2-8**, between the measured colorimetric tri-stimulus values and the ones predicted by the two models, respectively, are calculated as the index. Cross comparisons are made between the two models with data retrieved from the two designed images.
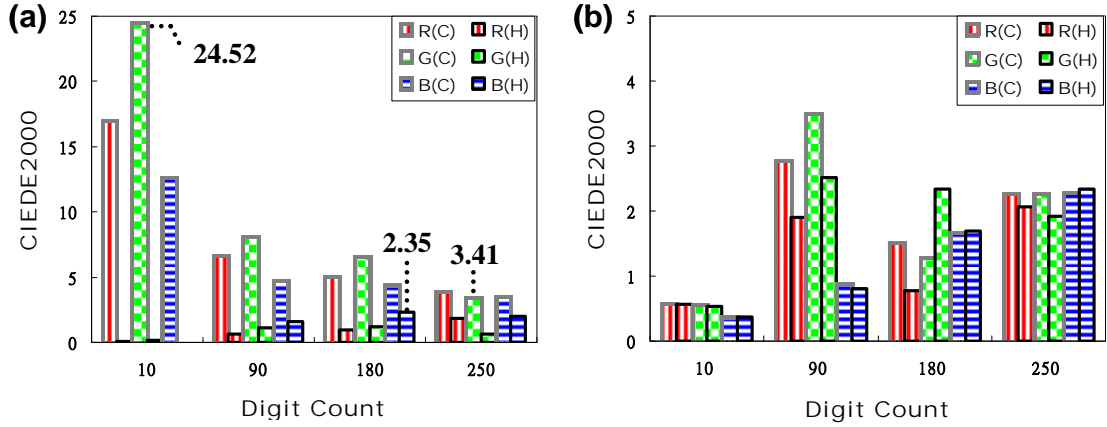
Fig. 2-8 *CIEDE2000 color, with respect to the proposed model (trips enclosed by solid boundary) and to the model for the conventional LCD (trips enclosed by dashed boundary), is computed with data retrieved from (a) the color-ramp and (b) the mosaic images. L in the computation is obtained by convolution.*

For the color-ramp image, the average CIEDE2000 values calculated from the conventional model are well-above 3.41 and up to 24.52 at the patch (0 10 0), as shown in **Fig. 2-8(a)**. Meanwhile, those from the proposed model are well-below 2.35. Large color differences occur at patches including digit 10, because large luminance errors are introduced by the conventional model by means of **Eq. (2-4)**, where the matrices parameters are constant that cannot reflect backlight variation. As for the mosaic image, the difference of the CIEDE2000 values between the two models became unnoticeable statistically, as shown in **Fig. 2-8(b)**. This result may be due to the fact that the backlight distribution of the mosaic image gets closer to that of the full-on backlighting, to which the conventional model is applied.

The proposed model is more suitable for the LCD with a spatially-modulated backlight than that for the conventional LCD, based the results shown in **Fig. 2-8**. However, a color model achieves color prediction to current degree of accuracy, say, with error tolerance greater than CIEDE2000 value of 1.0 is inapplicable in view of colorimetry. The backlight distribution L, currently obtained by convolution, may be the cause. For verification, color difference is re-computed with measured L.
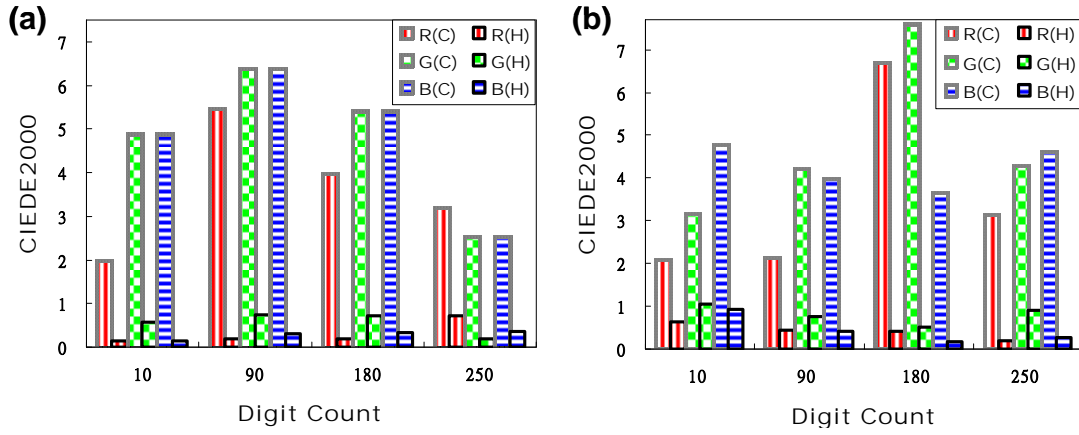
Fig. 2-9 *CIEDE2000 color, with respect to the proposed model (trips enclosed by solid boundary) and to the model for the conventional LCD (trips enclosed by dashed boundary), is computed with data retrieved from (a) the color-ramp and (b) the mosaic images. L in the computation is obtained by measurement.*

Overall speaking, reduced color differences are obtained when the measured backlight intensity L is used in the computation. The CIEDE2000 values, arising from the proposed model, are all less than or around 1, as shown in **Fig. 2-9**, for both the color-ramp images and the mosaic image. However, the CIEDE2000 values, resulting from the conventional model, are well-above 2, which is still inapplicable to color reproduction. Although the reduction of CIEDE2000 values are also observed in comparison with the results shown in **Fig. 2-8**, it is just due to the selection of another set of twelve measurement positions. In summary, the proposed model is applicable to the HDR LCD. Besides, the accuracy of backlight distribution remains a challenging engineering issue of the LCD with a spatially-modulated backlight [36,37].

It is worth noting that CIEDE2000 formula is preferred to evaluate colorimetric difference since more databases and corrections have been involved in the development. The CIEDE2000 value is much closer to subjective difference than the other prior color difference formulae. As the latest version of color difference metric, CIEDE2000 is therefore recommended by CIE for industrial applications.

2.5 Conclusion

This study clarifies the specific colorimetric property of one-to-many mapping of the LCD with a spatially-modulated backlight. This characteristic cannot be explained consistently by any existing color models. After investigation, the parameter, backlight distribution L, is identified to be the critical factor leading to such colorimetric behavior. Consequently, a proposed color model, implementing L as a crucial parameter, has been developed and verified to be of CIEDE2000 value around or less than 1 in color reproduction accuracy. The result strongly recommend that the widely-applied method nowadays, introduced in **Section 2.1**, must be replaced by the proposed color model in order to convey precise color information.

The model performance can be further enhanced by some strategies. A feasible solution, for instance, is to apply non-linear optimization onto the model equations to achieve results with least-square errors. However, the radical consideration must fall on how to improve the accuracy of backlight distribution L, which is certified to dramatically affect the model performance from the experiment outcome. This challenging issue will be worked out by a special optical design of light guide unit (LGU), as being elaborated in **Chapter 3**.

Chapter 3

Super-Gaussian LSF with Light Guide Unit

3.1 Introduction

The construction of an LCD with a spatially-modulated backlight gradually becomes a well-known craft, yet the colorimetric performance and manipulation efficiency remain to be improved. For example, unacceptable colorimetric reproduction error, arising from inaccurately estimated backlight distribution L discussed in **Chapter 2**, has not received sufficient attention. Although many efforts are made to facilitate such system [20,38,39], the development will be incomplete without pondering the impacts of L, or, more precisely, the effects of light spread function (LSF). Thus, it is the opportune moment to make in-depth analyses of the influences of LSF and the related issues.

3.1.1 Free-spreading LSF

The free-spreading or, specifically, Gaussian-shaped LSF has been regarded tacitly as the primitive light profile ever since the HDR LCD is proposed [3,4]. This customary law is formed because the Gaussian LSF, as shown in **Fig. 3-1**, is of compact mathematic expression and is, thus, convenient to derive L by convolution computation, at step 4 as shown in the flowchart **Fig. 1-12**. Nevertheless, a necessary condition, spatial shift-invariance, for the convolution computation is always violated in practical systems; that is, the LSF varies with the LED position, as exemplified in **Fig. 3-2**. The measured light distribution profiles, associated with three groups of LEDs (white highlight) as an example, are apparently non-identical

at bottom corner, center, and bottom edge of the backlight module, respectively. Analytically, the variation of LSF profile, dependent on relative position, mainly arises from the reflection of LED light energy from the edges of backlight module. Those spatially shift-variant LSFs lead to the inconsistency between the measured L and that by convolution computation, discussed in **Section 2.4**. In summary, the very first issue, color reproduction error, commonly exists and affects the colorimetric performance if without the improvement in accuracy of the estimated L.
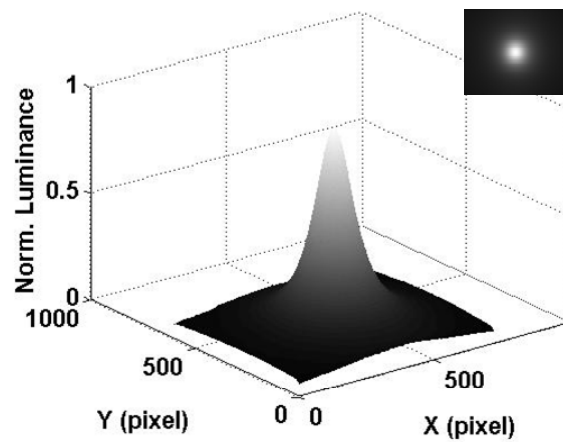
Fig. 3-1 *A two-dimensional Gaussian profile is most frequently-applied LSF in the HDR LCD or, say, an LCD with a spatially-modulated backlight*
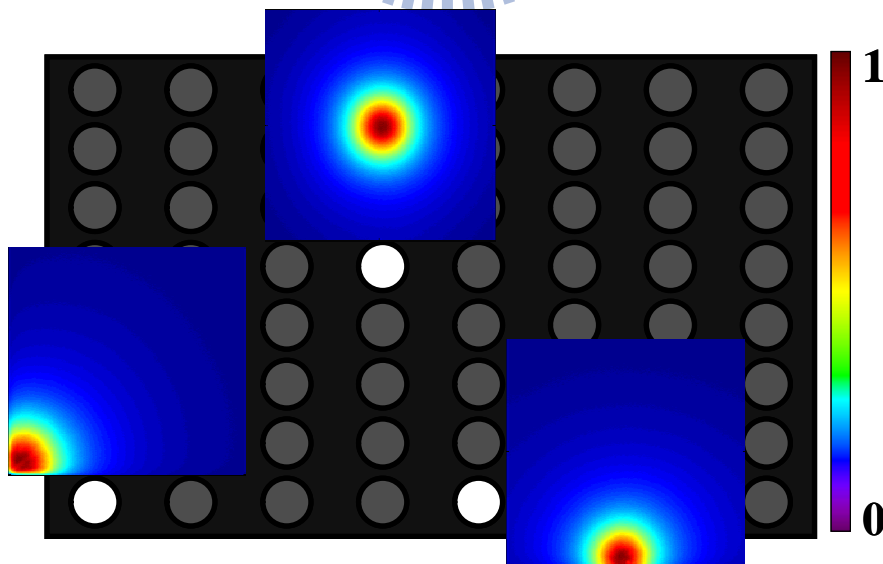
Fig. 3-2 *Spatially shift-variant LSFs always exist in a spatially-modulated backlight. Three groups of LEDs are located at bottom corner, center, and bottom edge, respectively, with the associated non-identical light profiles.*

The overall backlight uniformity is in general not as uniform as the conventional full-on backlight, which is treated as an entirety so the optomechanical layout can be optimized. An example *L*, as shown in **Fig. 3-3**, is synthesized by means of the Gaussian LSF shown in **Fig. 3-1** when all the LEDs are turned full-on. The resultant backlight intensity decreases from center to edges of the backlight module, in accordance with reducing number of LEDs that can contribute to energy overlap. Thus, for images with high brightness contents, like full white image, the intensity is on the decrease in outward direction, similar to the top-view inset in **Fig. 3-3**. The intensity variance is capable of being leveled off by lowering down the intensity around the central area by the front LC panel. However, the cost will be the energy waste and the overall luminance reduction of the whole system. This tradeoff turns into the second issue of free-spreading LSF.
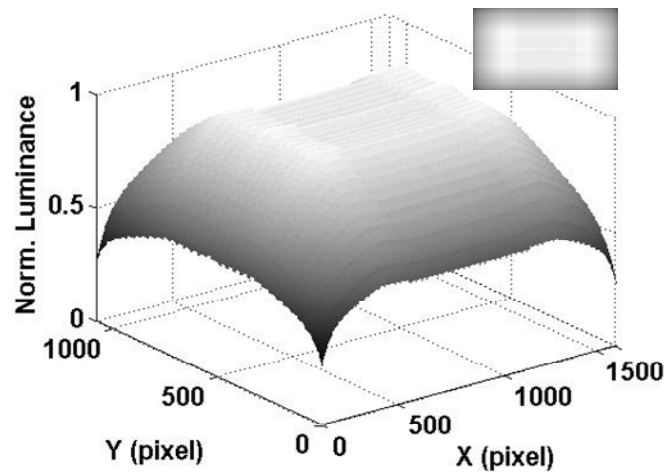
Fig. 3-3 *Overall backlight distribution L, resulted form all full-on LEDs, tends*
to reduce form center to backlight boundaries if free-spreading LSF is applied.

A further inspection is concerned with the contrast ratio and electric power consumption affected by the LSF. The image, as shown in **Fig. 3-4**, featuring high contrast ratio and high spatial frequency is taken as an example. The image is displayed on the system, introduced in **Section 2.3**, with 8-by-8 backlight divisions

separated by the green dashed lines. Point *a* in the enlarged part, enclosed by a red dot rectangle, is of maximum luminance. The backlight intensity for point *a* is always inefficient if the light energy is only provided by that division containing point *a*. In fact, the necessary backlight intensity has to be contributed by the additional next three layers of backlight divisions in current system. As a result, the flare term, $L*[X_k \ Y_k \ Z_k]^T$ from **Eq. (2-7)**, increases with L accumulated from a great number of backlight divisions. The contrast ration between points *a* and *b*, for example, is reduced. Besides, light energy is wasted in the neighboring dark areas, like that containing point *b*. Therefore, the free-spreading, wide LSF is particularly inadequate for image with contents of luminance varying at high spatial frequency.
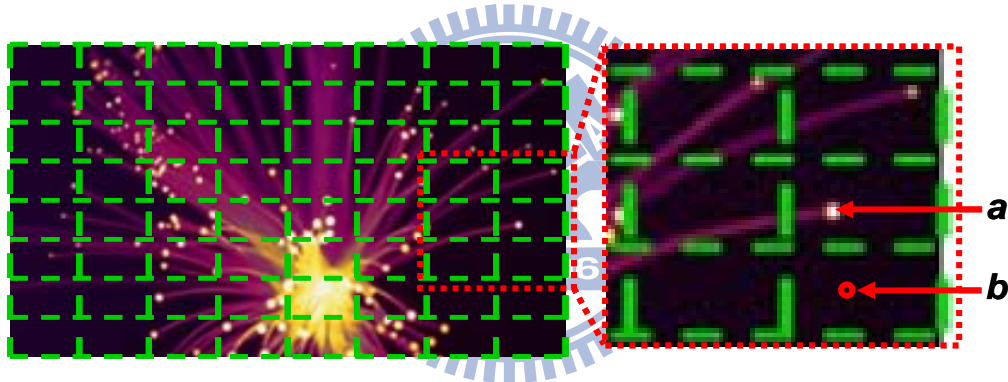
Fig. 3-4 *An image features high contrast ratio and high spatial frequency. 8-by-8 backlight divisions, underneath the image, are separated by the green dashed lines. Point **a** in the enlarged part of the image is the spark with high brightness while point **b** is a point of the dark background chosen arbitrarily.*

Finally, the manipulation efficiency is determined by the run time of derivation of driving signals. Among the procedures shown in **Fig. 1-12**, most of the processing time is spent on the estimation of L, step 4, which is strongly relevant to the size of LSF. The backlight intensity onto each pixel is contributed by the LSFs covering that pixel. Therefore, more LSFs are able to overlap together when the LSF spreads wider. In view of this, the free-spreading, wide LSF is inadequate for an LCD with a spatially-modulated backlight.

3.1.2 Localized LSF

The concept of localized LSF, on the contrary to the free-spreading one, is proposed to solve the aforementioned issues. Ideally, a rectangular LSF, as shown in **Fig. 3-5(a)**, is the optimized choice in the systematic point of view [40,41]. An apparent advantage is that a uniform backlight distribution can be achieved when those rectangular LSFs piece up periodically in the backlight module. However, perfect rectangular luminous distribution is not possible to be realized via current state-of-the-art backlit setup. Instead, the super-Gaussian LSF, **Fig. 3-5(b)**, is a reasonable approximation to the ideal one.
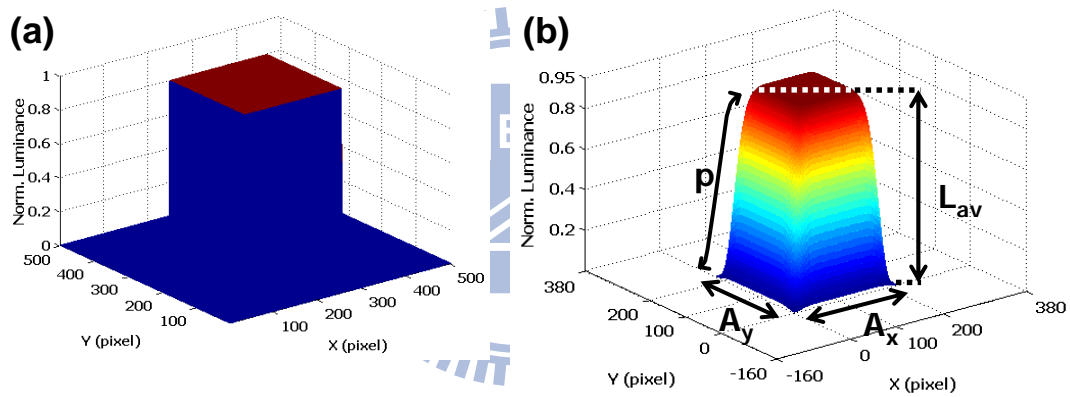
Fig. 3-5 (a) rectangular LSF, and (b) super-Gaussian LSF

The general formulation of a square super-Gaussian LSF, $LSF_{SG}(x,y)$, can be expressed as following [42,43]:

$$LSF_{SG}(x,y) = L_{av} \exp\left(-2(x/A_x)^{p_x}\right) \exp\left(-2(y/A_y)^{p_y}\right) \qquad (3\text{-}1)$$

L_{av} denotes the maximum luminance value at the center. A_x and A_y roughly define the dimensions of the LSF_{SG} in x and y directions, respectively. Particularly, the initial values of A_x and A_y are determined by the quotient of panel resolution divided by the number of backlight partition. The dimensionless parameters, p_x and p_y,

determine the edge decay from the central region. A cross-section family of super-Gaussian LSFs, being of identical luminance power with different values of A and p, is illustrated in **Fig. 3-6**. As the value of p is approaching to infinity, the $LSF_{SG}(x,y)$ will change into an ideal rectangle function with the width of A_x and A_y in x and y directions, respectively. Finally, the qualified LSF_{SG} is treated as the designated light profile for optomechanical design after perceptual assessment of grid pattern visibility on a dual-liquid-crystal-panel (DLCP) system [41], introduced in **Section 3.2.1**.
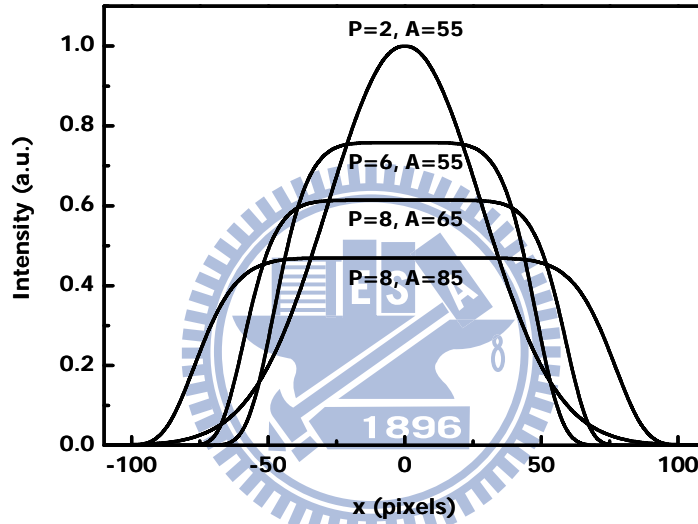
Fig. 3-6 *A series of one-dimensional super-Gaussian profile; energy conservation is preserved.*

3.1.3 Physical Constraints Revisited of FSC LCD

The localized LSF is also potential to overcome the issues of the FSC LCD arisen from the physical constraints, discussed in **Section 1.4.3.2**. The idea comes up from the so-called scanning backlight, as shown in **Fig. 3-7** [15,16]. The scanning order is the same as the data registration in the LC module, say, the top-down direction. The merit of this backlight technique is to save much time for color-field backlighting in FSC LCDs with moderate timing between LC data registration and backlight illumination.

TFT scan order   **LC module**

Divided backlight   **Backlight scan order**
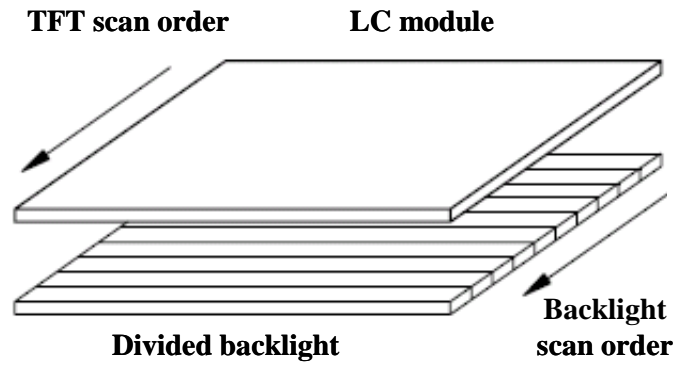
Fig. 3-7 *Configuration of an LCD with a scanning backlight [15]*

As an example, a schematic timing is drawn for an LCD with a 480-row LC module and a 10-block scanning backlight, as shown in **Fig. 3-8**. Referred to **Section 1.4.3.2**, time for backlight illumination is hard to be manipulated because of the field time delay, 5.56ms, of data registration between the first and the last rows of the LC module, as illustrated in **Fig. 1-9**. In current configuration, each backlight block is responsible for 48 rows of LC cells. Thus, the time delay in each block becomes only one-tenth the filed time, 0.556ms, which is 1 time division shown in **Fig. 3-8**. The LEDs in each block are ignited after 5 time divisions, which comprise 1 time division of data registration of LC cells in a block and 4 time divisions for the LC response. Consecutively, all the rows of LC cells in the block experience the same backlight illumination for 5 time divisions. Then, the backlight is turned off for 1 time division, followed by refreshing the data registration for the next color field at current backlight block. As for the next block of LC cells, the time delay is merely 1 time division following the preceding block.

The spatial arrangement of backlight block combined with adequate timing can, ideally, prevent filed crosstalk and, thus, the reduction of color gamut. If fast-response LC mode is implemented, backlight illumination can last longer by compress the time for LC transition. However, the challenge of backlight isolation hinders the implementation of this technique.
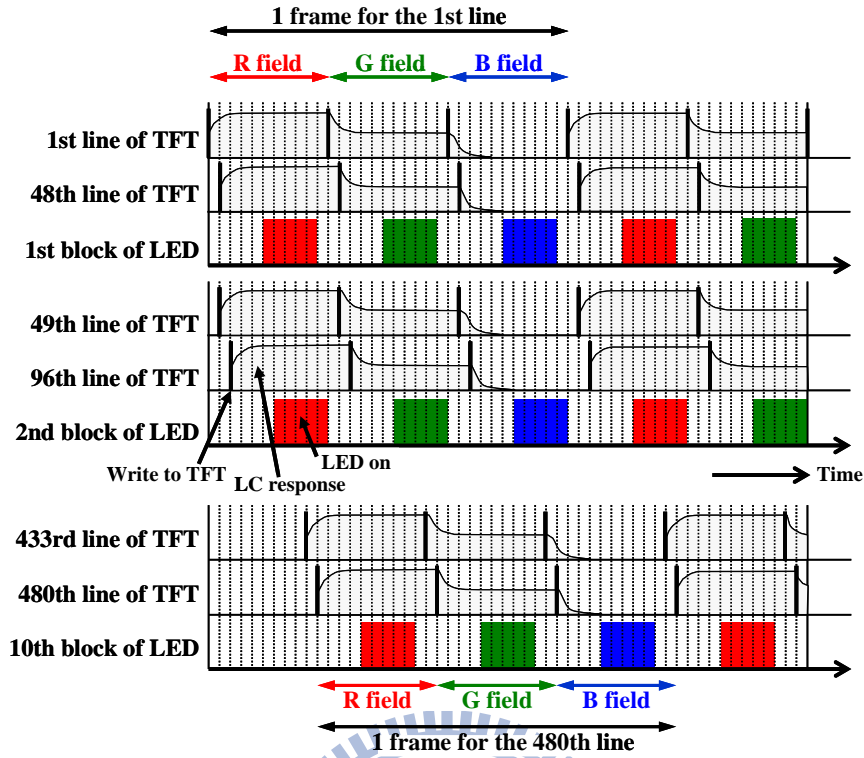
Fig. 3-8 *Timing for an LCD, composed of an LC module with 480 rows and a scanning-backlight with 10 blocks arranged in the top-down direction [15]*

The imperfect isolation of one-block backlight illumination from that of the others degrades the performance of this system set-up. Sharp, clear images can be formed, based on perfect isolation of block LSF, by turning off the blocks of backlight corresponding to regions of LC cells during transition, as shown in **Fig. 3-9(a)**. The practical situation, nevertheless, is that light form single backlight block always penetrates several neighboring blocks, as shown in **Fig. 3-9(b)**. Thus, erroneous images always result from discordant combination between the backlight illumination and the modulation state of LC cells, **Fig. 3-9(c)**. **Fig. 3-9(d)**, for example, is a snapshot image of pure red demonstrating visible periodic grids and erroneous colors, magenta-like (top) and yellowish (bottom) ones, due to backlight leakage. Although many efforts have been made to suppress the unwanted light penetration and the resultant visible artifacts, the costs are the reduction of output intensity and the extra design complexity [44].

44
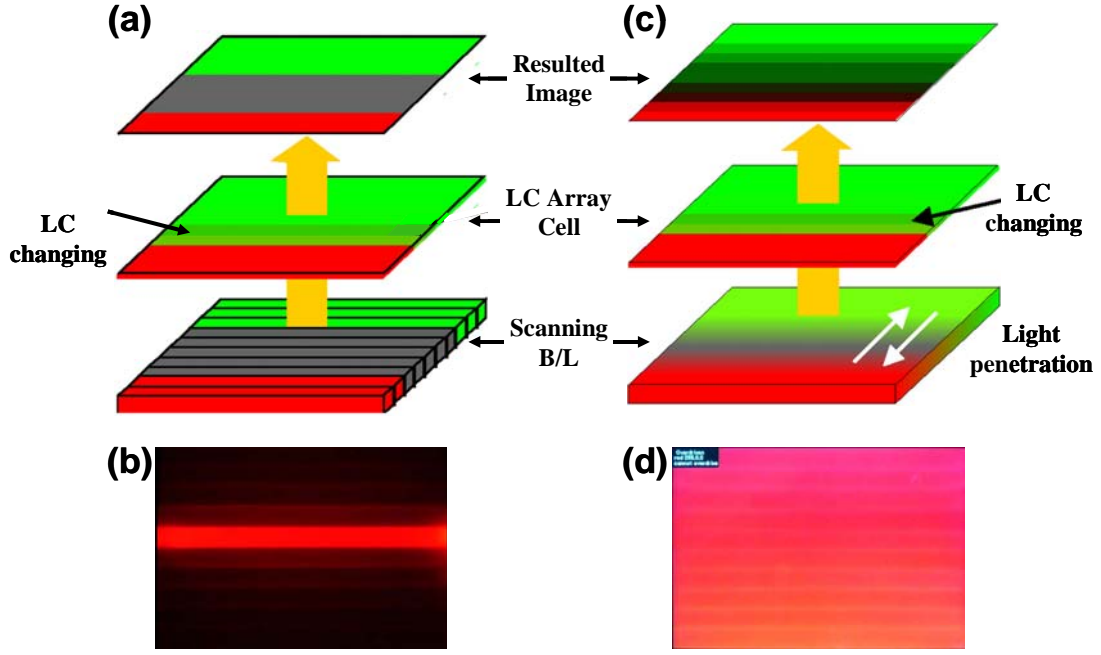
Fig. 3-9 *Images are formed from the scanning-backlight and the LC array cell in (a) the ideal case and (c) the practical situation. (b) The light distribution from single backlight block penetrates several neighboring blocks. (d) A snapshot image of a pure red with visible periodic grids and enormous colors, magenta-like (top) and yellowish (bottom) ones, due to backlight leakage [15]*

A spatially-modulated backlight, implementing the localized LSF, is also potential to function as a scanning backlight, simply by simultaneously driving the LSFs in the same row. The advantage is two-fold. First, concentrated LSF is effective to prevent light spreading widely. Second, compensation by the front LC module helps to achieve acceptable image quality. The procedures are introduced to define, optimize, and realize the desired LSF, which is then implemented in a platform, called DLCP [41]. Some system parameters are then measured on the platform to verify the applicability of the proposed design.

3.2 Light Guide Unit for Super-Gaussian LSF

3.2.1 Design Flow

The applicable super-Gaussian LSFs can be attained via two successive assessments along a methodical design flow. The design flow, as shown in **Fig. 3-10**, commences with a formulated LSF, denoted as LSF_{SG} expressed by **Eq. (3-1)**, which is then applied to the DLCP system (**Section 3.3**) to simulate the resultant backlight distribution. The initial values of the parameters A and p in **Eq. (3-1)** are deduced according to the panel dimension and the number of backlight division.

The undesirable grid pattern, detrimental to the implementation of super-Gaussian LSF, arises from the superposition of the tail intensity beyond the flat-topped region across the adjacent backlight divisions. The first assessment, therefore, is to perceptually judge the visibility of the grid lines, as shown in **Fig. 3-11(a)**. A set of qualified LSF_{SG}, obtained by iteratively adjusting the parameters in **Eq. (3-1)** to make grid pattern invisible as illustrated in **Fig. 3-11(b)**, is treated as the target for designing the optomechanical part, the light guide unit (LGU). The similarity, calculated by the correlation coefficient (CC), defined by **Eq. (3-2)** (**Section 3.2.3**) between the qualified LSF_{SG} and the emitting light profile of the LGU, denoted as LSF_{LGU}, is the second assessment to ensure the acceptability of designed LGU. Finally, the qualified LGU will be fabricated and pieced together to form a complete spatially-modulated backlight.
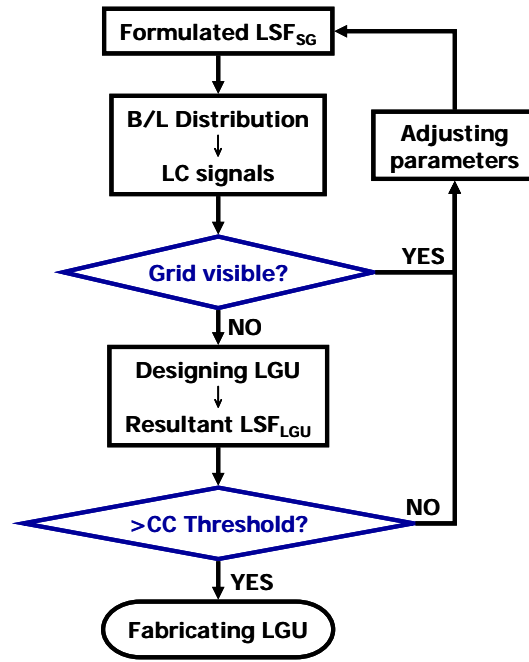
Fig. 3-10 *Design flow of retrieving applicable parameters for optical design*

(a)   **(b)**
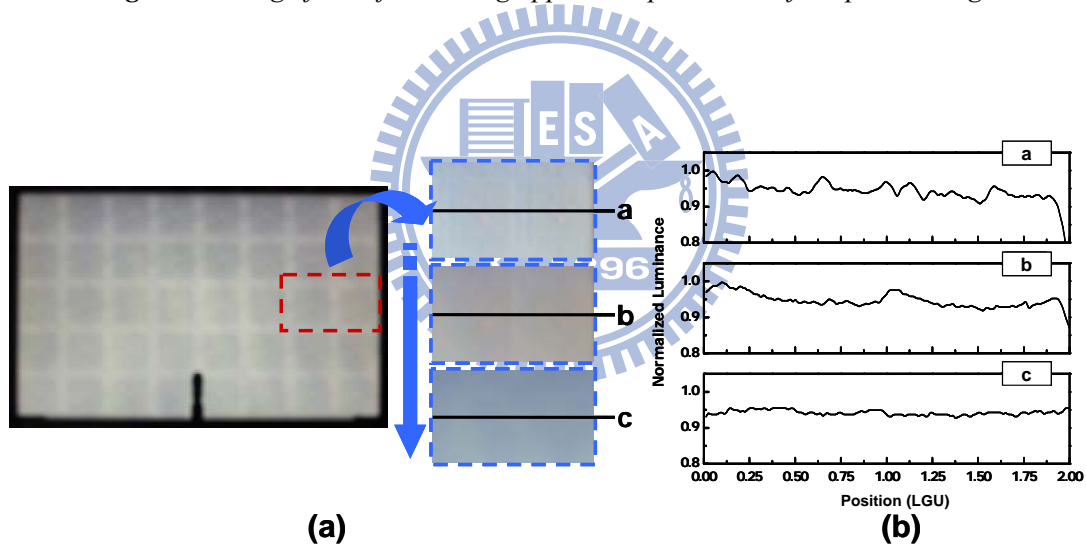
Fig. 3-11 *(a) The photographed image on the left is the intensity distribution of backlight by virtue of super-Gaussian LSF without compensation of the second LC panel. Nevertheless, the visible grid lines, shown in the photos on the right, can be gradually reduced from top to bottom (a to c) by modifying the parameters of the super-Gaussian LSF and the corresponding compensation of the second LC panel. (b) The corresponding cross-section profiles of central lines a through c. In the case of c, the adjusted parameters can achieve variation of 1.4%, which is less than the empirical value of 2% in the current DLCP system.*

3.2.2 Optomechanical Layout

A novel optomechanical layout, light guide unit (LGU), is proposed whose light spreading profile, denoted as LSF_{LUG}, is subjected to the qualified LSF_{SG}. The LGU consists of three major components: a side-emitting LED, a quadratic light guide (QLG), and a concentric prismatic sheet (CPS), as shown in **Fig. 3-12(a)**. The light emanating from the LED, following the light path as shown in **Fig. 3-12(b)**, finally exits the LGU in the normal direction to form a concentrated light distribution, super-Gaussian LSF.
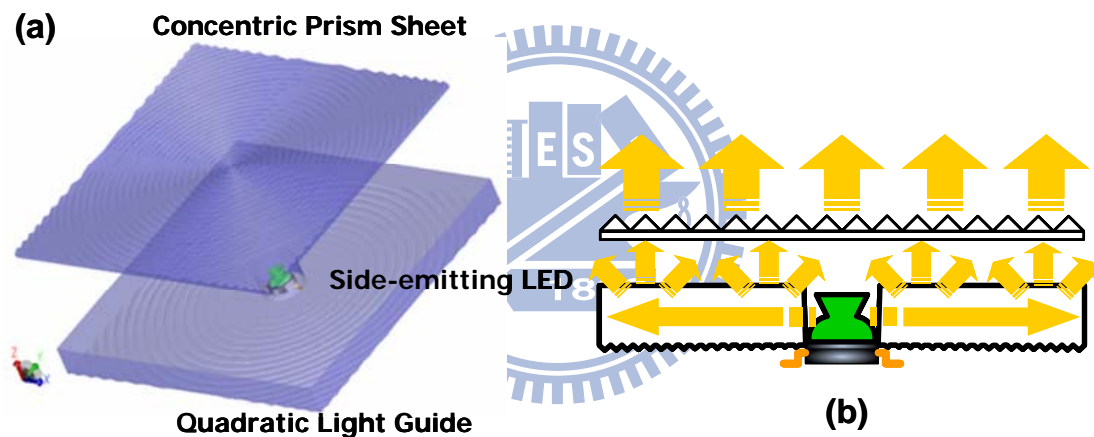
Fig. 3-12 *(a) Composition of LGU; (b) the light path from LED to output surface of CPS along the arrow direction*

LED

About 80% of luminous flux from the side-emitting LED is confined within ±20 degrees in the azimuthal direction [45]. The LED is located at the cavity center of a QLG, which mainly facilitates redirecting the azimuthal flux into the normal direction of the backlight surface. In current configuration, wide angle of light emanation in the azimuthal direction is preferred because it is helpful to achieve uniform distribution inside the flap-topped region.

QLG

The function of the QLG is to re-direct azimuthal light from LED to the output of backlight surface. Each QLG features a set of centric micro prismatic bumps on the bottom coated with highly reflective material, silver (Ag), underneath. The set of concentric prismatic bumps locates in parallel with increasing spacing from the center, LED, to the QLG side walls; the height of the prismatic bumps changes in corresponding sense as well, while the base angle θ_b is fixed, as shown in **Fig. 3-13(a)** [46]. Light incident on those Ag-coated prismatic bumps can be directly reflected into the concentric prism film, as shown in **Fig. 3-13(b)**. The amount of light leaving the CPS increases with the density of micro bumps in a QLG. The designed configuration of the QLG can also contribute to good uniformity. In addition, the edge planes of light guide are coated with reflective material as well not only to enhance the light efficiency but also to ensure that light can not influence other adjacent units.
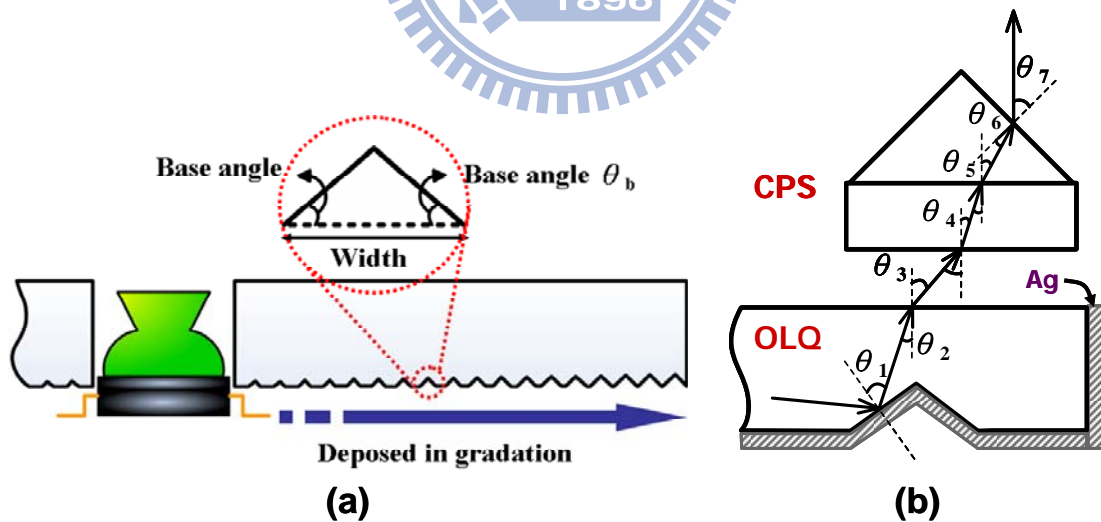
Fig. 3-13 (a) Cross-section of a QLG; (b) a light trace through QLG and CPS

CPS

A concentric prism sheet (CPS) is employed to collimate the divergent light from QLG toward the surface normal, as shown in Figure **Fig. 3-13(b)**. Light undergoes a

series of refraction by the CPS, and then results in the narrowed zenith angle of divergent light in all azimuth direction. The prismatic structure can also increase the throughput efficiency within the cone of small zenith angle around the normal direction. Furthermore, the square beam shape is achieved when light transmits a distance from QLG to panel. The structure of CPS is similar to that of the conventional brightness enhancement film (BEF) proposed by 3M™ [47], except the concentric arrangement.

Based on the proposed configuration of LGU, the luminous flux from the side-emitting LED can be transformed into a nearly square pattern, i.e. the super-Gaussian LSF. Since each LED module is regarded as an isolated secondary light source, the luminous pattern can be space-shift invariant and easily modified by changing the parameters of each unit.

3.2.3 Correlation

In order to evaluate the similarity between the LSF generated by the LGU (LSF$_{LGU}$) and the qualified super-Gaussian function (LSF$_{SG}$), a correlation coefficient (CC), is introduced as following [48]:

$$CC = \frac{\sum_x \sum_y \left[LSF_{SG}(x,y) - \overline{LSF}_{SG} \right]\left[LSF_{LGU}(x,y) - \overline{LSF}_{LGU} \right]}{\sqrt{\sum_x \sum_y \left[LSF_{SG}(x,y) - \overline{LSF}_{SG} \right]^2 \cdot \sum_x \sum_y \left[LSF_{LGU}(x,y) - \overline{LSF}_{LGU} \right]^2}} \quad (3\text{-}2)$$

where $\overline{LSF}_{SG}$ and $\overline{LSF}_{LGU}$ are the mean values of the two LSFs. The CC provides an important measure for the LGU design. After the qualified LSF$_{SG}$ is defined via the testing platform, the optical parameters of the LGU can be iteratively adjusted to ensure that the CC is at least higher than 95%, which empirically ensures the indistinguishable difference between the two LSFs.

3.3 Experiment

Testing Platform

A dual-liquid-crystal-panel (DLCP) platform [41] is constructed to attain the qualified LSF_{SG} as the design target, and then to verify the system performance with the resultant LSF_{LGU}. The pseudo display system is composed of two commercially available LCDs, ASUS VW193D [49], as depicted in **Fig. 3-14**. With a diffusing sheet on top, the rear LCD is served as a programmable backlight module with 8-by-5 local partition. Each unit is of square shape for the design convenience. Meanwhile, the front LC panel with resolution 1440-by-900 pixels, after removing the backlight module, functions as the substantial LC panel. The resultant uniformity, based on the ANSI-thirteen-point specification shown in **Fig. 3-15**, of the DLCP system is of 68% due to placement of the diffuser sheet. The maximum luminance of the DLCP system is of 10.2cd/m^2 while the minimum is of 0.01cd/m^2. The contrast range over 1,000:1 is sufficient for the following tests.

(a)   **(b)**
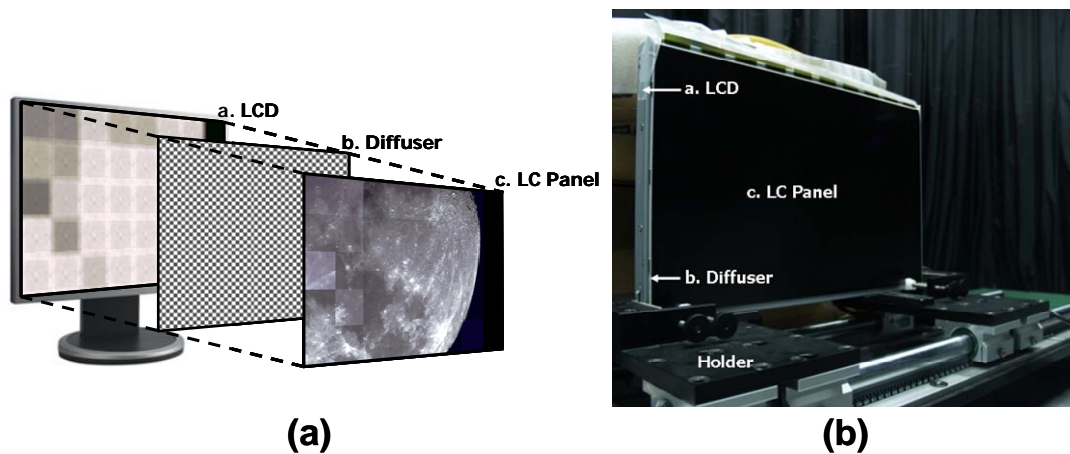
Fig. 3-14 (a) Schematic construction and (b) the practical apparatus of a DLCP system
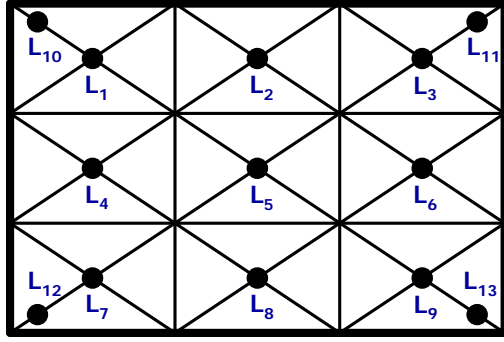
$$\text{Uniformity} = \frac{\text{Min. } \{L_1, ..., L_{13}\}}{\text{Max. } \{L_1, ..., L_{13}\}}$$

Fig. 3-15 *ANSI-thirteen-point uniformity measurement on flat-panel display*

Testing Items

The examination is divided into two categories. The first investigates the parameter adjustment to achieve invisible grids and the similarity between the LSF_{SG} and the LSF_{LGU}. Second, luminance uniformity, contrast ratio, and processing speed are three key parameters for evaluation of system performance. Those three comparisons are made based on the two different LSFs, that is, the general Gaussian LSF and the resultant super-Gaussian LSF, LSF_{LGU}; both LSFs are offered by the rear LCD in the DLCP system. The Gaussian LSF kernel is of size 540-by-540 pixels where the standard deviation, σ, is 90 pixels, which is half the width, 180 pixels, of the ideal square LSF. Meanwhile, the LSF_{LGU} kernel is of size 220-by-220 pixels, including the tails out of the ideal square area of size 180-by-180 pixels. In addition to kernel size, the summation of luminance value in both kernels is set equal in consideration of energy conservation.

3.4 Result and Discussion

The visibility of grid lines is varied with the adjustment of equation parameters, A_x, A_y P_x and P_y, as Lav is fixed. Certain range of parameter values is summarized as **Fig. 3-16** to explain the situation. The cross-sign region denotes inadequate

parameter values where the superimposed luminous intensity at the division boundary is less than the value of central region and thus insufficient for backlighting requirement. The slash regions indicate where the grid lines, incapable of being compensated by the front LC panel, are of unacceptable visibility to degrade the panel uniformity. Subsequently, the rest regions with number represent the acceptable parameter values; numbers in those regions denote the normalized uniformity rescaled to the uniformity, 68%, of the DLCP system with full-on backlighting. The uniformity 68% of the DLCP system arises from precision loss during manual construction. The normalized uniformity, up to 99.4%, implies that the localized LSF is potential to achieve the optimal uniformity of the conventional system with full-on backlight. Furthermore, the uniformity resulted from these applicable parameter values is perceptually indistinguishable, so any set of these values can be arbitrarily chosen in view of the fabrication tolerance.

Uniformity (%), rescaled to DLCP system

P_x, P_y \ A_x, A_y	98	100	102	104	106	108	110
6	✕	✕	✕	✕	✕	✕	✕
8	✕	✕	✕	✕	98.8	97.1	///
10	✕	✕	99.4	98.2	97.9	///	///
12	✕	98.9	98.9	98.5	///	///	///
14	99.3	98.5	97.5	///	///	///	///
16	97.8	96.8	98.2	///	///	///	///
18	96.5	99.4	///	///	///	///	///

A_x, A_y (pixels)
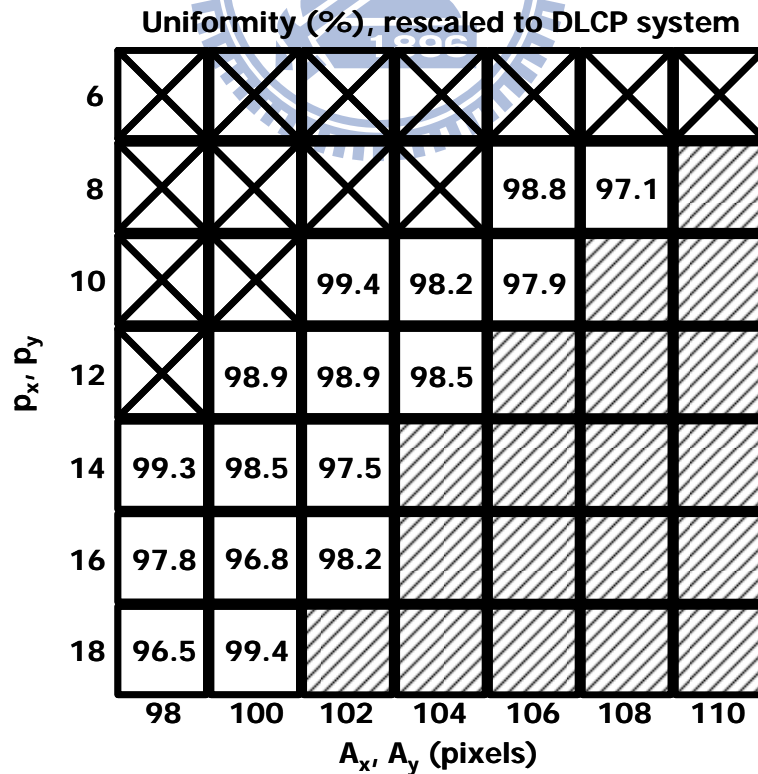
Fig. 3-16 *Parameter values correlated with gird-pattern visibility*

The proposed optomechanical layout, the LGU, is verified in terms of the correlation coefficient (CC) between the resultant LSF_{LGU} and an example qualified LSF_{SG}, with $L_{av} = 0.95$, $A_x = A_y = 102$ pixels, and $p_x = p_y = 10$. The intensity profiles of the two LSFs are shown in **Fig. 3-17(a)**. The ripples at the flat-top region of the LSF_{LGU}, as shown in **Fig. 3-17(b)**, can be confined within $\pm 10\%$ average luminance L_{av}. In this case, the CC is of 96.67%. The redundant light, trailing over the gray slash regions in **Fig. 3-17(b)** and attributed to the non-optimized design of the QLG edge, is the main cause to reduce the similarity between the two LSFs. Except for the slash area, the CC can achieve 98.91% which is more similar to the LSF_{SG}. Therefore, it is concluded that the proposed optical layout is applicable to create the nearly square light distribution for a spatially-modulated backlight.
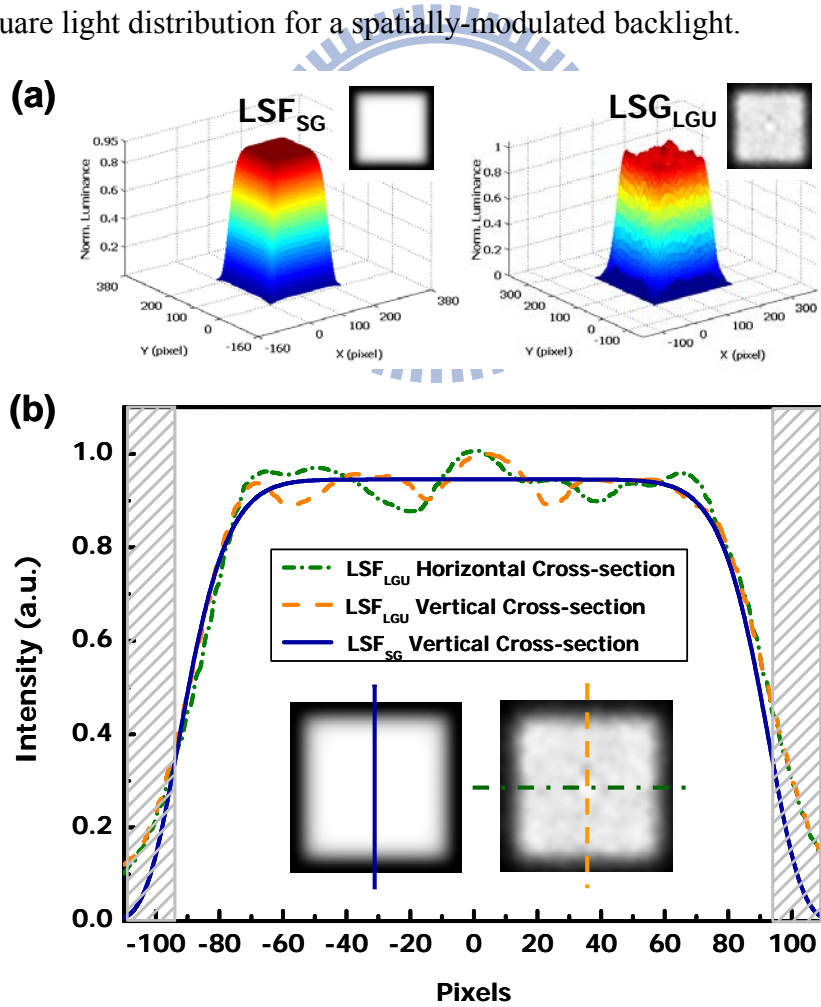
Fig. 3-17 (a) 3-D and top-view, and (b) cross-section profiles of the two super-Gaussian LSFs, LSF_{SG} and LSF_{LGU}

According to the ANSI-thirteen-point specification, the normalized uniformity is only of 60% when the whole screen is illuminated by the conventional Gaussian LSF ($A_x = A_y = 180$ pixels, and $p_x = p_y = 2$.). The normalized uniformity resulted from the LSF_{SG} with the parameter values $A_x = A_y = 102$ pixels and $p_x = p_y = 10$ is of 98.2%, whereas the one of the corresponding LSF_{LGU} 93.1%. All the three cases are measured after the compensation of the front LC panel. Again, the proposed super-Gaussian LSF and corresponding optomechanical setup are able to render an adequate backlighting solution for an LCD with a spatially-modulated backlight, without the expense of uniformity and optical efficiency.

The property of spatial shift-invariance is worth a further investigation on the proposed super-Gaussian LSF. As shown in **Fig. 3-18**, slight decrease of luminance occurs at the backlight edge. This fact implies that shift invariance is not hold around the boundary of backlight boundary. Specifically speaking, only the LSFs at the outmost location of the backlight module suffer this issue due to the imperfect tail of the super-Gaussian LSF. The other inner LSFs are still of the property of spatial shift-invariance. Thus, in comparison with the distribution from general Gaussian LSF, shown in **Fig. 3-3**, the uniformity is improved greatly.
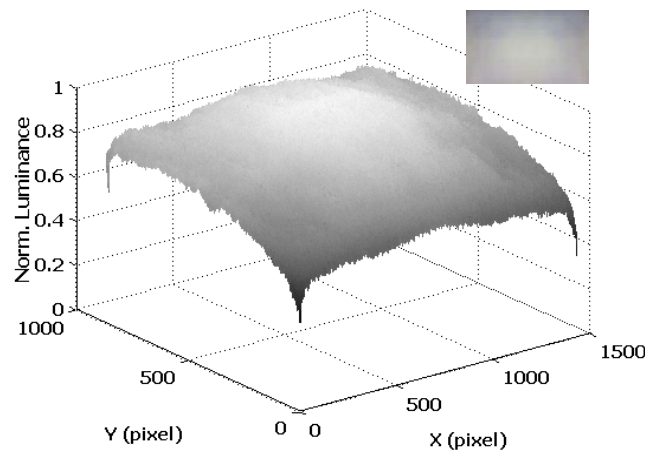
Fig. 3-18 *Resultant backlight distribution by means of LSF_{LGU}*

As for the examination of contrast ratio (CR), three testing images are displayed and measured under the illumination by the aforementioned Gaussian LSF and LSF$_{LGU}$, respectively. The measurement is made at the two-pair test points in each image, as shown in **Fig. 3-19(a)** - **Fig. 3-19(c)**. The CR values of the six pairs of test points are recorded as the bar chart, **Fig. 3-19(d)**. The improvement factor of CR by using LSF$_{LGU}$, labeled on top of each pair of bars, ranges between 1.9 and 4.2. In comparison with the Gaussian LSF, the LSF$_{LGU}$ has the superiority to maintain the luminance of the white areas and to suppress the luminance of the dark area adjacent to the white ones. That is, the proposed LSF is in general useful to achieve high CR for images with abrupt luminance variation.
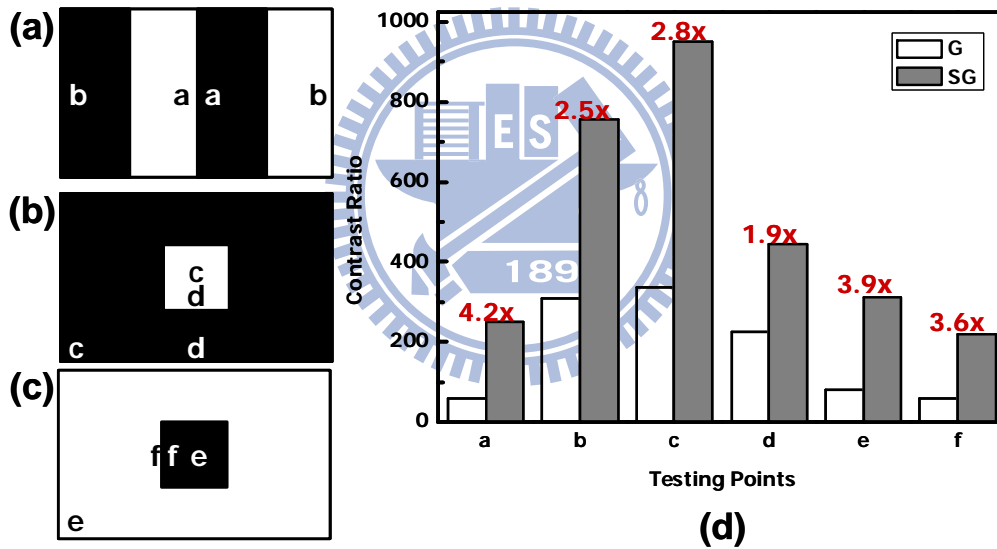
Fig. 3-19 *(a)-(c) are three test images with abrupt luminance change, and (d) the bar chart records the contrast ratio (CR) of six pairs of test points, in which white bars denote CR resulted from general Gaussian (G) LSF while gray ones from super-Gaussian (SG) LSF.*

Finally, the processing time is tested using the same computation procedure and program. In current situation, speed for the convolution computation with LSF$_{SG}$ is a factor of 4.82 faster than with current Gaussian LSF. The improvement is roughly in accordance with the factor of 6.02 of the reduction on the LSF$_{LGU}$ kernel size.

3.5 Fabrication

A. Process

The CPS can be fabricated by the following procedures. The UV (ultraviolet)-curable epoxy resin, of refractive index 1.553 close to that of PMMA (Polymethylmethacrylate), is applied to the surface of the metal mold, as shown in **Fig. 3-20**. A PET (Polyethylene Terephthalate) film, which is placed on the top of the layer of epoxy resin, is then imprinted by the rolling imprint. UV illumination is then incident on the PET to form the desired optical structure. The designed CPS can be obtained cutting out the resultant PET film to the appropriate shape. The photographs of the metal mold and the resultant film of the CPS are shown in **Fig. 3-21(a)** and **Fig. 3-21(b)** respectively, in which the inset shows the structure at point **b** of the CPS film, magnified by an optical microscope. The parallel bumps imply that current process is suitable for the fabrication of CPS film.
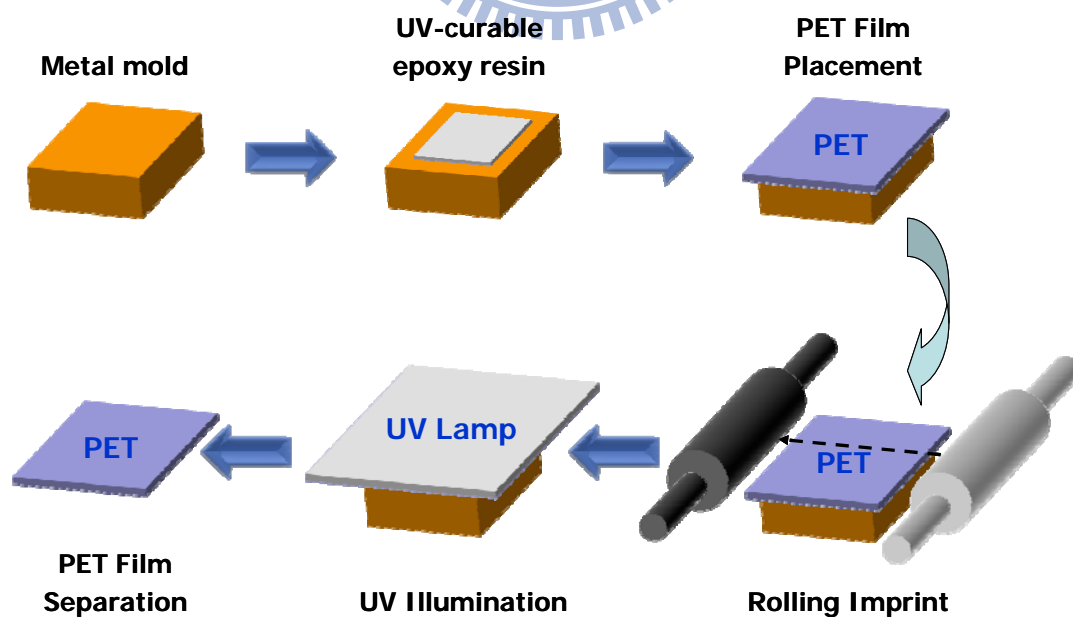
Fig. 3-20 *Fabrication process of the CPS*

(a) **(b)**
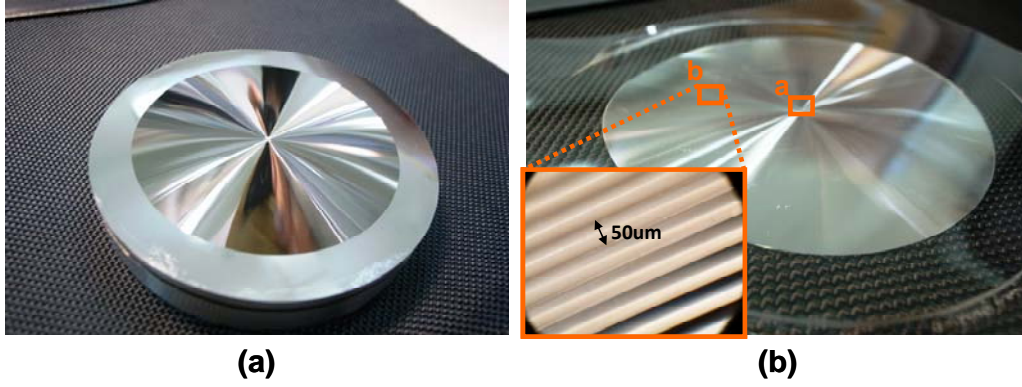
Fig. 3-21 Photographs of (a) the metal mold of the CPS and (b) a CPS film;
*angular light distribution will be measured on points **a** and **b**; the inset of point*
***b** is the magnified image by a optical microscope*

B. Optical Measurement

The angular light distribution of the CPS is measured to examine the light concentration property of the CPS. The measurement is done on a conventional, uniform full-on backlight module with the CPS film on top of it. The angular light distribution of the backlight module only, as shown in **Fig. 3-22(a)**, is first measured by ConoScope® [50], as the reference. The results of those with the CPS film measured at points **a** and **b** are shown in **Fig. 3-22(b)** and **Fig. 3-22(c)**, respectively. In comparison with **Fig. 3-22(a)**, the angular light distribution shown in **Fig. 3-22(b)** is more circular and symmetric that conforms to the collimation function of the CPS. The modulation is also observed in **Fig. 3-22(c)** with the variation with respective to the position. The cross-sectional profile of **Fig. 3-22(a)** and **Fig. 3-22(b)** along the

(a) **(b)** **(c)**
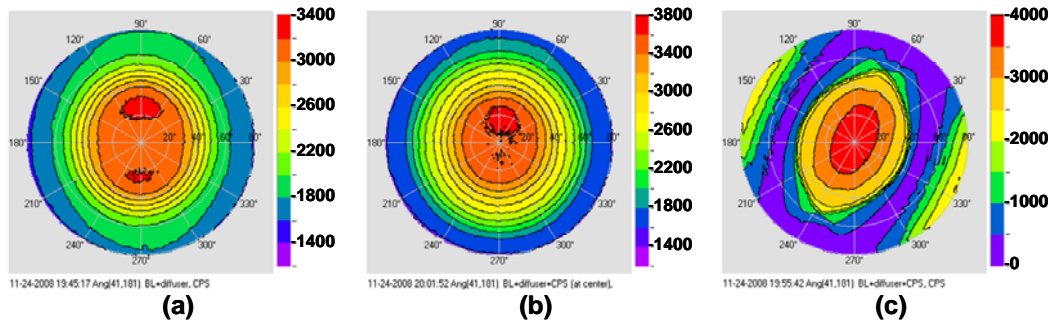
Fig. 3-22 Angular light distributions of the backlight module (a) without the
*CPS, (b) with the CPS at point **a**, and (c) with the CPS at point **b**, respectively*

azimuthal angle 0°~180°, as shown in **Fig. 3-23(a)**, exhibits the energy concentration of the CPS. More light energy exits the backlight module along the normal direction. Similar phenomenon is observed in **Fig. 3-23(b)**, in which the profiles are obtained from **Fig. 3-22(a)** and **Fig. 3-22(c)** along the azimuthal angle 156°~180°. The raised tails at both sides of the profile with CPS in **Fig. 3-23(b)** are the light energy contributed from the backlight module at large incident angles.
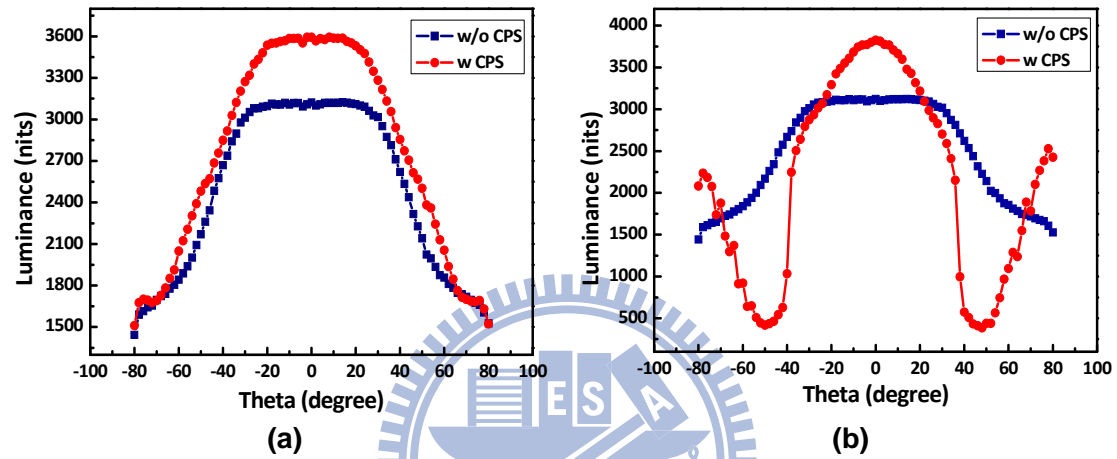
Fig. 3-23 *Cross-sections of the angular light distribution of the backlight module (a) with the CPS at point **a** with azimuthal angle 0°~180° and (b) with the CPS at point **b** azimuthal angle 156°~336°, respectively*

C. Issues on QLG Fabrication

The fabrication of the QLG is different from that of the CPS. Since the pitch and the height of the bumps of the QLG vary along the radical direction, difficulty arises in carving those structures. In addition to the varied micro structures, the QLG is much thicker than the CPS, the rolling imprint and the UV-curing procedures may be ineffective. Thus, a fabrication process, called vacuum compression forming, will be tried to realize the QLG. More details are described in **Section 6.2.1**. Once the fabrication of the QLG is finished, the following tasks are the construction and the optical measurement of the LGU, and then the constitution of a complete backlight module.

3.6 Conclusion

The applicability of the proposed methodology, based on two-dimensional super-Gaussian light spread functions (LSF), is demonstrated via the platform of the dual-liquid-crystal-panel (DLCP) system. In the experimental setup, luminance uniformity, contrast ratio and processing speed of the proposed high-dynamic-range system can be improved by factors of 1.55, 1.95-4.15 and 4.82, respectively. The enhancement on contrast ratio (CR) shows that such LSF is particularly effective to improve CR of image contents subjected to the abrupt luminance variance in an LCD with a spatially- modulated backlight. In addition, the methodology is capable of scaling the light guide unit (LGU) to meet any panel dimension with moderate design parameters. Finally, the proposed optomechanical layout is applicable to both the LCDs with the conventional full-on backlight and a spatially-modulated one.
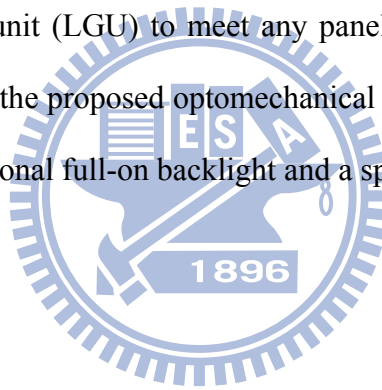
Chapter 4

Two-field Driving Scheme and System

4.1 Introduction

The issues, field crosstalk and tradeoff of output backlight intensity, of the FSC LCD theoretically can be solved by the technique of scanning backlight (**Section 3.1.3**). Besides, the localized super-Gaussian LSF (**Section 3.1.2**) can mend another crosstalk arisen from leakage light between backlight divisions. However, if the timing chart, shown in **Fig. 3-8**, is carefully analyzed, the effectiveness of this configuration of scanning backlight must also be attributed to the short LC response time. In the example as shown in **Fig. 3-8**, time for LC response is of around 2ms when the adopted optically-compensated bend (OCB) LC mode has response time of 0.6ms to a couple of milliseconds at gray-level transitions [15,16].

It is worth noting that the response time of 2ms has been quite marginal under three-filed driving scheme. If the same constitution is driven by a multi-filed scheme, e.g. four fields, either backlight intensity reduces more than 50% or color gamut shrinkage occurs. Moreover, most commercial LC modes, being of response time 4ms~8ms, are inapplicable to the present configuration. As a result, all those tradeoffs induce the preference for long field time in the FSC LCD and thus hasten the emergence of the two-field driving scheme.

4.2 Prior Art

A plausible method, hybrid spatial-temporal color synthesis, has been proposed to facilitate the FSC LCD driven at only two color fields per frame [51,52,53]. A

special color filter (CF) film, composed of only two CFs, and the constituent successive two fields denominate the terms "spatial" and "temporal", respectively. Two configurations have demonstrated the feasibility of such color synthesis mechanism, as shown in **Fig. 4-1**. The CF film in configuration 1 is composed of magenta and cyan CFs arranged in a checkerboard pattern. Yellow and blue light sources successively illuminate the LCD panel to form images based on a red-green and a full blue patterns, respectively, which then result in a full color image after the integration by the human visual system. In the similar manner, full color images can be obtained under configuration 2, in which the color filter film consists of magenta and green CFs while yellow and cyan light sources are used. The optical throughput is enhanced by a factor of 1.5 in comparison with the conventional LCD with a red/green/blue CF film. However, the cost of CF film remains and the optical throughput is still not as good as that of an LCD without a CF film.
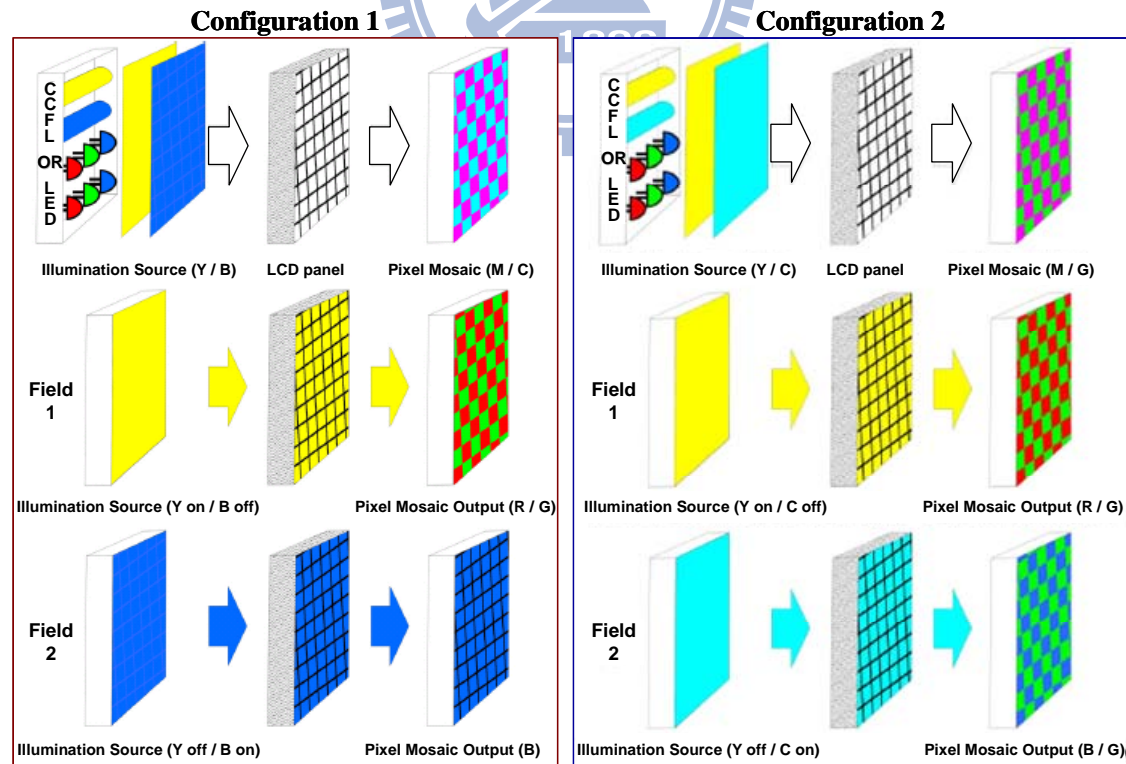
Fig. 4-1 *Two feasible configurations for hybrid spatial-temporal color synthesis, wherein Y denotes yellow, B blue, M magenta, C cyan, R red, and G green, respectively*

4.3 Proposed Two-field Driving Scheme

A novel displaying method, two-field driving scheme, is proposed for FSC LCDs without a CF film. The challenge of a two-field driving scheme on an LCD without a CF film is the lack of the third temporal degree of freedom for displaying the third primary information. That is the reason why a special CF film is still required in the hybrid spatial-temporal color synthesis. For this, the proposed method incorporates a spatially-modulated color backlight that can make up for the required third temporal degree by the spatial degrees of freedom embedded in such system. The system configuration, concept, algorithm, and color difference formula are declared below.

4.3.1 System Configuration

The system configuration for the proposed two-field driving scheme consists of an LC module without a CF film and a spatially-modulated color backlight, as shown in **Fig. 4-2**. Specifically, each pixel is now of single TFT unit, but not of three-in-one sub-pixel structure as the conventional LCD. The signal derivation and the corresponding color model are similar to those of the system based on white LED as the light source and the LC module with a CF film, as shown in **Fig. 1-11**, except for moderate modifications. That is, the processes of signal derivation of LED and LC module are the same as that shown in **Fig. 1-12**, but now based on each color backlight. Besides, the corresponding color model, modified from **Eqs. (2-5)** and **(2-7)**, becomes **Eqs. (4-1)** and **(4-2)**, respectively, where j denotes the field number and i indexes r, g, and b, each for red, green, and blue light. I and L represent radio-metric scalar and backlight intensity, individually. For example, $I_{r,1}$ and $L_{r,1}$ represent radio-metric scalar R and red light intensity in the first field, respectively. The flare term becomes triple to account for three-primary backlight.

| LED Array | OPTICS | LC Module |
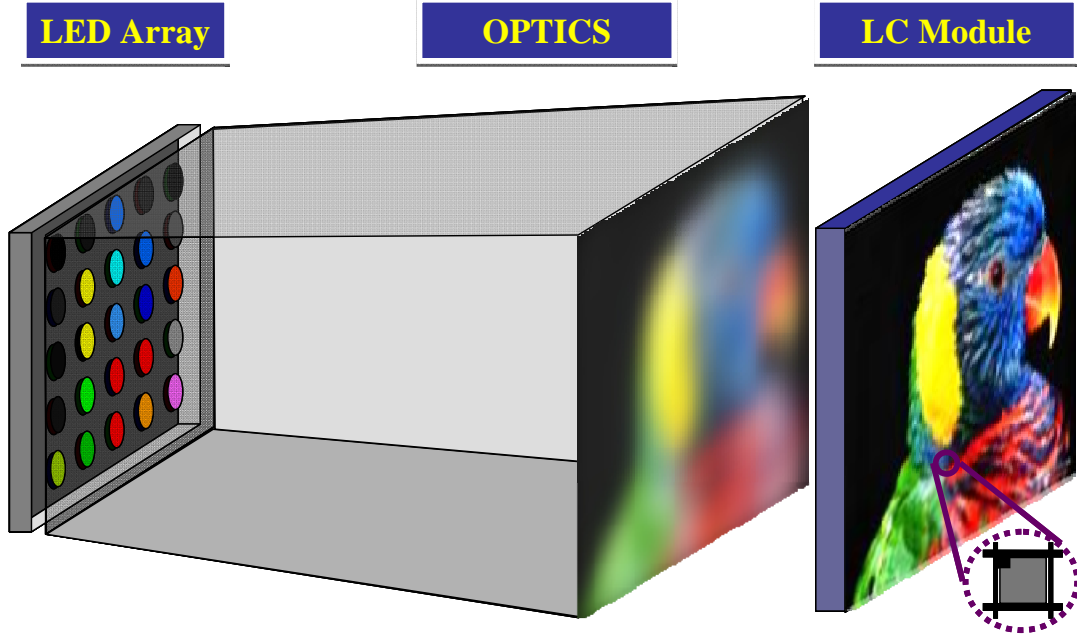
Fig. 4-2 *The system configuration for the proposed two-field driving scheme consists of an LC module without color filter film and a spatially-modulated color backlight.*

$$I_{i,j} = LUT_i(d_j{}')$$
$$0 \le I_{i,j} \le 1 \qquad\qquad (4\text{-}1)$$
$$0 \le L_{i,j} \le 1$$

$$\begin{bmatrix} X \\ Y \\ Z \end{bmatrix} = \sum_j \left\{ \sum_i \begin{bmatrix} X_{i,\max} - X_{i,k} \\ Y_{i,\max} - Y_{i,k} \\ Z_{i,\max} - Z_{i,k} \end{bmatrix} I_i L_i + \begin{bmatrix} X_{i,k} \\ Y_{i,k} \\ Z_{i,k} \end{bmatrix} L_i \right\}_j \qquad (4\text{-}2)$$

4.3.2 Concept

The two-field driving scheme is to sequentially display two field images, which are produced on a color-filterless LCD with a spatially-modulated backlight, as shown in **Fig. 4-3**. This driving scheme begins at primary assignment. The first field image comprises the first primary and a part of the third primary information while the other includes the second primary and the remaining part of the third primary information. Red, green, and blue, as an example shown in **Fig. 4-3**, are assigned as

the first, the second, and the third primary, respectively. Blue as the third primary is beneficial to reduce visual deviation of images reproduced by the two-field method since the human visual system is less sensitive to blue information. As a result, the first field represents a magenta-like image while the second field is cyan-like. In this case, the color model, simplified from **Eq. (4-2)**, can be explicitly expressed as **Eq. (4-3)**. Color difference as an evaluation metric of the proposed method will be calculated with the tri-stimulus values predicted by **Eq. (4-3)**.

$$
\begin{bmatrix} X \\ Y \\ Z \end{bmatrix} = \begin{bmatrix} X_{r,\max} - X_{r,k} \\ Y_{r,\max} - Y_{r,k} \\ Z_{r,\max} - Z_{r,k} \end{bmatrix} R_1 L_{r,1} + \begin{bmatrix} X_{r,k} \\ Y_{r,k} \\ Z_{r,k} \end{bmatrix} L_{r,1} + \begin{bmatrix} X_{b,\max} - X_{b,k} \\ Y_{b,\max} - Y_{b,k} \\ Z_{b,\max} - Z_{b,k} \end{bmatrix} B_1 L_{b,1} + \begin{bmatrix} X_{b,k} \\ Y_{b,k} \\ Z_{b,k} \end{bmatrix} L_{b,1} +
$$

$$
\begin{bmatrix} X_{g,\max} - X_{g,k} \\ Y_{g,\max} - Y_{g,k} \\ Z_{g,\max} - Z_{g,k} \end{bmatrix} G_2 L_{g,2} + \begin{bmatrix} X_{g,k} \\ Y_{g,k} \\ Z_{g,k} \end{bmatrix} L_{g,2} + \begin{bmatrix} X_{b,\max} - X_{b,k} \\ Y_{b,\max} - Y_{b,k} \\ Z_{b,\max} - Z_{b,k} \end{bmatrix} B_2 L_{b,2} + \begin{bmatrix} X_{b,k} \\ Y_{b,k} \\ Z_{b,k} \end{bmatrix} L_{b,2}
$$

$$(4\text{-}3)$$

$d_{BL-R} + d_{BL-B1}$ $L_{BL-R} + L_{BL-B1}$ d_{LC-1} $I'_R + I_{B1}$

$d_{BL-G} + d_{BL-B2}$ $L_{BL-G} + L_{BL-B2}$ d_{LC-2} $I'_G + I_{B2}$
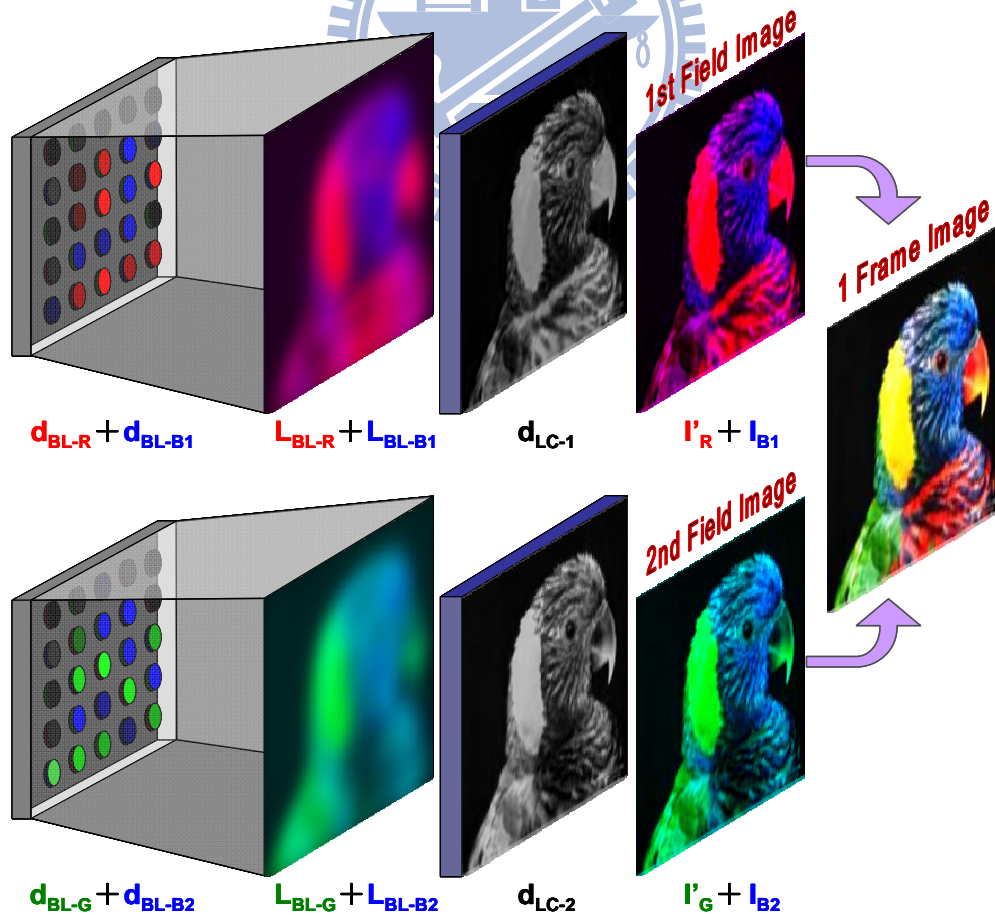
Fig. 4-3 Concept of the proposed two-field driving scheme

4.3.3 Algorithm Flowchart

The process flow with the previous primary setting is further detailed below. Similarly, the process starts at transforming the digits (d_r d_g d_b) of an input image into the corresponding target intensity I_R, I_G, I_B of red, green, and blue information, as show in **Fig. 4-4**. In the first field, the LED and the LC signals of the red information, I_R, are derived by the aforementioned "forward" process, defined in **Section 1.5.2**. The red backlight distribution, L_{BL-R}, is shown in **Fig. 4-4** instead of red LED signals, d_{BL-R}. Besides, the red LC signals are defined as the LC compensation signals for the first field, d_{LC-1}. The blue LED signals, d_{BL-B1}, and the corresponding backlight distribution, L_{BL-B1}, are acquired through the "backward" process, defined in **Section 1.5.2**, based on I_B and d_{LC-1}. The first field image, thus, consists of the reproduced red and blue information, I'_R and I_{B1}, together. As for the second field, the procedure is almost the same as that of the first one except that the blue target intensity is changed to the difference between the original and the produced blue intensity in the first field, i.e. I_B-I_{B1}. This difference, in general, arises from the fact that $\hat{I}_L$ derived from **Eq. (1-3)** only achieves least-square errors between $\hat{L}$ and **L**. The compensation, I_B-I_{B1}, in the second field can improve the reproduction accuracy of blue information toward I_B.
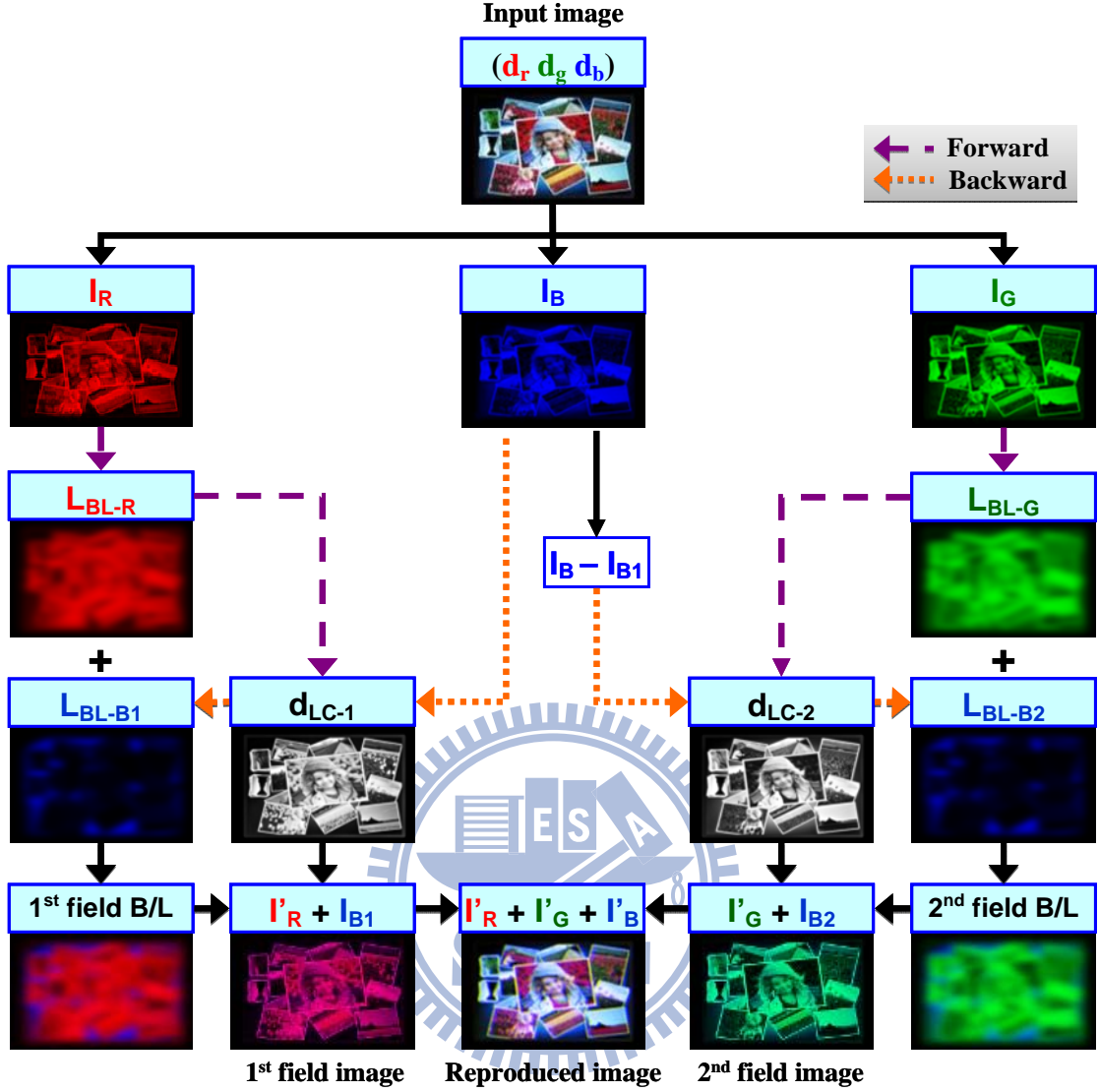
Fig. 4-4 *Flowchart of the proposed two-field driving scheme*

4.3.4 Color Difference Indexes

The performance of the proposed two-field driving scheme is evaluated by the color difference between the original input image and the reproduced one. Two formulae of color difference, CIE 2000 color difference (CIEDE2000, denoted as ΔE_{00}) [34] and the spatial-extension of CIEDE2000 (S-ΔE_{00}) [54] are applied to the evaluation. Briefly speaking, S-ΔE_{00} features the spatial filtering performed on the opponent colors, (A C_1 C_2), as shown in **Fig. 4-5**. This step accounts for the

phenomenon that visual perception of the field of view is affected by the neighboring stimuli in a complex image. In the following evaluations, ΔE_{00} is applied in the induction of optimal system parameters, the size of LSF and the number of localized backlight division. In that experiment, the test images will be the color-patch images, which are close to the sample images of database formulating ΔE_{00}. As for the evaluation of simulated complex images, on the other hand, S-ΔE_{00} will be implemented.

Original   **Reproduced**

Original and Reproduced Images $(d_r\ d_g\ d_b)$

Device-independent Representation $(X\ Y\ Z)$

Opponent Color Space Representation $(A\ C_1\ C_2)$

Spatial Filtering   **Spatial Filtering**

Device-independent Representation (inversed) $(X'\ Y'\ Z')$

Color Difference Image ΔE_{00}
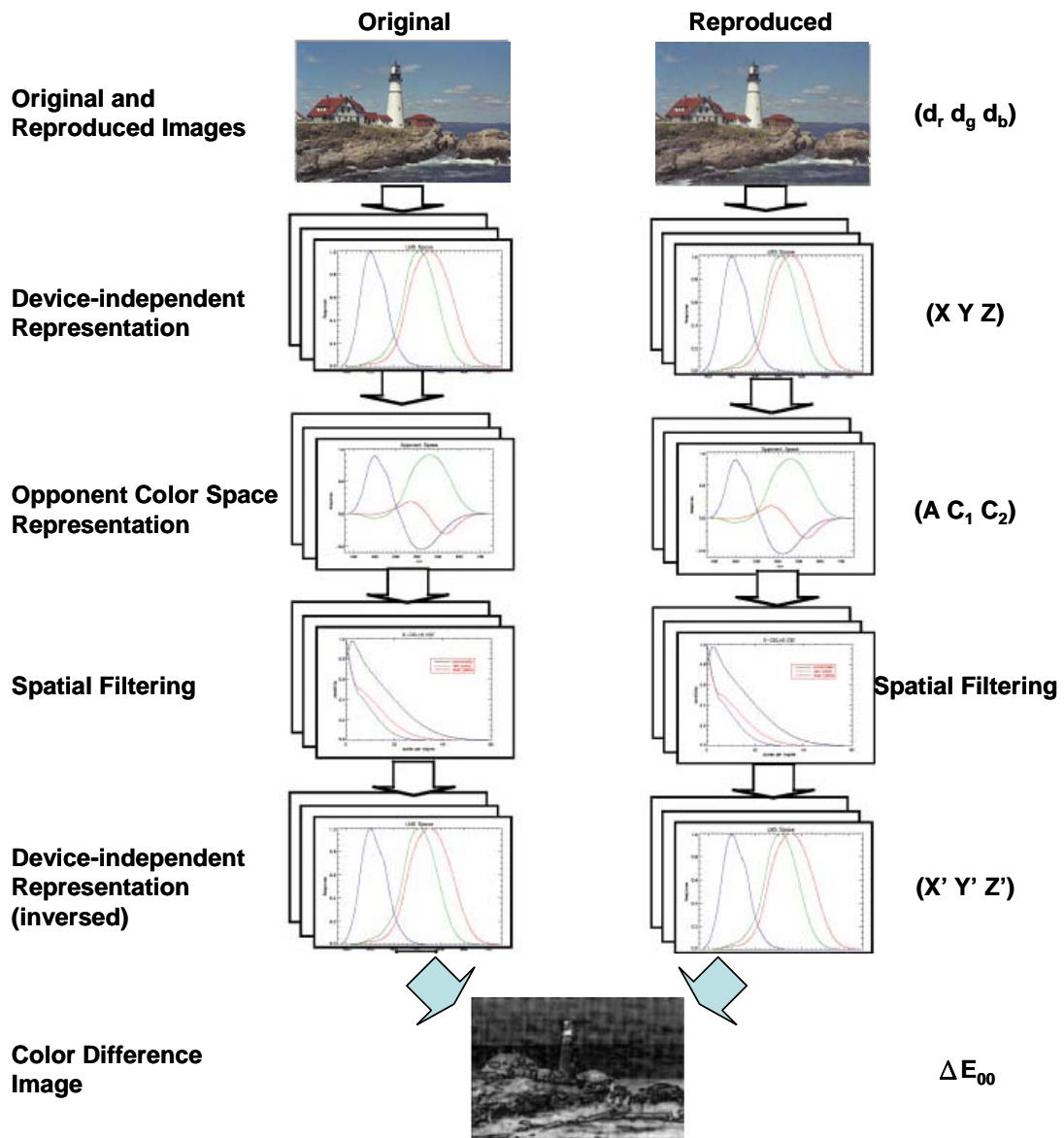
Fig. 4-5 Flowchart illustrating the spatial-extension of CIEDE2000 [54]

4.4 Experiment, Optimization, and Visual Difference

A. Experiment

The feature of spatial degrees of freedom embedded in an LCD with a spatially-modulated color backlight is crucial for facilitating the proposed method. The influences of system characteristics on the colorimetric reproduction are thus worth a further investigation. This examination is performed on the same platform introduced in **Section 2.3**, that is, an LC module of resolution 1920-by-1080 pixels and a backlight module with 8-by-8 divisions, wherein three-in-one LEDs are the light source. The composed red, green, and blue LEDs in a package are now controlled independently, but not simultaneously as in the experiment described in **Section 2.3**.

The current platform, however, is not specifically designed for the proposed driving scheme so some considerations must be put on the experiment. The platform functions in two ways, either as a conventional HDR LCD at frame rate 60Hz or a two-field LCD at frame rate 30Hz. The differentiation between these two modes is the control of three sub-pixels. Three sub-pixels of a pixel are manipulated independently in the conventional one while those in the other one are controlled by the same driving signal to simulate a color filterless LC panel. In order to precisely estimate the backlight distribution L, all the 8-by-8-by-3 LSFs, from different divisions and of three primaries, are recorded faithfully and implemented in the computation. For example, the recorded LSFs, from left to right as shown in **Fig. 4-6**, belong to three single backlight divisions located at the backlight edge, near center, and bottom corner, respectively. Thus, linear superposition, **Eq. (1-2)**, is applied instead of commonly-used convolution. It is worth noting that each LSF covers quite a large area, leading to a heavy computation loading.

69
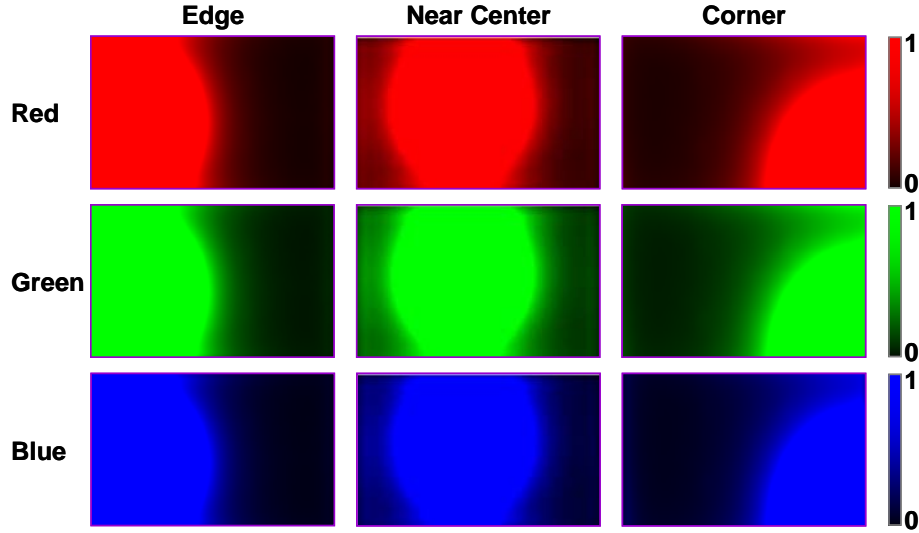
Fig. 4-6 *LSFs, from left to right, belong to three backlight divisions located at the backlight edge, near center, and bottom corner, respectively. From top to bottom rows are arranged in the sequence of red, green, and blue.*

A series of random color-patch images are designed as the testing inputs. The variation of patch number is to examine the dependency of color reproduction accuracy on the spatial frequency of images, as shown in **Fig. 4-7(a)**. For energy conservation, the magnitude of image digits in the first mode is scaled by a factor of one-half since the tri-stimulus values measured on each patch by a colorimeter are the time-average results. Color difference, ΔE_{00}, is calculated between the same images separately displayed by the two modes. As a result, the average ΔE_{00}, as shown in **Fig. 4-7(b)**, increases with the spatial frequency, i.e. the patch number. In view of Fourier analysis, large LSF area can only contribute to the components of low spatial frequency. In other words, wide-spreading LSFs, like those shown in **Fig. 4-6** of the current platform, are detrimental to manipulate complex images accurately. A postulation is induced that color reproduction accuracy of the proposed driving scheme depends on the correlation between the image content and both the backlight division and LSF property. The following discussion is to derive adequate specifications of the backlight module for the proposed method.
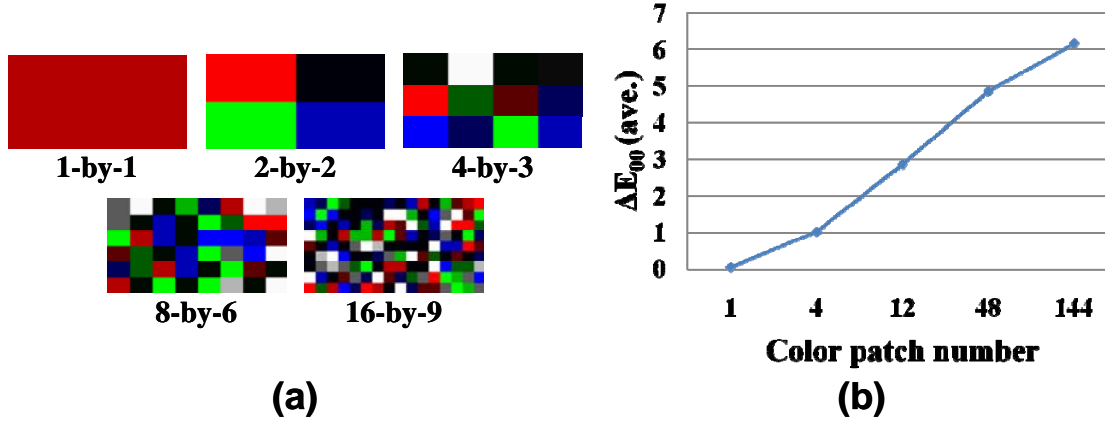
Fig. 4-7 *(a) A series of random color-patch images are designed as the testing inputs; (b) The average color difference, ΔE_{00}, against the color-patch number*

B. Optimization on Backlight Parameters

The number of backlight division and the size of LSF are the two backlight parameters to be optimized. Currently, the optimization can only be done by simulation on two pseudo systems because the present platform lacks modulation flexibility on the backlight parameters. Firstly, an LCD with a spatially-modulated color backlight is expressed mathematically by **Eqs. (4-4) and (4-5)**, which are modified from **Eqs. (2-5)** and **(2-7)** [55]. In short, the variables in **Eqs. (2-5)** and **(2-7)** must be threefold for the red/green/blue color backlight, denoted by the suffix *i*. As for the two-field LCD, **Eqs. (4-1)** and **(4-3)** are implemented. The numeric values of these two models are adopted from the current platform. Color difference, ΔE_{00}, is then calculated between the tri-stimulus values predicted by the two sets of equations. Besides, Gaussian profile, as the ideal LSF, is applied to the simulation for mathematic simplicity [4,56]; in addition, the shift-invariance is assumed so convolution is utilized to estimate backlight distribution. The LSF is represented by a square matrix with width of 6σ, where σ denotes the standard deviation of a Gaussian profile. The amplitude of the Gaussian LSF is carefully adjusted with the number of backlight division to maintain constant maximum panel luminance.

71

$$R_i = LUT_i(d_r')$$
$$G_i = LUT_i(d_g')$$
$$B_i = LUT_i(d_b') \qquad \text{, where } \textbf{\textit{i}} \text{ denotes red/green/blue light} \qquad (4\text{-}4)$$
$$0 \le R_i, G_i, B_i \le 1$$
$$0 \le L_i \le 1$$

$$\begin{bmatrix} X \\ Y \\ Z \end{bmatrix} = \sum_i \left\{ \begin{bmatrix} X_{i,r,\max} - X_{i,k} & X_{i,g,\max} - X_{i,k} & X_{i,b,\max} - X_{i,k} \\ Y_{i,r,\max} - Y_{i,k} & Y_{i,g,\max} - Y_{i,k} & Y_{i,b,\max} - Y_{i,k} \\ Z_{i,r,\max} - Z_{i,k} & Z_{i,g,\max} - Z_{i,k} & Z_{i,b,\max} - Z_{i,k} \end{bmatrix} \begin{bmatrix} R_i \\ G_i \\ B_i \end{bmatrix} L_i + \begin{bmatrix} X_{i,k} \\ Y_{i,k} \\ Z_{i,k} \end{bmatrix} L_i \right\} \qquad (4\text{-}5)$$

The variation of backlight division is tested at first. As a result, the average ΔE_{00} is reduced along with the increasing backlight division, shown in **Fig. 4-8(a)**. **Fig. 4-8(b)** implies that narrow LSF generally adapts to represent complex images with less color difference. The results can be explained by the increment of spatial degrees of freedom for complex images. More backlight division and narrow LSF are, thus, the design rules of the hardware for the proposed driving scheme.
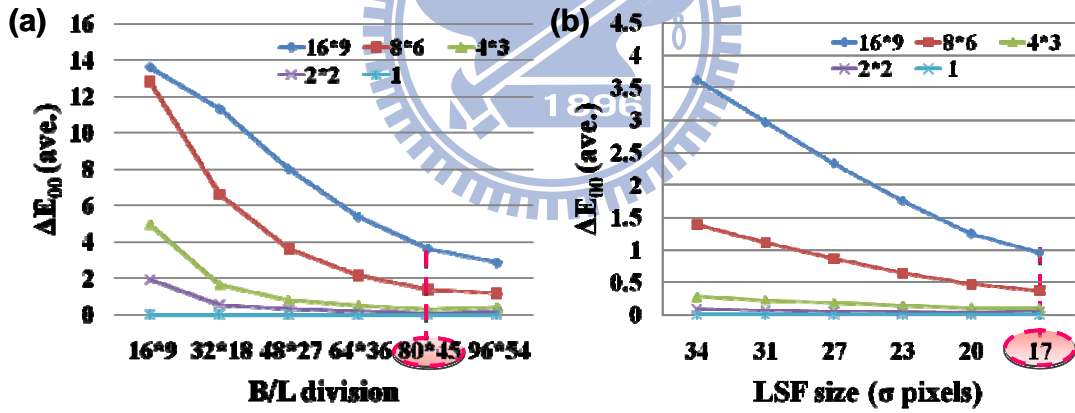
Fig. 4-8 *The optimization on (a) backlight division and (b) LSF size to reduce average ΔE_{00}*

If without additional notification, 80-by-45 backlight divisions and 17-pixel σ will be implemented in the following examination of image reproduction. Those optimized values are selected for the practical feasibility and the minimal color difference. Color difference is compared between the target and the reproduced images, which correspond to the simulated images from the LCD with a spatially-modulated backlight and the two-field LCD, respectively.

C. Visual Difference

A debate easily falls on the situation that the proposed driving scheme achieves color reproduction accuracy of less than 100%, in general. Theoretically, this argument is true since it is inefficient to implement the same amount of LEDs as the LC panel resolution to provide equal spatial degrees of freedom to the pixel numbers. However, our viewpoint is that acceptable accuracy of visual experience is more significant than the exact accuracy of pixel-to-pixel colorimetric reproduction. Some natures of the human visual system (HVS), e.g. band-pass or low-pass filtering on the opponent visual signals [57], can dramatically reduce the necessary bandwidth of spatial frequency in reproducing indistinguishable perception.

The standpoint in the evaluation of image reproduction accuracy, therefore, suggests that the spatial-filtering effect be taken into account [54,57]. Two simulated images, corresponding to the conventional HDR LCD and the two-field LCD, are shown in **Fig. 4-9(a)** and **Fig. 4-9(b)**, respectively. While the color difference map, **Fig. 4-9(c)**, is directly computed by ΔE_{00}, the other one, **Fig. 4-9(d)**, results from computing S-ΔE_{00}. At first glance, **Fig. 4-9(c)** implies that the reproduced image by the two-field driving scheme exhibits apparent color difference, including average $\Delta E_{00} = 1.39$ and maximum $\Delta E_{00} > 30$. However, the implication is contrary to the observers' response, which is much similar to that shown in **Fig. 4-9(d)** where average S-ΔE_{00} is 0.16 and maximum S-ΔE_{00} less than 4.3. Specifically, current blurring masks, i.e. the low- and band-pass filters, are designed for the viewing distance of one diagonal size with viewing angle of 2°. When the viewing distance increases, say, more than 2 times in watching TV, the visual difference decreases generally. Therefore, the image reproduction accuracy can be promoted effectively with the spatial filtering nature of the HVS. S-ΔE_{00}, henceforth, is recommended to be the index evaluating the proposed two-field driving scheme.
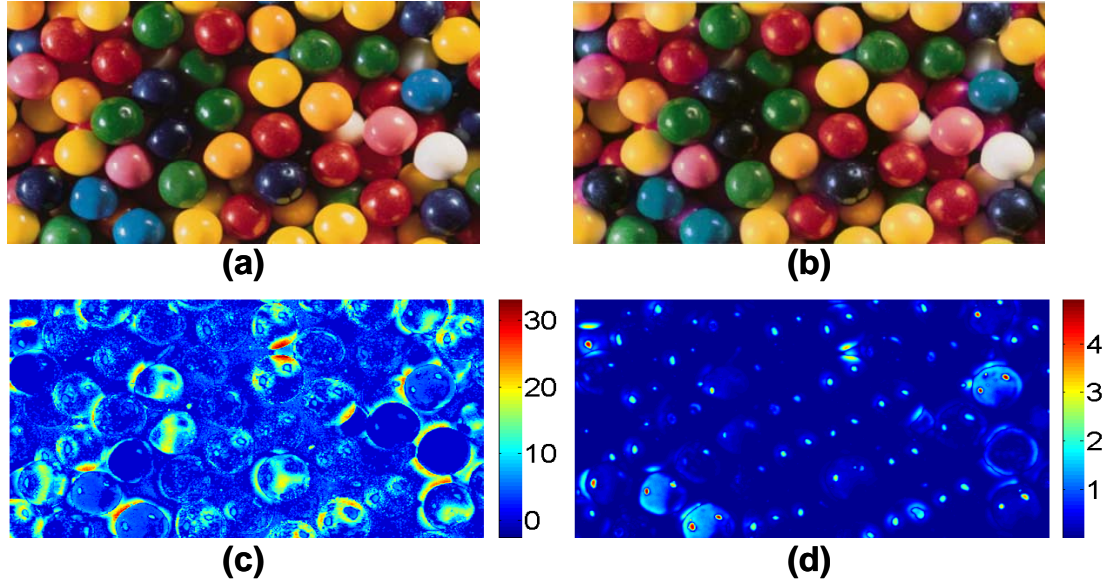
Fig. 4-9 *Color difference between (a) the target image and (b) the one produced by the two-field driving scheme is exhibited by the color difference maps of (c) ΔE_{00} and (d) S-ΔE_{00}, respectively.*

4.5 Demonstration

A. Image Reproduction

A further comparison is made by simulation, using the proposed driving scheme, between the current platform and the pseudo-platform with the optimized backlight parameters. Four images, Butterfly, Color Balls, Lily, and Parrot, as shown in the middle of **Fig. 4-10(a)** through **Fig. 4-10(d)**, are the testing images representing natural scene, global color variation, high contrast, and detailed color, accordingly. The reproduced image and the S-ΔE_{00} color difference map, resulted from 8-by-8 backlight division, are in the left side while those, resulted form 80-by-45 backlight division, are in the right. Generally, both the average and the standard deviation of S-ΔE_{00} of the reproduced images, as shown in **Fig. 4-10(e)**, are all below 1.0, which confirms the applicability of the proposed method. Moreover, the optimized backlight parameters, more backlight division and localized LSF, are indeed effective to improve color reproduction accuracy.

8 x 8   **Target Image**   **80 x 45**

(a)

(b)

(c)

(d)

(e)
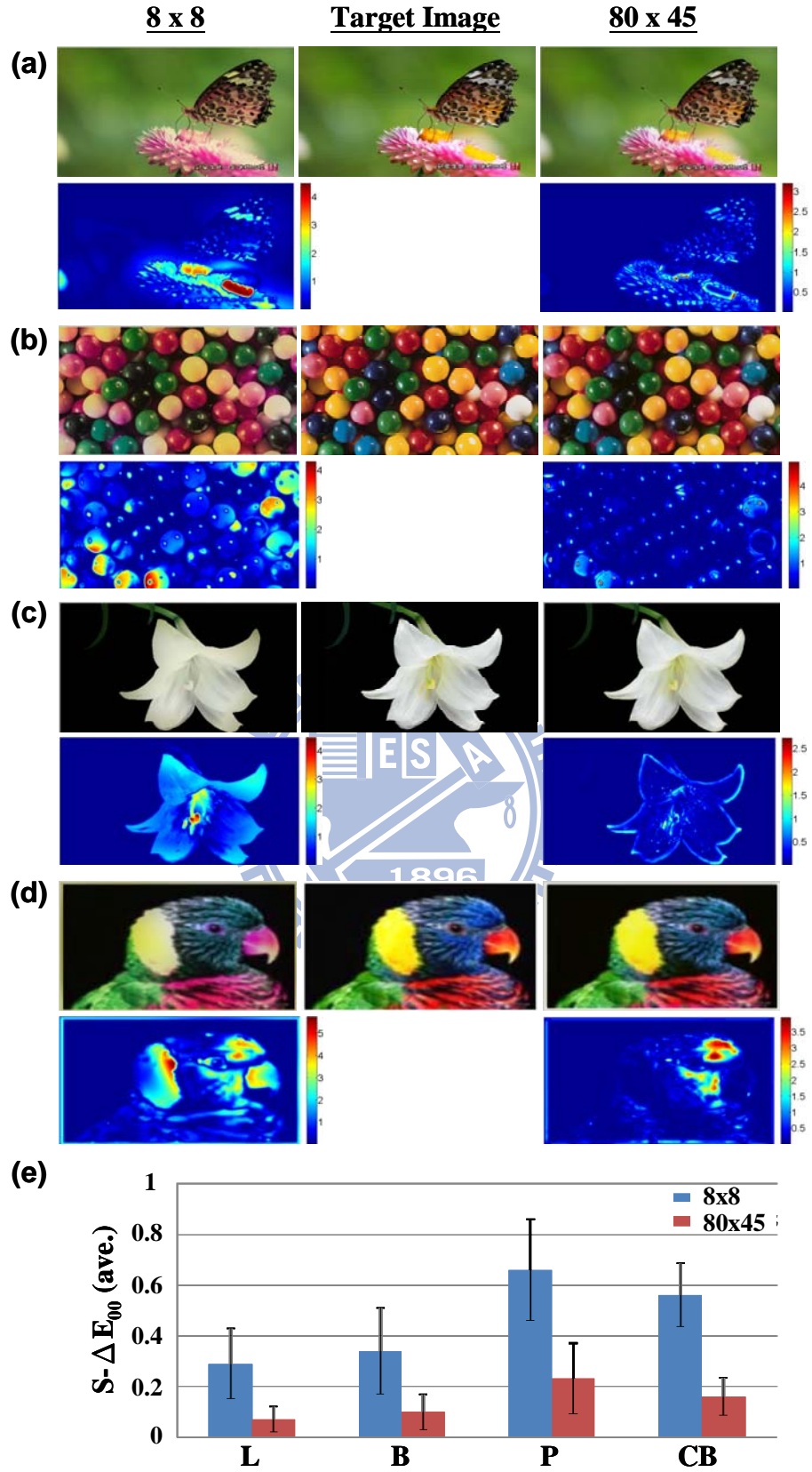
Fig. 4-10 *Target images, Butterfly (B), Lily (L), Parrot (P), and Color Balls (CB), are reproduced and compared in terms of in (a)-(d). (e) Comparison of the average S-ΔE_{00} from the two color difference maps of each image*

According to the proposed method, the reproduced first and the second primary information are basically the same as those of the targets. That is, color difference in principle arises from the inexact reproduction of the third primary information. This deduction is observed easily in the reproduced images based on 8-by-8 backlight division. Those images are de-saturated and blurred in comparison with the other reproduced images because more blue information than necessary is introduced to achieve global target luminance. On the contrary, the stamens of the flowers in Butterfly and Lily resulted from 80-by-45 backlight division, for example, become saturated towards the targets because of rather accurate blue information involved. This observation conforms that the proposed method works well for large backlight division amount and narrow LSF.

Some strategies can further improve the color reproduction accuracy. The global analysis, firstly, is to compile primary information statistically to decide the least significant one, which is chosen as the third primary redistributed into the two fields. **Fig. 4-11**, with 51% of blue information greater than the other two primaries, is an example illustrating that blue is improper to be the third primary. Errors from reproducing blue information easily occur when the LC signals, based on red information, tend to be minimized in **Fig. 4-11**. The local analysis, furthermore, decides the third primary dependent on the image detail. Take for example the reproduced images of Color Balls and Parrot based on 80-by-45 backlight division, as shown in **Fig. 4-10(b)** and **Fig. 4-10(d)**. In color difference maps of these reproduced images, larger color deviation occurs at the cyan-like areas, such as the cyan balls and parrot head around the eye. It is difficult to manipulate blue information in those areas since the LC signals here approach zeros because of less red and green information to be displayed. In such case, three combinations of two primary LEDs, R-G, G-B, or B-R, may be turned on at different location in each of

the two fields. The least significant primary selected by either the global or the local

analyses is expected to achieve minimum color reproduction errors.
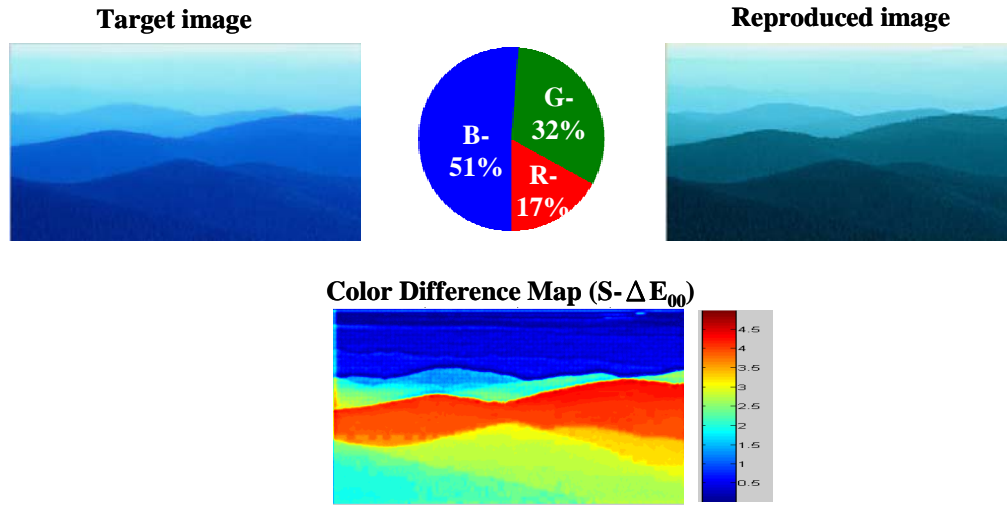
Fig. 4-11 *An image in which blue is inadequate to be the third primary*

B. Color Break-up (CBU) Examination

CBU visibility is compared between two images formed by the conventional

three-field (R/G/B) and the proposed two-field methods. A high-speed camera

moves horizontally in front of an LCD, with refreshing rate 120Hz, to simulate eye

movement to capture CBU images, as shown in **Fig. 4-12(a)**. The capturing time of

the camera in both cases is well-arranged to ensure equal CBU width. The CBU

images arise from the R/G/B three-field and the proposed two-field methods are

shown in **Fig. 4-12(b)** and **Fig. 4-12(c)**, respectively. The extracted pink ball in **Fig.

4-12(b)** displays clear reddish and bluish bands; that in **Fig. 4-12(c)** shows

de-saturated magenta bands which are perceived less color separation. Similarly, the

extracted white ball in **Fig. 4-12(b)** incurs more apparent contrast of color bands

than that in **Fig. 4-12(c)**. The result agrees with the innate feature of the two-field

driving scheme in reducing CBU visibility [58]. Namely, the contrast sensitivity

between the magenta-like and cyan-like fields is generally lower than that between

the opponent color, red and green, fields [59,60,61].
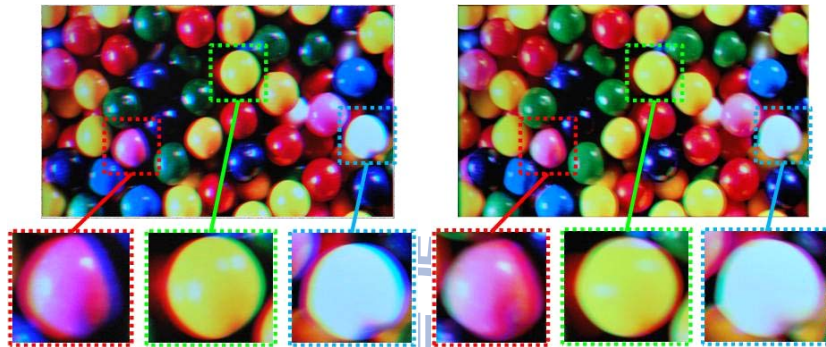
Fig. 4-12 *(a) The apparatus of capturing CBU image by a high-speed camera moving horizontally. The CBU images arise from (b) the R/G/B three-field and (c) the proposed two-field methods, respectively. (An example video of synthesizing the image, Color Balls, can be browsed via the hyperlink: http://adolab.ieo.nctu.edu.tw/app/news.php?Sn=32.)*

Some derivative issues are worth review on the examination of CBU visibility. First, the capture of CBU image is dependent on the viewing condition. **Fig. 4-12(b)** and **Fig. 4-12(c)** are photographed under specific conditions, at a position close to the LCD and with rather fast speed of the camera movement, which are suitable for capturing apparent CBU fringes but are not the real ones. The discrimination of CBU fringes is the second debatable point. The visibility of CBU fringes, e.g. **Fig. 4-12(b)** and **Fig. 4-12(c)**, varies with observers because the judgment relates to psychophysical response rather than simple colorimetric tri-stimulus difference. Those considerations induce the demand for a metric, based on psychophysical nature of the HVS, introduced in **Chapter 5**.

4.6 Conclusion

A two-field driving scheme is proposed to facilitate the field-sequential-color LCD. The color reproduction achieves average CIEDE2000 color difference of less than 3. Moreover, the average CIEDE2000 values are well-below 1.0 by simulation when the low- and band-pass features of the human visual system are taken into account. In addition, the color breakup visibility is suppressed by reducing the contrast sensitivity between the two color fields. Some comparisons on the system properties with the other driving schemes are summarized in **Table 4-1**. The promoted optical efficiency and the reduced material cost can be realized by removing the CF film. Power consumption is also reduced since a spatially-modulated backlight is utilized. Particularly, some commercial LC modes, e.g. MVA (Multi-domain Vertical Alignment) mode, can be utilized without extra cost to perform two fields sequentially in displaying color images on LCDs. Therefore, the proposed driving scheme, accompanied by the corresponding system configuration, is an applicable candidate to large-size, green display.

Table 4-1 Comparisons between the proposed two-field and the other driving schemes

	Full-on B/L	RGB-field	Prior Two-field [53]	NCTU Two-field [64]
Color Filters	3	0	2	0
Field / Frame	1	3	2	2
Refresh Rate (Hz)	60	180	120	120
Light Source	1x CCFL	3x LED	3x LED	3x LED
BL System	Global	Global	Global	Local
Optical Throughput	100%	300%	150%	300%
Resolution	100%	300%	150%	300%
LC Response Time (ms)	< 8	< 2 [15]	< 5	< 5
Color Breakup [58]	None	High	Medium	Medium

Chapter 5

Relative Contrast Sensitivity as CBU Index

5.1 Introduction

Although many driving schemes for color break-up (CBU) suppression have been proposed [62,63,64], no concrete evaluation metric can assert the effectiveness of those methods. Amongst the prior works, the device-dependent method, fitting empirical formula based on the display parameters, is commonly applied to the evaluation of CBU effect [65,66,67,68]. The advantage is that the fitted formulae are useful to predict the width of CBU fringe or to derive the cut-off frequency of the field rate, etc. However, the utility is limited due to the lack of generality and efficiency. That is, the formula deduced from one display under certain viewing condition may not be effective in other displays under different viewing conditions.

As for the device-independent method, the well-developed CIE color differences, CIEDE2000 (ΔE_{00}) for instance, are the candidates. Nevertheless, the applicability of CIE color difference to CBU phenomenon must be reviewed carefully. The CIE color difference formulae are developed to measure the color difference between uniform color patches with small color difference, e.g. **Fig. 5-1(a)**, after moderate chromatic adaptation [69,70]. CBU phenomenon, on the contrary, occurs at any image contents, simple or complex, with large color difference, red-green as shown **Fig. 5-1(b)**, for example. Although color differences of the opponent colors, e.g. red-green and yellow-blue, still can be calculated by formulae, the real perception is generally non-linear to large color difference values. Moreover, CBU stimuli are always glanced in a short period, which is insufficient for chromatic adaptation [71].
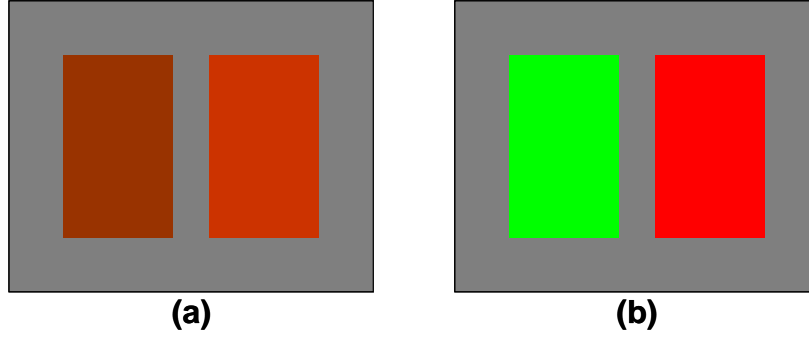
Fig. 5-1 *Pairs of color patches with (a) small and (b) large color differences*

An example is given to further exemplify the disagreement between the visual response of CBU and the calculated ΔE_{00} value. A series of synthesized CBU images, as shown in **Fig. 5-2**, are the simulated results of a white bar moving horizontally from left to right in black background at speeds of 200mm/s, 400mm/s, 600mm/s and 800mm/s, respectively. Observers report unanimously that the awareness of CBU effect increases along with increasing moving speed. However, the averaged ΔE_{00} values, calculated by **Eq. (5-1)**, of the four CBU images are the same, 68.03, in the experiment platform. The disagreement results from the fact that the accumulated average ΔE_{00} value of CBU fringe is proportional to the moving speed, thus the fringe width, so the common factor is cancelled by the division.

$$\Delta E_{00}(ave.) = \frac{\sum \text{CIEDE2000 value of each pixel of CBU fringe}}{\text{total pixel number of CBU fringe}} \qquad (5\text{-}1)$$
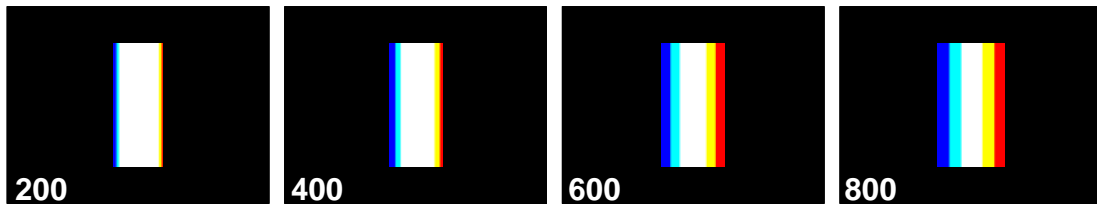
Fig. 5-2 *Synthesized CBU images of a white block moving horizontally;*
numbers at the bottom-left corner are the moving speeds in unit of mm/s.

The objective of this study is to establish a robust method, which can closely reflect the real response of the human visual system to evaluate the CBU effect effectively. An overview of the procedures of the proposed method and the verification by psychometric experiments are described. An application of this proposed index will be given as well.

5.2 Evaluation Method and the Index

Visual sensitivity based on the pattern-color-separable appearance pathways [61] is proposed to correlate with the sensibility of CBU. In our hypothesis, CBU stimulus is presumed to be strongly related to the neural signals, just leaving the lateral geniculate nucleus (LGN) cells, as shown in **Fig. 5-3** [72], with incomplete chromatic adaptation because of very short existing time period. According to the theory of pattern-color separability, the raw neural signals are proportional to the product of three terms: the stimulus strength, the pathway's sensitivity to the pattern color, and the pathway's sensitivity to the spatial pattern [59,60]. The procedures of reckoning sensitivity, as shown in **Fig. 5-4**, are modified from S-CIELAB [54,57] and described below.
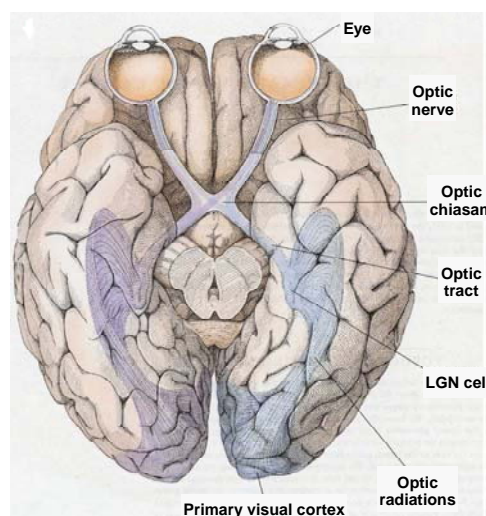
Fig. 5-3 *Visual pathway from the eye ball to the visual cortex, in which the LGN cell is the intermediate node [72]*
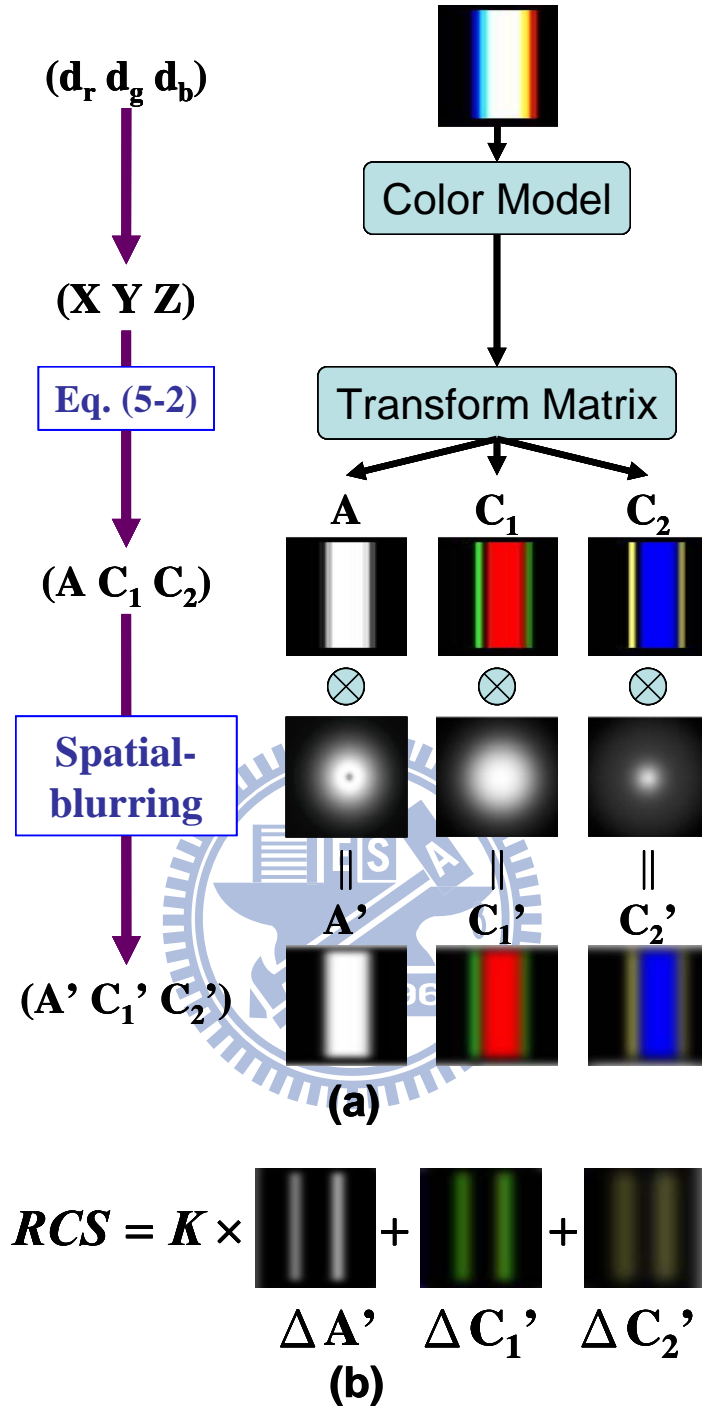
Fig. 5-4 *The computation flowchart of relative contrast sensitivity: (a) from input digits (d_r d_g d_b) to spatially-blurred opponent signals (A' C_1' C_2'), and (b) weighting sum performed on the subtracted CBU fringe signals, where **K** is the scale ratio between the luminance and the chrominance channels.*

The procedures of the proposed method start at tri-stimulus conversion, from the device-dependent input digits to the device-independent tri-stimulus values, CIE

1931 XYZ. Tri-stimulus values XYZ are then transformed into opponent-color space, AC_1C_2, where A denotes the luminance-related channel and C_1, C_2 the chrominance-related ones. Sometimes, AC_1C_2 representation is referred to as luminance, red-green, and blue-yellow channel signals, respectively. Each channel of opponent-color signals is then spatially filtered by the corresponding spatial contrast sensitivity function (CSF) to simulate the spatial blurring by the human visual system. Finally, subtraction is performed to extract the filtered signals of CBU fringe, followed by the weighting sum between the opponent channels pixel by pixel. The outcome is termed as relative contrast sensitivity, RCS.

A. Tri-stimulus Conversion

Since CBU effect is studied on LCDs, a mapping rule of LCDs is required for the tri-stimulus conversion. In current situation, all the CBU images, based on different driving schemes, are processed, synthesized, and then displayed on an FSC LCD. The color model expressed by **Eqs. (2-3)** and **(2-4)**, except for some modifications [73], can be applied to the conversion of tri-stimulus value from the input digits. The color model has to be implemented correspondingly once if other type of LCD is the testing platform.

B. XYZ to AC_1C_2

The opponent-color sensitivity signals, AC_1C_2, are determined through psychophysical experiments for pattern-color separability [61]. Mathematically, A set of AC_1C_2 is linearly transformed from a set of XYZ by **Eq. (5-2)** [54,57] since the application is focused on transformation of XYZ tri-stimulus values on LCDs.

$$\begin{bmatrix} A \\ C_1 \\ C_2 \end{bmatrix} = \begin{bmatrix} 0.297 & 0.72 & -0.107 \\ -0.449 & 0.29 & -0.077 \\ 0.086 & -0.59 & 0.501 \end{bmatrix} \cdot \begin{bmatrix} X \\ Y \\ Z \end{bmatrix} \qquad (5\text{-}2)$$

C.   Spatial Filtering

The spatial filtering on the opponent-color signals can be operated in the frequency domain. A, C_1, and C_2 signals are transformed into frequency domain by Fourier transformation. Multiplications are then performed channel by channel between the opponent signals and the corresponding CSFs. The frequency version of CSFs is expressed by **Eqs. (5-3)** and **(5-4)** [54], where csf_{lum} and csf_{chrom} respectively denote CSFs of luminance and chrominance channels, f the spatial frequency in unit of cycle per degree. The numerical values of the fitted parameters are summarized in **Table 5-1** [54], and the normalized one-dimensional CSFs are depicted in **Fig. 5-5**. **Fig. 5-5(a)** represents the 1-D cross-section profile while **Fig. 5-5(b)** corresponds to the blurring masks as shown in **Fig. 5-4(a)**. The CSF of channel A exhibits band-pass nature, while the other two are low-pass filters.

$$csf_{lum}(f) = a \cdot f^c \cdot e^{-b \cdot f} \tag{5-3}$$

$$csf_{chrom}(f) = a_1 \cdot e^{-b_1 \cdot f^{c_1}} + a_2 \cdot e^{-b_2 \cdot f^{c_2}} \tag{5-4}$$

Table 5-1 Numerical values of the coefficients of Eqs. (5-3) and (5-4) [54]

Parameters	Values (Channel A)	Parameters	Values (Channel C_1)	Values (Channel C_2)
a	75	a_1	109.1413	7.0328
b	0.2	b_1	0.00038	0.000004
c	0.5	c_1	3.4244	4.2582
		a_2	93.5971	40.6910
		b_2	0.00367	0.10391
		c_2	2.1677	1.6487
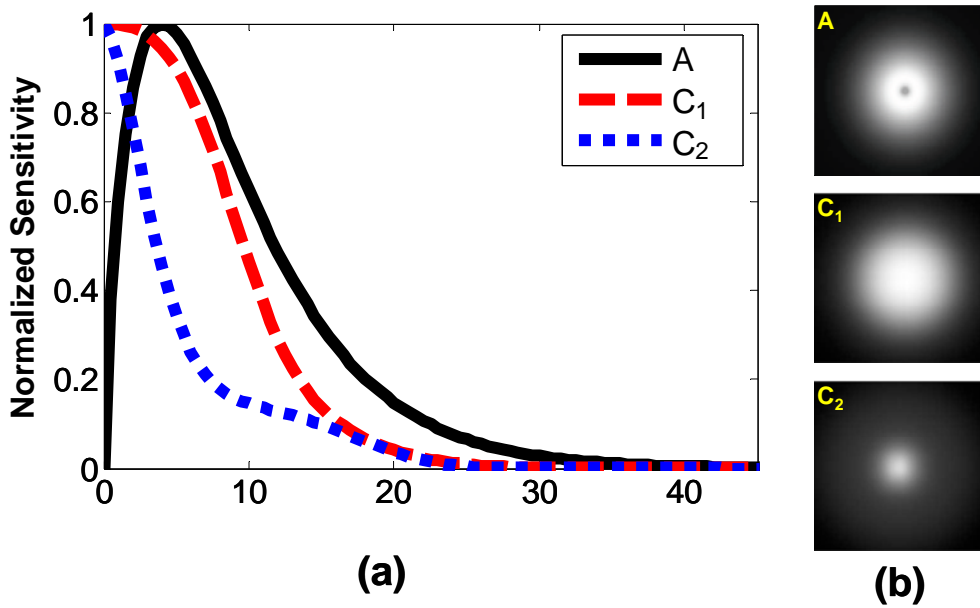
***Fig.* 5-5** *Normalized frequency filters in (a) 1-D cross-section and (b) 2-D distribution to approximate the spatial contrast sensitivity functions in unit of cycle per degree*

D. Single-valued Index: Subtraction and Weighting Sum

CBU fringe is the object for the RCS computation. As shown in **Fig. 5-2** for example, the separate color fields form the colored bands at both sides of the white bar in the horizontal direction. These two color bands in both sides are the CBU fringe here. The filtered A, C_1, and C_2 signals are extracted by subtracting the signals at the white area channel by channel, followed by weighting sum of the difference values among three channels, as shown in **Fig. 5-4(b)**. The scale ratio, K, is an empirical value deduced from the psychophysical experiments.

Before finishing the summation, two more considerations must be dealt with. First, the values of opponent signals, C_1 (red-green) and C_2 (blue-yellow) must use the absolute values. The positive and the negative signs in the representation of opponent signals just show the concept of opposite polarity. Second, the summation between the luminance channel and the chrominance channels requires a suitable scale ratio to account for the fact that the human visual system has different modulation responses to the two kinds of channels [59].

5.3 Experiment

The experiments are divided into three steps. The first is aimed at retrieving the scale ratio between the luminance and the chrominance channels. The second is to evaluate the proposed RCS index. Finally, a useful application is demonstrated.

Apparatus

A 32", optically-compensated-mode (OCB) FSC LCD is constructed as the testing platform. Three-in-one light emitting diodes (LEDs) are the light sources, supporting the red, green, and blue field rate at 180Hz, as shown in **Fig. 5-6**.
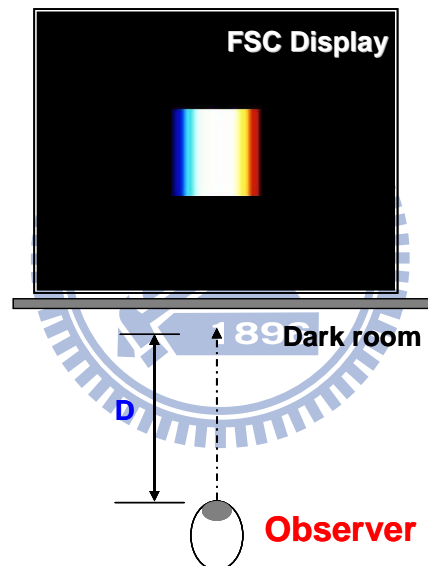
Fig. 5-6 Apparatus of the psychophysical experiments viewed in a dark room, where D denotes the viewing distance

Observers

There are undergraduate and graduate observers (three females and eight males) of ages ranging from 23 to 36 years old. All observers, some wearing their correcting lenses, perform normally on Snellen acuity pattern test for visual acuity and on Ishihara test for color blindness. All the experiments are performed in a dark room.

Test Images

A series of CBU images are synthesized as the testing images. The original images are square, uniform blocks of different colors in the center of the black ground. The width of the blocks is 2cm, subtending around 2-degree viewing angle at viewing distance of three-fifths the diagonal size. Color fringes appear in the horizontal direction to simulate the bar moving horizontally, like the case of white bar shown in **Fig. 5-2**. Color fringe width is above 0.1 degree, depending on the velocity applied to the synthesis.

Experiment (I): Mean Opinion Score and Absolute Threshold

Experiments of mean opinion score (MOS) and absolute threshold are performed to retrieve the scale ratio between the luminance and the chrominance channels and to examine the proposed index. In this experiment, color fringes are synthesized, based on three-field scheme, onto a white block; the color fringe width extends along with simulating velocity, ranging from 200mm/s to 800mm/s, separated by every 100mm/s. The blocks are of four luminance levels, 18, 28, 42, and 56cd/m^2.

MOS is one of the ordinal scales, category scaling [74]. Synthesized CBU images are rated by assigning a score, summarized in **Table 5-2**. The sensibility of CBU fringe increases from "Imperceptible" to "Vary annoying" of the CBU fringe along with the decrease of MOS from 1 to 5. Particularly, an anchoring CBU image, with the widest color fringe arising from the velocity 800mm/s, is scored 5 since it is regarded most annoying. Each CBU image pops up on the LCD and vanishes after three seconds to imitate closely to the real situation. A full dark image is inserted between any two succeeding CBU images to reduce after-image effect. Each test round for an observer, the CBU images are shown in random sequence. The comparison will be made between the MOS and the computed RCS.

Table 5-2 *Mean opinion score definition*

Score	Evaluation result
1	Imperceptible
2	Perceptible, but not annoying
3	Slight annoying
4	Annoying
5	Very annoying

The absolute threshold is determined manually based on method of adjustment [74]. The same series of CBU images, as those in MOS experiment, are displayed on the LCD. Observers are asked to adjust the viewing distance till the CBU fringe is imperceptible; this distance is termed as indistinguishable viewing distance, denoted as D_{InD}. The resultant indistinguishable CBUA (CBU angle), as shown in **Fig. 5-7**, denoted as InD-CBUA can be obtained by substituting D_{InD} into **Eq. (5-5)**, where D denotes the viewing distance, T the target width, V the moving speed, and F the field rate, respectively [75]. Cross comparisons are then made between InD-CBUA and the computed RCS.

$$CBUA = \tan^{-1}(\frac{T}{2D} + \frac{V}{FD}) - \tan^{-1}(\frac{T}{2D}) \qquad (5\text{-}5)$$
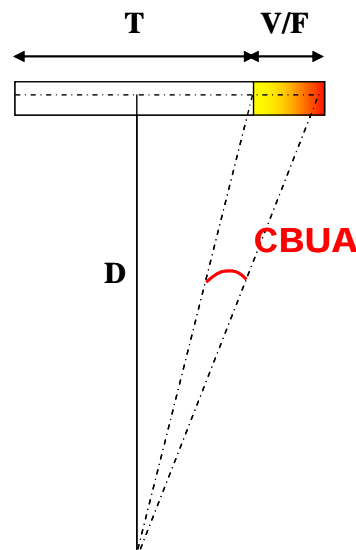

Fig. 5-7 Illustration of the geometric relation of CBUA with other parameters

Experiment (II): Optimization

The RCS index is applied to the comparison between various CBU suppression driving schemes: RGB, RYGB, RGBWmin, and RGBCY [76,77], as shown in **Fig. 5-8**. For those multi-primary methods being tested, the CBU images are synthesized according to the method and then are decomposed to the signals that can be used in the testing platform. Specific colors are used for comparison: White (255, 255, 255), Asia Skin (213, 139, 112), Light Skin (205, 163, 144), Strong Red (186, 70, 73), and Sky Blue (65, 75, 163), as shown in **Table 5-3**. The input digits, White (255, 255, 255) for example, follow the definition of that shown in **Eq. (2-3)**. The color fringes for all color blocks are synthesized based on velocity 800mm/s because of the widest color fringe width. The way to decide the MOS here is the same as that performed in the MOS decision of Experiment (I). The anchoring CBU image, scored 5, here becomes the white block with color fringes resulted from RGB driving scheme because all observers agree that it is most annoying. The luminance of the white block is 56cd/m^2. MOS values will be compared with RCS values and CIEDE2000 values, respectively.
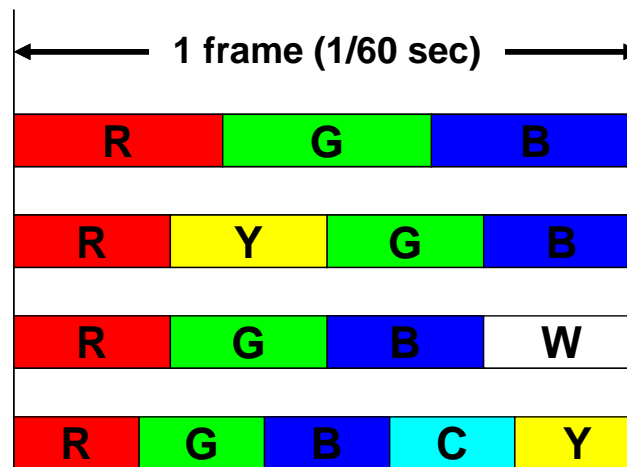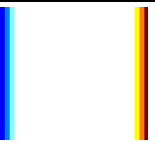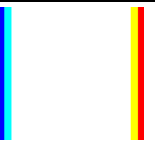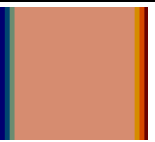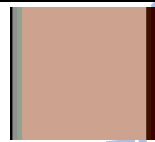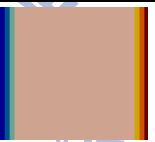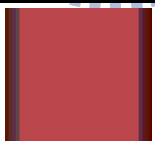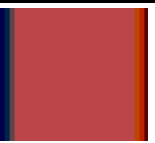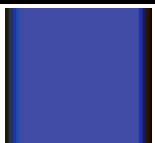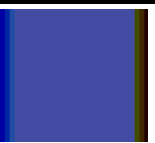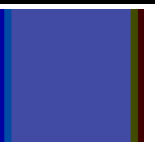

Fig. 5-8 *Different driving schemes: RGB, RYGB, RGBWmin, and RGBCY in top-down direction. R denotes red, G green, B blue, Y yellow, W white, and C cyan*

Table 5-3 *Comparison between different driving schemes by means of relative*
contrast sensitivity (RCS). CC denotes the correlation coefficient.

Driving Scheme	RGBWmin	RGBCY	RYGB	RGB	C.C.(%)
White (255, 255, 255)					
MOS	1	2.7	3.7	4.8	
RCS	0.215	0.408	0.807	1	97.2
CIEDE2000	0	45.859	58.662	68.587	96.8
Asia Skin (213, 139, 112)					
MOS	2.9	2.4	4.1	4.7	
RCS	0.299	0.312	0.840	1	97.7
CIEDE2000	23.67	27.277	33.594	38.417	91.0
Light Skin (205, 163, 144)					
MOS	3.1	2.2	3.7	4.8	
RCS	0.394	0.337	0.827	1	93.8
CIEDE2000	23.518	29.108	37.257	42.647	80.2
Strong Red (186, 70, 73)					
MOS	3.2	2.3	4.2	4.8	
RCS	0.254	0.255	0.849	1	94.0
CIEDE2000	16.276	24.648	26.392	27.329	46.2
Sky Blue (65, 75, 163)					
MOS	1.6	2.7	3.7	4.6	
RCS	0.271	0.475	0.887	1	98.1
CIEDE2000	5.6316	12.745	18.055	20.34	98.9

5.4 Result and discussion

The scale ratio between the luminance and the chrominance channels is obtained by analyzing the correlation coefficient in Experiment (I). The data set of white CBU images is used, because of the largest response to the CBU fringe in comparison with the other color bars. The correlation coefficient is examined as a function of the scale ratio, as shown in **Fig. 5-9**. Number 10 is selected as the scale ratio because the average correlation coefficient is as high as 98.9% and is around the turning point reaching the maximum. In addition, this value is close to that from the prior research [59].
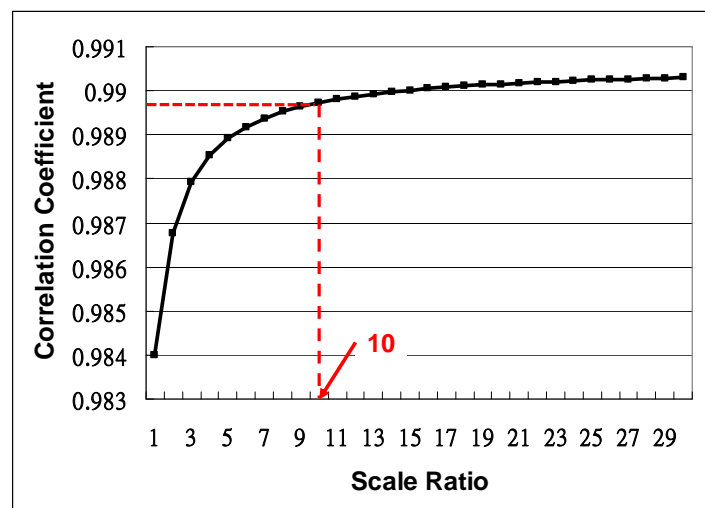
Fig. 5-9 *Correlation coefficient against the scale ratio between the luminance channel and the chrominance channels*

Both MOS and InD-CBUA are subjective judgments, which are meaningful to verify the proposed RCS index. The correlation coefficients between MOS and RCS, and between InD-CBUA and RCS are up to 96.8% and 94.1%, respectively, as shown in **Fig. 5-10(a)** and **Fig. 5-10(b)**, while the lowest is still of as high as 83.6%. Therefore, RCS, as presumed, is capable of reflecting the sensitivity of CBU fringe moderately. In general, the correlation coefficients between MOS and RCS are

higher than those between InD-CBUA and RCS. It is believed that this result arises from the different time for chromatic adaptation, since MOS is given within three seconds while the adjustment to achieve indistinguishable CBUA lasts several tens seconds [75]. Hence, time constraint is important in CBU evaluation experiment.
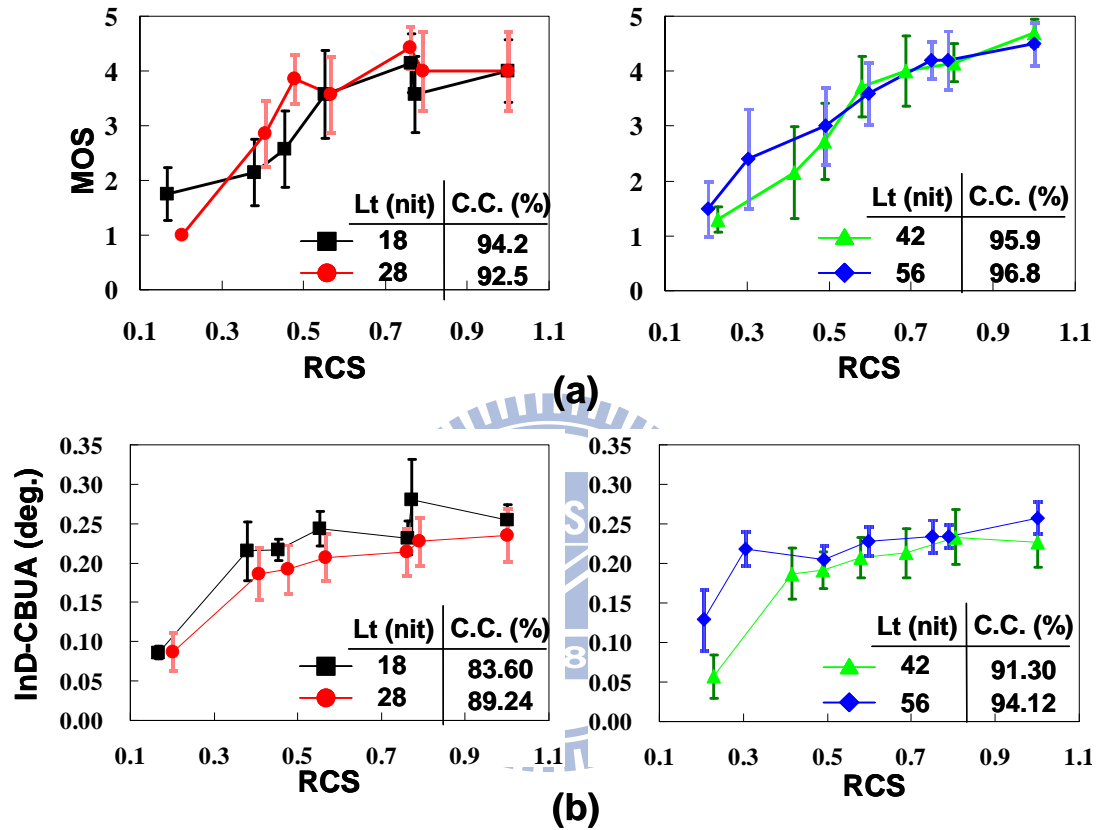
***Fig. 5-10** xy scattering plots of (a) Mean Opinion Score, and (b) Indistinguishable CBUA as a function of Relative Contrast Sensitivity. Lt in the inset is the target luminance (cd/m^2), and C.C. the correlation coefficient (%).*

As for Experiment (II), the mean, normalized RCS values of RGBWmin, RGBCY, RYGB, and RGB methods of the five colors, as summarized in **Table 5-3**, are 0.27, 0.37, 0.82, and 1, respectively, which are well correlated with the mean MOS values, 2.4, 2.5, 3.9, and 4.7, accordingly. Therefore, the results demonstrates the RCS is useful to sort different driving schemes dependent on perceived CBU effect; RGBWmin is the preferred one in current situation. It is worth noting that only one

sequence of color field of each driving scheme is examined. The result may vary when the color-field sequence of the driving scheme is exchanged due to spatial modulation, i.e. contrast sensitivity functions.

The CIEDE2000 as the evaluation index of CBU is further examined in Experiment (II). Compared with the RCS values, the CIEDE2000 values are compatible in colors White and Sky Blue, worse in colors Asian Skin and Light Skin, and the worst in color Strong Red. In average, the CIEDE2000 values exhibit less correspondence with the psychophysical response to CBU fringe than that of the RCS index. Specifically, the correlation coefficient between the CIEDE2000 values and the MOS values is less than one-half of that between the RCS values and the MOS values. This result conforms to the hypothesis that CBU stimuli are perceived without complete chromatic adaptation, so the CIEDE2000 is inadequate for CBU evaluation.

The application of current spatial CSFs, rather than temporal CSFs, is worth further discussion. The relative retinal motion is known to alter the curve shape of CSFs on the modulation of contrast sensitivity and the shift alone with frequency [78,79]. Generally, the modulation is more significant than the shift, especially in the case of smooth eye-tracking movement [79]. Since the RCS index is a relative number, the difference between the obtained RCS indexes from the spatial and the temporal CSFs is roughly a constant, which is accounted for in the normalization computation. In summary, the adaptation of the spatial CSFs is a trial. Although current results reveal the coincidence between the observation and the index, temporal CSFs should be considered when the experiment of CBU evaluation is improved to be in-situ operation, instead of static CBU images captured by a camera or by synthesis.

5.5 Two-field Driving Scheme Evaluated by RCS

The CBU suppression of the proposed two-field driving scheme, described in **Chapter 4**, can now be examined be means of RCS. A series of CBU images, as shown in **Fig. 5-11(a)**, are synthesized based on the proposed two-field method following the same way as described in Experiment (II). In comparison with the aforementioned driving schemes, the RCS values of the CBU images from the proposed method are almost less than all the others. However, it cannot carelessly conclude that the proposed method is better than others in CBU suppression. What is true is that the optimization introduced in **Chapter 4** is effective to achieve current results when the other driving schemes are not optimized.
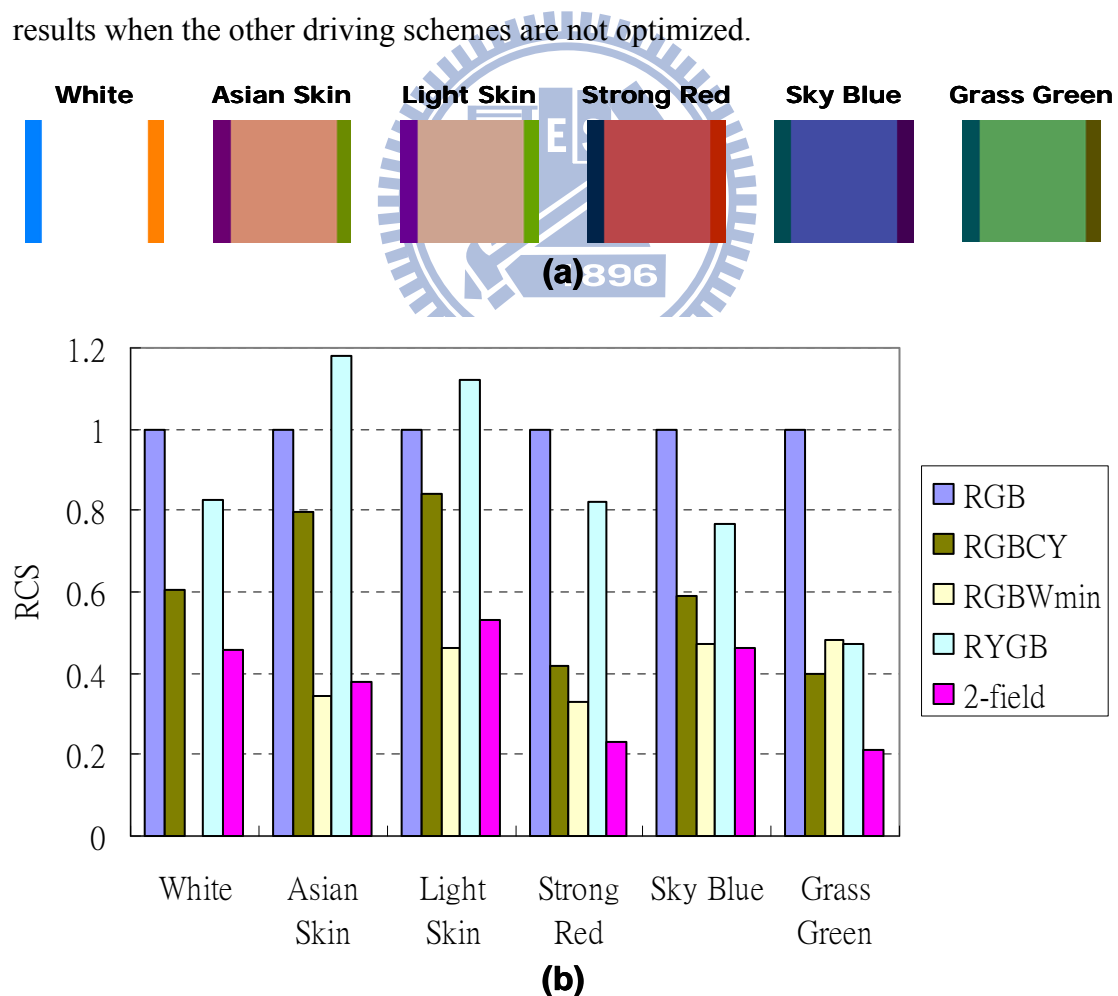
Fig. 5-11 (a) A series of CBU images synthesized based on the proposed two-field driving scheme; (b) comparison with other driving schemes by means of RCS

5.6 Conclusion

The single-valued index, relative contrast sensitivity (RCS), is proposed to evaluate color break-up (CBU) in field-sequential-color (FSC) LCDs. The vision-based methodology is verified in accordance with the visual responses of CBU fringes, in that the absolute correlation coefficients, between the computed RCS values and the psychophysical judgments in mean opinion score (MOS), are of well-above 80% and up to 98.9% in certain cases. The comparison between four driving schemes is performed based on the criterion of minimum of RCS values. The results demonstrate that the RCS is more adequate to evaluate CBU effect than the CIEDE2000. The simplicity and the robustness of the RCS computation are beneficial for facilitating the practical applications to FSC LCDs.

Several tasks remain to be dealt with to improve the RCS. First, while the RCS is potentially applicable to two-dimensional complex image, the separation of CBU fringe from complex CBU images is a challenge. Second, more psychophysical data are required from various FSC LCDs (different multi-primary driving schemes, wide luminance range, different panel size, etc.) under different viewing conditions (from dark, through dim, to bright environment, etc.). Third, capturing CBU images by high-speed camera for RCS computation is recommended to replace current synthesized CBU images, but the viewing conditions must be carefully defined.

Chapter 6

Conclusion and Future Work

6.1 Conclusion

A novel two-field driving scheme and the associated system have been proposed to facilitate the FSC LCD without color filter. A spatially-modulated color backlight is implemented to provide degrees of freedom in spatial domain in addition to the two temporal ones for conveying full-color information. This configuration of FSC LCD specifically features the feasibility of commercial LC modes, e.g. MVA, without colorimetric issues such as color gamut shrinkage, color crosstalk between successive fields, and insufficient backlight intensity. The corresponding color model and the localized light guide unit (LGU) are developed to achieve precise colorimetric reproduction and to improve system manipulation efficiency, respectively. Additionally, the innate nature of reduced contrast sensitivity between two primary-mixed fields suppresses the CBU to be less sensitive than that appears in the fundamental three-field FSC LCD. Finally, the psychophysical index, relative contrast sensitivity (RCS), has demonstrated the applicability to evaluate CBU among various driving schemes, which can be a useful feedback for system optimization. The related research topics are illustrated in **Fig. 6-1**, and more detailed summaries are described as follows.

In summary, the contributions of this dissertation are the following: (1) a feasible configuration for the FSC LCD, to which commercial LC modes are applicable; (2) the first color model and the efficient light guide unit for LCDs with a spatially-modulated backlight; (3) the first psychophysical index for CBU evaluation.
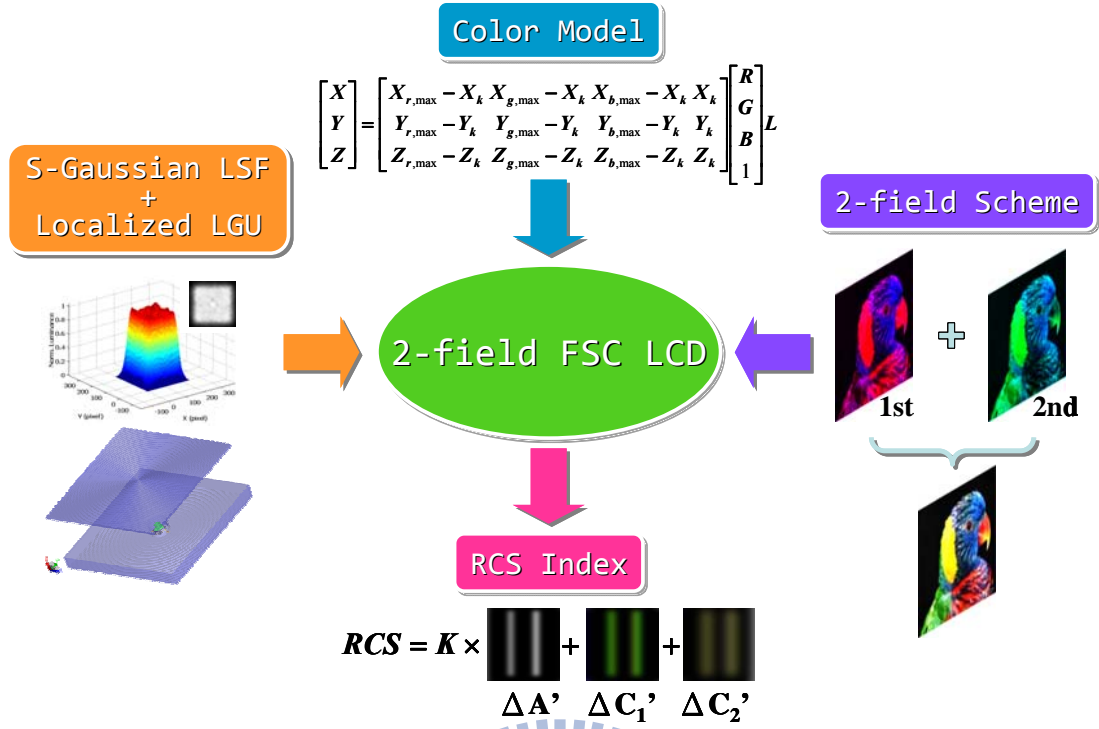
Fig. 6-1 *Research topics in this thesis*

6.1.1 Colorimetric Characterization of an LCD with a Spatially-modulated Backlight

The color model, expressed by **Eqs. (2-5)** and **(2-7)**, has been developed to ensure accurate colorimetric reproduction on an LCD with a spatially-modulated white backlight. The crucial parameter, backlight intensity distribution, is incorporated into the model for the first time. This model achieves the accuracy of CIEDE2000 value around or less than 1.0 with the measured backlight intensity distribution. Significantly, the color models for an LCD with a spatially-modulated color backlight, expressed by **Eqs. (4-4)** and **(4-5)**, and for the proposed two-field LCD, expressed by **Eqs. (4-1)** and **(4-2)**, are derived from the aforementioned one with moderate modifications.

6.1.2 Super-Gaussian Light Spread Function with Localized Light Guide Unit

A localized super-Gaussian light spread function (LSF) has been proposed to resolve several issues in an LCD with a spatially-modulated backlight. A dual-liquid-crystal-panel system is constructed as a pseudo high-dynamic-range (HDR) LCD to evaluate the super-Gaussian profile. The proposed solution is verified via the current platform: overall luminance uniformity, contrast ratio and processing speed can be improved by factors of 1.55, 1.95-4.15 and 4.82, respectively. An associated LED-based optomechanical configuration is also proposed to realize the desirable luminous pattern. The design flexibility makes the methodology applicable to any panel dimension and backlight division of LCDs with a spatially-modulated backlight, and to the conventional full-on backlighting LCDs as well.

6.1.3 Two-field Driving Scheme and System

The two-field driving scheme is proposed to facilitate an FSC LCD without color filters. With some modifications, the aforementioned color model and the spatially-modulated color backlight are integrated in the proposed method to achieve adequate colorimetric properties. The simulation results show that the proposed method achieves acceptable color reproduction accuracy, average CIEDE2000 color difference (ΔE_{00}) < 3. The least number of fields particularly alleviates the demand for fast-response LC modes in sequential-type LCDs. Furthermore, color break-up suppression is observed due to less chrominance difference between the two fields. Finally, the proposed method with the optimized manipulation, in average, exhibits minimal relative contrast sensitivity (RCS) values in comparison with the other four driving schemes.

6.1.4 Relative Contrast Sensitivity as Color Break-up Index

A single-valued index, relative contrast sensitivity (RCS), is developed to quantitatively evaluate color break-up (CBU) phenomenon. The sensibility of CBU fringe is hypothesized to strongly correlate with RCS, which is defined as the integrated difference of the opponent-color signals filtered by spatial contrast sensitivity functions. Psychometric experiments, based on methods of category scaling and adjustment respectively, are conducted to examine the proposed numerical metric. The results show that the maximal correlation coefficient is of as high as 98.9% between the subjective judgments and the computed numerical values of the experimental results. A useful application of RCS index is demonstrated by the evaluation of five driving schemes, including the proposed two-field one, for CBU visibility.
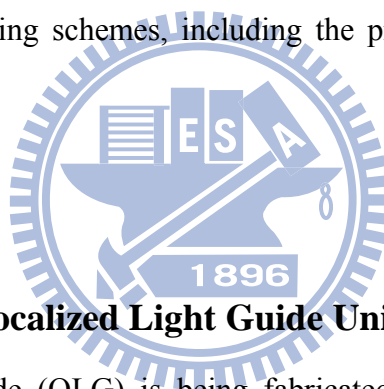
6.2 Future Works

6.2.1 Fabrication of Localized Light Guide Unit

The quadratic light guide (QLG) is being fabricated. In comparison with the concentric prism sheet (CPS), the fabrication process, introduced in **Section 3.5A**, is not suitable for the QLG because of the thickness and the non-identical pitch and height of the bumps, as shown in **Fig. 6-2**. The vacuum compression forming, as shown in **Fig. 6-3**, will be utilized to fabricate the QLG. Briefly, the metal mold compresses the heated PMMA substrate. After removing the metal mold, silver (Ag) is then coated onto the surface of the micro structure. The Ag-coated PMMA substrate is cut to obtain the designed shape to form a unit of QLG. Once the fabrication of the QLG is finished, the following tasks are the construction and the optical measurement of the LGU, and then the constitution of a complete backlight module.
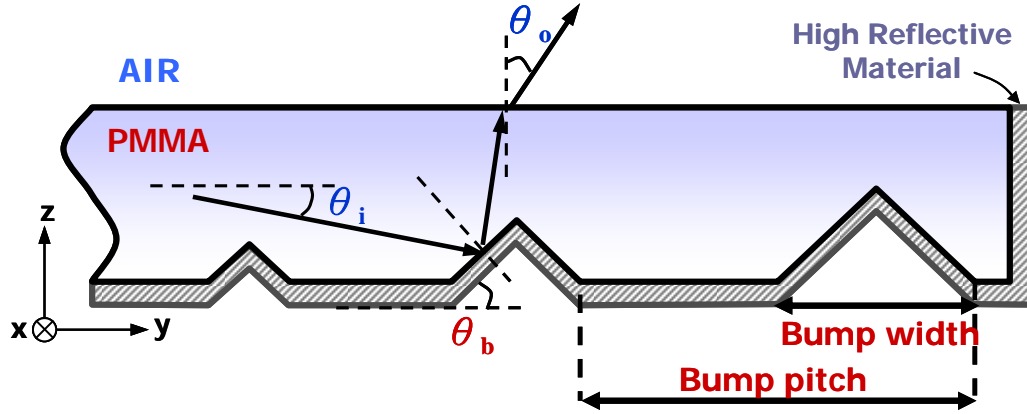
Fig. 6-2 *Schematic illustration of a quadratic light guide*
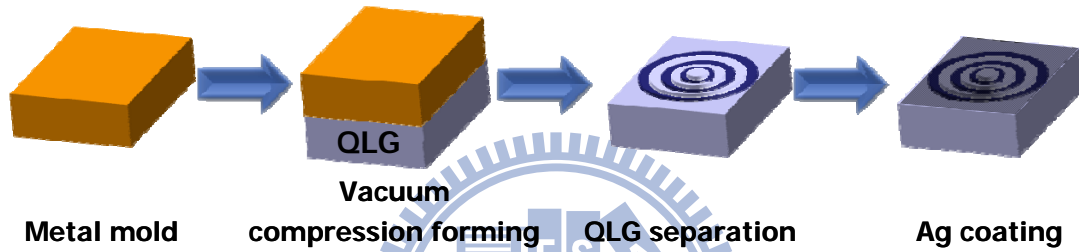
Fig. 6-3 *Vacuum compression forming process for the QLG*

6.2.2 Global and Local Analyses for the Two-field Driving Scheme

The color reproduction accuracy can be further improved by some means. Blue information, currently selected as the third primary because of the least luminance sensitivity, may be not the optimal choice. The global analysis, firstly, is to compile primary information statistically to decide the least significant one, which is chosen as the third primary redistributed into the two fields. The weight of red primary of the example image, as shown in **Fig. 6-4**, is the least significant so red information is suitable to be divided into the two fields. The local analysis, furthermore, can be regarded as the advanced modification from the global one. The area of statistical analysis is based on that of each backlight division, instead.

Color separation

Target image

Statistics

15%
30%
55%

R
Least significant

G-R1

B-R2
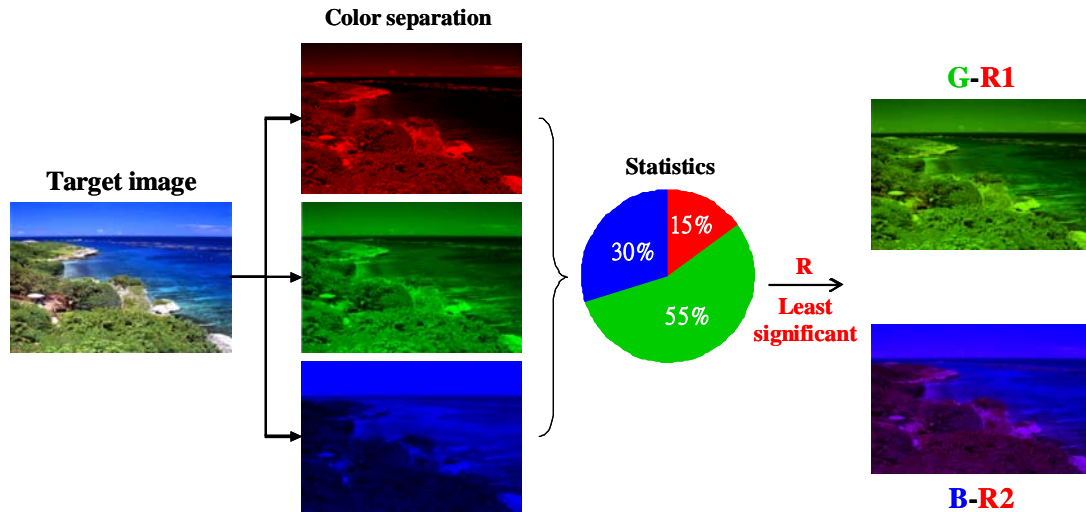
Fig. 6-4 *Example of global analysis for improving color reproduction accuracy*

6.2.3 Database for Optimization of RCS Index

The application of the RCS index, at current stage, is restricted in certain conditions because of the limited database till now. In view of psychometric scaling [74], current RCS index is regarded as an ordinal scale which is useful to rate the sequence of samples. However, when the conditions change, the results may be different correspondingly. More psychophysical data are required from various FSC LCDs (wide luminance range, different multi-primary driving schemes, different panel size, etc.) under different viewing conditions (from dark, through dim, to bright environment, etc.). With the additional parameters of the viewing conditions, modifications on some color appearance models, such as CIECAM02 [21], may be necessary to calculate RCS value.

References

1 M. G. Clark and I. A. Shanks, "A Field-Sequential Color CRT Using a Liquid Crystal Color Switch," *SID Symposium Digest of Technical Paper*, 13, pp. 172-173 (1982)

2 R. Vatne, P. A. Johnson, and P. Bos, "A LC/CRT Field-Sequential Color Display," *SID Symposium Digest of Technical Paper*, 14, pp. 28-29 (1983)

3 H. Seetzen, L. Whitehead, and G. Ward, "A high dynamic range display using low and high resolution modulators," *SID Symposium Digest of Technical Paper*, 34, 1450-1453 (2003)

4 H. Seetzen, W. Heidrich, W. Stuerzlinger, G. Ward, L. Whitehead, M. Trentacoste, A. Ghosh, and A. Vorozcovs, "High Dynamic Range Display System," *ACM Transactions on Graphics*, **23**(3), pp. 760-768, (2004)

5 R. G. W. Hunt, *The Reproduction of Colour: Sixth Edition*, Voyageur Press (MN); 6th edition (2004)

6 L. Arend, J. Lubin, J. Gille, and J. Larimer, "Color Breakup in Sequentially Scanned LCDs," *SID Symposium Digest of Technical Papers*, **25**, pp. 201- 204 (1994)

7 D. Eliav, E. H. A. Langendijk, S. Swinkels, and I. Baruchi, "Suppression of Color Breakup in Color-Sequential Multi-Primary Projection Displays," *SID Symposium Digest of Technical Papers*, **36**, pp. 1510- 1513 (2005)

8 F. Yamada, H. Nakamura, Y. Sakaguchi, and Y. Taira, "Color Sequential LCD Based on OCB with an LED Backlight," *SID Symposium Digest of Technical Papers*, **31**, pp. 1180-1183 (2000)

9 T. Ishinabe, Y. Ohno, T. Miyashita, T. Uchida, H. Yaginuma, and K. Wako, "Development of Super High Performance OCB Mode for High Quality Color-field Sequential LCDs," *SID Symposium Digest of Technical Papers*, **37**, pp. 717-720 (2006)

10 F.-C. Lin, Y.-P. Huang, C.-M. Wei, and H.-P. D. Shieh, "Color Breakup Suppression and Low Power Consumption by Stencil-FSC Method in Field- Sequential LCDs," *Journal of the Society*

for Information Display, **17**(3), pp. 221-228 (2009)

11 C.-H. Chen, F.-C. Lin, Y.-T. Hsu, Y.-P. Huang, and H.-P. D. Shieh, "A Field Sequential Color LCD Based on Color Fields Arrangement for Color Breakup and Flicker Reduction," *Journal of Display Technology*, **5**(1), pp. 34-39 (2009)

12 "How DLP® Technology Works." Retrieved Nov. 8, 2009, from: http://www.dlp.com/tech/what.aspx

13 K. T. Mullen, "The Contrast Sensitivity of Human Colour Vision to Red-Green and Blue-Yellow Chromatic Gratings," *The Journal of Physiology*, **359**, pp 381-400 (1985)

14 A. B. Poirson, and B. A. Wandell, "Appearance of colored patterns: pattern-color separability," *Journal of the Optical Society of America A*, **10**, No. 12, pp 2458-2470 (1993)

15 K. Käläntär, T. Kishimoto, K. Sekiya, T. Miyashita, and T. Uchida, "Spatio-temporal scanning backlight mode for field-sequential-color optically-compensated-bend liquid-crystal display," *Journal of the Society for Information Display*, **14**(2), pp. 151-159 (2006)

16 K. Sekiya, "Design Scheme of LED Scanning Backlights for Field Sequential Color LCDs," *SID Symposium Digest of Technical Papers*, **40**, pp. 1026-1029 (2009)

17 K. Takatori, "Field-sequential Smectic LCD with Twin-gate-TFT Pixel Amplifiers," *Displays*, **25**, pp. 37-44 (2004)

18 S. Kobayashi, J. Xu, H. Furuta, Y. Murakami, S. Kawamoto, M. Oh-kouchi, H. Hasebe, and H. Takatsu, "Fabrication and electro-optic characteristics of polymer-stabilized V-mode ferroelectric liquid crystal display and intrinsic H-V-mode ferroelectric liquid crystal displays: their application to field sequential full color active matrix liquid crystal displays," *Optical Engineering*, **43**(2), pp. 290-298 (2004)

19 L. J. Hornbeck, "Digital light processing for high-brightness, high-resolution applications," *Proc. SPIE Projection Displays III*, **3013**, pp 27-40 (1997)

20 F. Li, X. Feng, I. Sezan, and S. Daly, "Deriving LED Driving Signal for Area-Adaptive LED
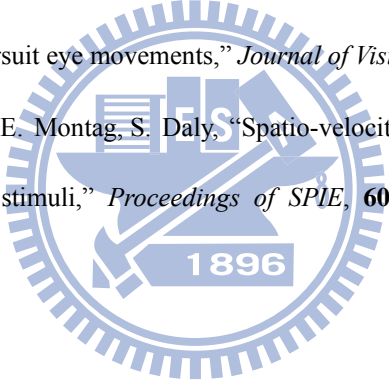
Backlight in High Dynamic Range LCD Display," *SID Symposium Digest of Technical Papers*, **38**, pp. 1794-1797 (2007)

21 CIE, "A Colour Appearance Model for Colour Management Systems: CIECAM02," *TC8-01 Technical Report*, CIE Publication, **159**:2004

22 F. H. Imai, D. Kuo, and R. J. Motta, "Colorimetric characterization of a HDR display system," *Proceeding of the 10th Congress of the International Colour Association AIC Colour '05*, Granada, Spain, pp. 653-656 (2005)

23 Y.-L. Chen, Y.-K. Cheng, Y.-P. Huang, H.-P. D. Shieh, and S.-C. Yeh, "Color Optimization Model for High Dynamic Range LCDs with RGB Color Backlights," *SID Symposium Digest of Technical Papers*, **40**, pp. 636-639 (2009)

24 S. Luka and J. A. Ferwerda, "Colorimetric Image Splitting for High-Dynamic- Range Displays," *SID Symposium Digest of Technical Papers*, **40**, pp. 1298-1301 (2009)

25 L. Kerofsky and S. Daly, "Brightness Preservation for LCD Backlight Reduction ," *SID Symposium Digest of Technical Papers*, **37**, pp. 1242-1245 (2006)

26 R. S. Berns, "A Generic Approach to Color Modeling," *Color Research & Application,* **22**(5), pp. 318-325 (1997)

27 R. S. Berns, R. J. Motta, and M. E. Gorzynski, "CRT Colorimetry. Part I: Theory and Practice" *Color Research & Application*, **18**(5), pp. 299-314 (1993)

28 R. S. Berns, R. J. Motta, and M. E. Gorzynski, "CRT Colorimetry. Part II: Metrology," *Color Research & Application*, **18**(5), pp. 315-325 (1993)

29 M. D. Fairchild and D. R. Wyble, "Color Characterization of the Apple Studio Display (Flat Panel LCD)," *Munsell Color science Laboratory Technical Report* 1998, http://www.cis.rit.edu/mcsl/research/PDFs/LCD.pdf

30 E. A. Day, L. Taplin, and R. S. Berns, "Colorimetric Characterization of a Computer-Controlled Liquid Crystal Display," *Color Research & Application*, **29**(5), pp. 365-373 (2004)

31 G. Marcu and K. Cheng, "Gray tracking correction for TFT-LCDs," *Proceedings of the IS&T/SID Tenth Color Imaging Conference*, pp. 272-276 (2002)

32 Y. Yoshida and Y. Yamamoto, "Color Calibration of LCDs," *Proceedings of the IS&T/SID Tenth Color Imaging Conference*, pp. 305-311 (2002)

33 N. Tamura, N. Tsumura, and Y. Miyake, "Masking Model for Accurate Colorimetric Characterization of LCD," *Proceedings of the IS&T/SID Tenth Color Imaging Conference*, pp. 312-316 (2002)

34 CIE, "Improvement to Industrial Colour Difference Evaluation," *TC1-47 Technical Report*, CIE Publication, **142**:2001

35 Topcon Technohouse Corp.: Spectroradiometer SR-UL1R, retrieved Nov. 22, 2009, from: http://www.topcon-techno.co.jp/eng/products/110383.html

36 Y.-H. Lu, Y.-K. Cheng, and C.-H. Tien, "A Localized Pattern Approach for High-Dynamic-Range Display," *SID Symposium Digest Technical Paper*, **38**, 449-452 (2007)

37 Y.-K. Cheng, Y.-H. Lu, P.-I. Lu, C.-H. Tien, and H.-P. D. Shieh, "Super-Gaussian Light Spread Function for High Dynamic Range Displays," *SID Symposium Digest Technical Paper*, **39**, 983-985 (2008)

38 F.-C. Lin, C.-Y. Liao, L.-Y. Liao, Y.-P. Huang, H.-P. D. Shieh, P.-J. Tsai, T.-M. Wang, and Y.-J. Hsieh, "Inverse of Mapping Function (IMF) Method for Image Quality Enhancement of High Dynamic Range LCD TVs," *SID Symposium Digest Technical Paper*, **38**, pp. 1343-1346 (2007)

39 L.-Y. Liao, Y.-P. Huang, and S.-C. Yeh, "A Real-Time Image Compensation for High Dynamic Range LCDs," *SID Symposium Digest Technical Paper*, **39**, pp. 764-767 (2008)

40 Y.-W. Wan, Y.-K. Cheng, H.-P. D. Shieh, T.-M. Wang, and R. H.-W. Lin, "Analyses of Point Spread Function in High Dynamic Range Display System," *Optics and Photonics Taiwan* 2005, Serial No. G-SA-X 4-3.

41 S. Swinkels, R. Muijs, E. Langendijk, and F. Vossen, "Effect of Backlight Segmentation on

Perceived Image Quality for HDR Display," *Proceeding of International Display Workshop'06*, pp. 1451-1454 (2006)

42 A. Parent, M. Morin, and P. Lavigne, "Propagation of super-Gaussian field distributions," *Optical and Quantum Electronics*, **24**, S1071-S1079 (1992)

43 J. A. Hoffnagle and C. M. Jefferson, "Beam shaping with a plano-aspheric lens pair," *Optical Engineering*, **42**(11), pp. 3090-3099 (2003)

44 K. Käläntär, M. Okada, and H. Ishiko, "Monolithic Block-Wised Light Guide with Controlled Optical Crosstalk for Field-Sequential Color/Scanning LCD," *SID Symposium Digest Technical Paper*, **40**, pp. 1038-1041 (2009)

45 Philips Lumileds LED Lighting, "Luxeon III Emitter Technical Datasheet (03/31/2006)", Retrieved Mar. 17, 2008 from the: http://www.lumileds.com/pdfs/DS45.PDF

46 K. Käläntär, "Functional Light-Guide Plate for Backlight Unit", *SID Symposium Digest Tech Paper*, **30**, pp. 764-767 (1999)

47 Vikuiti™ Business Partner Website, Vikuiti™ BEF III, Retrieved Mar. 17, 2008, from the: http://multimedia.3m.com/mws/mediawebserver?66666UuZjcFSLXTtlx&2MXfcEVuQEcuZgVs 6EVs6E666666--

48 K. Erwin, *Introductory Mathematical Statistics*, (Wiley, New York, 1970)

49 ASUSTek Computer Inc.: LCD Monitors, 19" Widescreen VW193D, retrieved Nov. 23, 2007, from the:
http://usa.asus.com/products.aspx?l1=10&l2=87&l3=545&l4=0&model=1688&modelmenu=2

50 Autronic-Melchers GmbH Inc., ConoScope®, retrieved Oct. 12, 2009, from the
http://old.autronic-melchers.com/products/measurement/conoscope/index.htm

51 L. D. Silverstein, "STColor: Hybrid Spatial-Temporal Color Synthesis for Enhanced Display Image Quality," *SID Symposium Digest of Technical Papers*, **36**, pp. 1112-1115 (2005)

52 M. J. J. Jak, G. J. Hekstra, J. J. L. Hoppenbrouwers, F. J. Vossen, N. Raman, and O. Belik,

"Spectrum Sequential Liquid Crystal Display," *SID Symposium Digest of Technical Papers*, **36**, pp. 1120-1123 (2005)

53 L. D. Silverstein, S. J. Roosendaal, and M. J. J. Jak, "Hybrid spatial-temporal color synthesis and its applications," *Journal of the Society for Information Display*, **14**(1), pp. 3-13 (2006)

54 G. M. Johnson and M. D. Fairchild, "A Top Down Description of S-CIELAB and CIEDE2000," *Color Research and Applications*, **28**(6), pp 425-435 (2003)

55 Y.-K. Cheng and H.-P. D. Shieh, "Colorimetric Characterization of High Dynamic Range Liquid Crystal Displays and Its Application," *Journal of Display Technology*, **5**(1), pp. 40-45 (2009)

56 Y.-K. Cheng, Y.-H. Lu, C.-H. Tien, and H.-P. D. Shieh, "Design and Evaluation of Light Spread Function for Area-Adaptive LCD System," *Journal of Display Technology*, **5**(2), pp. 66-71 (2009)

57 X. Zhang and B. A. Wandell, "A Spatial Extension of CIELAB for Digital Color Image Reproduction," *SID Symposium Digest Technical Papers*, **27**, pp. 731-734 (1996)

58 E. H. A. Langendijk, "A Comparison of Three Different Field Sequential Color Displays," *Proceeding of International Display Workshop '05*, pp. 1809-1812 (2005)

59 G. J. C. Van der Horst, and M. A. Bounman, " Spatiotemporal chromaticity discrimination," *Journal of the Optical Society of America A*, **59**, No. 11, pp 1482-1488 (1969)

60 K. T. Mullen, "The Contrast Sensitivity of Human Colour Vision to Red-Green and Blue-Yellow Chromatic Gratings," *The Journal of Physiology*, **359**, pp 381-400 (1985)

61 A. B. Poirson, and B. A. Wandell, "Appearance of colored patterns: pattern-color separability," *Journal of the Optical Society of America A*, **10**, No. 12, pp 2458-2470 (1993)

62 T. Kurita, and T. Kondo, "Evaluation and Improvement of Picture Quality for Moving Images on Field-Sequential Color Displays," *Proceeding of the 7th International Display Workshops*, pp 69-72 (2000)

63 N. Koma, and T. Uchida, " A new field-sequential-color LCD without moving- object color

break-up," *Journal of the Society for Information Display*, **11/2**, pp 411-417 (2003)

64 Y.-K. Cheng, Y.-P. Huang, Y.-R. Cheng, H.-P. D. Shieh, "Two-Field Scheme: Spatiotemporal Modulation for Field Sequential Color LCDs," *Journal of Display Technology*, **5**(10), pp 385-390. (2009)

65 D. L. Post, P. Monnier, and C. S. Calhoun, "Predicting color breakup on field-sequential displays," *Proceedings of SPIE*, **3058**, pp 57-65 (1997)

66 D. L. Post, A. L. Nagy, P. Monnier, and C. S. Calhoun, "Predicting Color Breakup on Field-Sequential Displays: Part 2," *SID International Symposium Digest Technical Papers*, **29**, pp 1037-1040 (1998)

67 X. Zhang, and J. E. Farrell, "Sequential color breakup measured with induced saccades," *Proceedings of SPIE*, **5007**, pp 210-217 (2003)

68 T. Jarvenpaa, "Measuring Color Breakup of Stationary Images in Field-Sequential-Color Displays," *SID International Symposium Digest Technical Papers*, **35**, pp 82-85 (2004)

69 M. R. Luo, G. Cui, and B. Rigg, "The Development of the CIE 2000 Colour Difference Formula," *Color Research and Applications*, **26**, pp 340-350 (2001)

70 G. Sharma, W. Wu, and E. N. Dalal, "The CIEDE2000 color-difference formula: Implementation notes, supplementary test data, and mathematical observations," *Color Research and Applications*, **30**, pp 21-30 (2005)

71 M. D. Fairchild, and L. Reniff, "Time Course of Chromatic Adaptation for Color-appearance Judgments," *Journal of the Optical Society of America A*, **12**, No. 5, pp 824-833 (1995)

72 D. H. Hubel, *Eye, Brain,* and *Vision*, New York: Scientific American Library No. 22, c1988

73 Y.-K. Cheng and H.-P. D. Shieh, "Relative Contrast Sensitivity for Color Break-up Evaluation in Field-Sequential-Color LCDs," *Journal of Display Technology*, **5**(10), pp 379-384. (2009)

74 P. G. Engeldrum, *Psychometric Scaling: A Toolkit for Imaging System Development*, Imcotex Press; 1st edition (2000)

75 S.-P. Yan, Y.-K. Cheng, F.-C. Lin, C.-M. Wei, Y.-P. Huang, and H.-P. D. Shieh, "A Visual Model of Color Break-Up for Designing Field-Sequential LCDs," *SID International Symposium Digest Technical Papers*, 38, pp 338-341 (2007)

76 C.-C. Chen, Y.-F. Chen, T.-T. Liu, C.-H. Chen, M.-T. Ho, K.-H. Chen, and H.-P. D. Shieh, "Spatial-temporal Division in Field Sequential Color Technique for Color Filterless LCD," *SID International Symposium Digest Technical Papers*, **38**, pp 1806-1809 (2007)

77 F.-C. Lin, Y.-P. Huang, C.-M. Wei, and H.-P. D. Shieh, "Stencil-FSC Method for Color Break-Up Suppression and Low Power Consumption in Field-Sequential LCDs," *SID International Symposium Digest Technical Papers*, **39**, pp 1108-1111 (2008)

78 A. C. Schütz, E. Delipetkos, D. I. Braun, D. Kerzel, and K. R. Gegenfurtner, "Temporal contrast sensitivity during smooth pursuit eye movements," *Journal of Vision*, **7(13):3**, pp 1-15 (2007)

79 J. Laird, M. Rosen, J. Pelz, E. Montag, S. Daly, "Spatio-velocity CSF as a function of retinal velocity using unstabilized stimuli," *Proceedings of SPIE*, **6057**, pp. 605705-1－605705-12 (2006)

Appendix: Acronym

BEF	brightness enhancement film	HVS	human visual system
CAM	color appearance model	InD-CBUA	indistinguishable CBUA
CBU	color break-up	LCD	liquid crystal display
CBUA	CBU angle	LED	light-emitting-diode
CC	correlation coefficient	LGU	light guide unit
CCFL	cold cathode fluorescent lamp	LGN	lateral geniculate nucleus
CRT	cathode-ray tube	LSF	light spread function
CF	color filter	LUT	look-up table
CIE	Commission Internationale de L'Eclairage	MOS	mean opinion score
		MVA	Multi-domain Vertical Alignment
CIECAM02	CAM proposed by CIE in 2002	OCB	optically-compensated bend
CIEDE2000	color difference calculated by the CIE 2000 color difference formula	OETF	opto-electronic transfer function
CPS	concentric prismatic sheet	PET	Polyethylene Terephthalate
CR	contrast ratio	PMMA	Polymethylmethacrylate
CSF	contrast sensitivity function	QLG	quadratic light guide
DLCP	dual-liquid-crystal-panel	RCS	relative contrast sensitivity
DLP®	Digital Light Processing®	S-CIEDE2000	spatial-extension of CIEDE2000
DMD	Digital Micro-mirror Device		
		TN	Twisted Nematic
FSC	field-sequential-color	TFT	thin-film-transistor
HDR	high-dynamic-range	UV	ultraviolet

Publication List

Journal Papers

1. **<u>Yu-Kuo Cheng</u>**, Han-Ping D. Shieh, "Colorimetric Characterization of High Dynamic Range Liquid Crystal Displays and Its Application," *Journal of Display Technology*, VOL. 5, NO. 1, pp 40-45. (2009) (I.F.:)

2. **<u>Yu-Kuo Cheng</u>**, Yen-Hsing Lu, Chung-Hao Tien, Han-Ping Shieh, "Design and Evaluation of Light Spread Function for Area-adaptive LCD System," *Journal of Display Technology*, VOL. 5, NO. 2, pp 66-71. (2009) (I.F.:)

3. **<u>Yu-Kuo Cheng</u>**, Han-Ping D. Shieh, "Relative Contrast Sensitivity for Color Break-up Evaluation in Field-Sequential-Color LCDs," *Journal of Display Technology*, VOL. 5, NO. 10, pp 379-384. (2009) (I.F.:)

4. **<u>Yu-Kuo Cheng</u>**, Yi-Pai Huang, Yi-Ru Cheng, Han-Ping D. Shieh, "Two-Field Scheme: Spatiotemporal Modulation for Field Sequential Color LCDs," *Journal of Display Technology*, VOL. 5, NO. 10, pp 385-390. (2009) (I.F.:)

International Conference Papers

1. **<u>Yu-Kuo Cheng</u>**, Han-Ping D. Shieh, "Color Gamut Enlargement and Adjustment by Using Multi-color LEDs in Time Sequential," *IDMC 2005 Proceeding*, p565-567

2. **<u>Yu-Kuo Cheng</u>**, Yu-Wen Wang, Han-Ping D. Shieh, "High Dynamic Range Display Adopting High Dynamic Range Imaging Technique," *IEEE/LEOS 2006 Proceeding*, p715-716

3. Yong-Jhih Chen, **<u>Yu-Kuo Cheng</u>**, and Han-Ping D. Shieh, "Optimum Design of Four-primary Color Gamut for Reproducing Maximum Input Encoded Color," *IDMC 2007 Proceeding*, p236-239

4. Shu-Ping Yan, **<u>Yu-Kuo Cheng</u>**, Fang-Cheng Lin, Ching-Ming Wei, Yi-Pai Huang, Han-Ping D. Shieh, "A Visual Model of Color Break-Up for Design Field-Sequential LCDs," *SID 2007 DIGEST*, p338-341

5. Yen-Hsing Lu, **Yu-Kuo Cheng**, Chung-Hao Tien, "A Localized Partition Approach for High-Dynamic-Range Display," *SID 2007 DIGEST*, p449-452

6. **Yu-Kuo Cheng**, Yen-Hsing Lu, Po-I Lu, Chung-Hao Tien, Han-Ping D. Shieh, "Super-Gaussian Light Spread Function for High Dynamic Range Displays," *SID 2008 DIGEST*, p983-985

7. **Yu-Kuo Cheng**, Han-Ping D. Shieh, "Colorimetric Characterization of High-Dynamic-Range LCDs," *SID 2008 DIGEST*, p1332-1335

8. **Yu-Kuo Cheng**, Yi-Ru Cheng, Yi-Pai Huang, Han-Ping D. Shieh, "Two-Color-Field Sequential Method for Color-Filter-Free MVA-LCDs," *SID 2009 DIGEST*, p 239-242 **(Distinguished Student Paper Award)**

9. Yi-Ling Chen, **Yu-Kuo Cheng**, Yi-Pai Huang, Han-Ping D. Shieh, "Color Optimization Model for High Dynamic Range LCDs with RGB Color Backlights," *SID 2009 DIGEST*, p 636-639

Domestic Conference Paper

1. Yu-Wen Wang, **Yu-Kuo Cheng**, Han-Ping D. Shieh, "Analyses of Point Spread Function in High Dynamic Range Display System," *OPT 2005*, Serial No.: G-SA-X 4-3.

2. Sue-Ping Yan, **Yu-Kuo Cheng**, Han-Ping D. Shieh, "Simulation of Color Breakup Phenomenon in Field-sequential Display," *OPT 2005*, Serial No.:

Patents

Taiwan

1. **鄭裕國**、謝漢萍,「一種應用於色序型液晶顯示器之色域及色溫調變裝置及調變方法」,中華民國專利,證書號:I315859

2. **鄭裕國**、陳勇智、謝漢萍,「發光二極體裝置以及其製造方法」,中華民國專利,證書號:I311381

3. 田仲豪、陸彥行、**鄭裕國**、呂柏毅,「應用於高動態對比顯示器之二維可控制局部區域性光場背光模組與其他影像處理系統」,中華民國專利,申請案號:096140524

4. **鄭裕國**、鄭宜如、黃乙白、謝漢萍,「雙色場之場色序顯示方法」,中華民國專利,申請案號:097139039

USA

1. Chung-Hao TIEN, Yen-Hsing LU, **Yu-Kuo CHENG**, Po-Yi LU
   Optical Element Apparatus for Two-dimensional Controllable Localized
   Partition Backlight Module
   US patent App. No.: 12/003,407 (pending)

2. **Yu-Kuo CHENG**, Yi-Ru Cheng, Yi-Pai Huang, Han-Ping D. Shieh
   DISPLAYING METHOD FOR FIELD SEQUENTIAL COLOR DISPLAYS
   USING TWO COLOR FIELDS,
   US patent App. No.: 12/359,346 (pending)

Vita

Name: Yu-Kuo Cheng 鄭裕國

Day of birth: July 7, 1975

E-mail: ykcheng.eo92g@nctu.edu.tw

- **Education**

  - 2003/09 – 2010/01   Ph.D., Institute of Electro-optical Engineering
    National Chiao Tung University, Hsinchu, Taiwan

  - 1997/09 – 1999/06   Master, Institute of Electrophysics
    National Chiao Tung University, Hsinchu, Taiwan

  - 1993/09 – 1997/06   Bachelor, Department of Electrophysics
    National Chiao Tung University, Hsinchu, Taiwan

- **Work and the Other**

  - 2001/03 – 2002/09   Electronic Engineer, DMD/LCD projector,
    BenQ Corp., Taoyuan, Taiwan

  - 2006/09 – 2007/08   Visiting scholar, Munsell Color Science Laboratory,
    Rochester Institute of Technology, Rochester, NY,
    USA.